Department of Electrical and Computer Engineering

Control and Data Communication Required for Hierarchical Control of Future Smart Microgrids

I Made Andik Setiawan

This thesis is presented for the Degree of
Doctor of Philosophy
of
Curtin University

June 2017

Declaration

To the best of my knowledge and belief this thesis contains no material previously published by any other person except where due acknowledgment has been made.

This thesis contains no material which has been accepted for the award of any other degree or diploma in any university.

Signature : …….

Date : ……...

Abstract

A Microgrid (MG) encourages the use of renewable energy resources due to its many recognised advantages, including reduced network expansion costs, minimisation of power loss in long feeders, increased network reliability, and faster recovery. It is expected that in the near future all MG operations will be fully automated. Information and Communication Technology (ICT) is essential for transmitting and exchanging the required data; however, because the number of MG devices to be connected can be numerous, it can lead to an increase in costs and also delays in data communication.

To solve this problem, this thesis presents a wireless data communication system for the future MG. The communication system is responsible for transmitting and receiving data among MG controllers. It is assumed that each MG has a central controller and each Distributed Generation (DG) unit in the MG has a local controller. The communication system is based on ZigBee technology, but — although it is a low cost and low power consumption device — it is limited by a low data transfer rate. To reduce the number of data transactions, this thesis presents the proposed data management scheme. The required data to be transferred are defined and a suitable coding is proposed. Then the number of transmitted symbols, including the processing time of the proposed data management scheme, are numerically analysed. Finally, the dynamic operation of an MG is evaluated, taking into account any delays that are imposed by this communication system.

In addition, by increasing the amount of digital technology that is powered in DC form, any power losses caused by AC-DC conversion can be drastically reduced. A DC MG network offers a significant reduction in power loss during conversion, and also less complexity when combining multi-renewable energy sources. The combination of several renewable energy sources into a single DC MG network leads to new issues such as voltage regulation and power/current load sharing among sources; on the other hand, the renewable energy sources have an intermittent characteristic, and their energy output depends on environmental conditions. The new technique presented in this thesis aims to regulate the voltage across the DC MG loads. The thesis also proposes and

discusses other advantages of the technique including: proper load current sharing among the DG units, which can operate simultaneously and precisely; scalability of multi-loads and multi-sources; it's simple to be implemented; it has a faster response time; and it is suitable for plug-and-play characteristics.

The dynamic performance of the investigated DC MG under different operating conditions is examined through extensive digital simulation analyses. The simulation results reveal the effectiveness of the proposed technique to achieve simultaneous voltage regulation and proper load current sharing. It is tested under different MG operating and loading conditions including constant-impedance, a communication link failure, and the plug and play feature of the DG units.

Various configurations can be considered for a DC MG, which is composed of DG units and loads, because renewable energy sources and energy storage systems of a plug-and-play nature can change the MG configuration at any time. Each configuration has a distinct and unique representation that influences the operation of the MG. The voltage profile of the future MG must be regulated within an acceptable limit, regardless of the configuration, load demand, and the number of DGs or loads. This thesis analyses, discusses and simulates the characteristics of various possible configurations of DC MGs with respect to voltage regulation and power/current sharing among DGs and using the proposed technique.

The required communication technology in the MG application should be capable of covering the scattered location of the DGs, ESSs and loads, and handling numerous and massive number of sensors/meters, spread over a geographical area. However, because there are significant installation costs associated with establishing an MG data communication infrastructure, to reduce costs, it is vital to identify a short distance without compromising reliability. In this thesis, the shortest distance algorithms for establishing an MG data communication infrastructure are proposed, discussed and simulated.

To perform the proper control for voltage regulation and power/current sharing, data exchange and communication among DGs, loads, and ESSs is required and essential for updating and synchronising the outputs via the established communication infrastructure. There are two types of data exchange

and communication scheme proposed and discussed in this thesis: centralised and distributed. Using the proposed voltage regulation and power/current sharing technique — with multi-sources and multi-loads in various data communication infrastructures — the dynamic performances of the MG are evaluated in MATLAB/Simulink through simulation analyses.

Acknowledgements

I am deeply grateful to my supervisors, Associate Professor Dr. Ahmed Abu-Siada, Dr. Farhad Shahnia, and Prof. Arindam Ghosh, for their incomparable guidance, support, encouragement, and continuous patience throughout the duration of my doctoral study. Their valuable ideas and advice both encouraged and helped me to generate and produce a quality research and publication, and also to successfully complete the writing of this thesis.

I would like to express my gratitude to my sponsors, Lembaga Pengelola Dana Pendidikan – LPDP (Indonesian Funds for Education) and the Ministry of Finance, Government of Indonesia, for their financial support, and also my institution, Politeknik Manufaktur Negeri Bangka Belitung, for giving me the opportunity to pursue doctoral study at Curtin University.

Thanks also to my parents for their encouragement and support, and finally, to my beloved wife, Yang Fitri Arriyani, and my amazing children, Husna Zahidah Mardhiyah, Ibrahim Muhammad Yusuf and Hasif Muhammad Ilyas, whose support and patience over the years is much appreciated.

List of Publications

It is acknowledged that most of the work in this thesis has been published in the following papers.

Journals:

- **Setiawan, M. A**., Shahnia, F., Rajakaruna, S., & Ghosh, A. (2015). ZigBee-Based Communication System for Data Transfer Within Future Microgrids. *IEEE Transactions on Smart Grid*, *6*(5), 2343–2355. http://doi.org/10.1109/TSG.2015.2402678.
- **Setiawan, M. A.**, Abu-Siada, A., Shahnia, F. (2017). A New Technique for Simultaneous Load Current Sharing and Voltage Regulation in DC Microgrids. *IEEE Transactions on Industrial Informatics*, Nov 2016 (submitted), Oct 2017 (**accepted**).
- **Setiawan, M. A.**, Abu-Siada, A., Shahnia, F. (2017). Proposing a Voltage Regulation and Power Sharing Method for Various Circuit Configurations of DC Microgrid. *Electric Power Systems Research*, Elsevier group, (submitted).
- **Setiawan, M. A.**, Abu-Siada, A., Shahnia, F. (2017). Performance Evaluation of a Proposed Centralised and Decentralised Data Communication Scheme for Voltage Regulation and Power Sharing in DC Microgrids. *Sustainable Energy, Grids and Networks*, Elsevier group, (submitted).

Conference Papers:

- **Setiawan, M. A**., Abu-Siada, A., & Shahnia, F. (2016). New Technique for Power sharing in DC Microgrids. In *IEEE Southern Power Electronics Conference* (pp. 1–5). Auckland: IEEE Conference Publications. http://doi.org/10.1109/SPEC.2016.7846021.
- **Setiawan, M. A.**, Abu-Siada, A., & Shahnia, F. (2016). Voltage Regulation in DC Microgrids with Various Circuit Configurations. In

IEEE Southern Power Electronics Conference (pp. 1–6). IEEE Conference Publications. http://doi.org/10.1109/SPEC.2016.7846021.

- **Setiawan, M. A.**, Shahnia, F., Chandrasena, R. P. S., & Ghosh, A. (2014). Data Communication Network and its Delay Effect on the Dynamic Operation of Distributed Generation Units in a Microgrid. In *IEEE PES Asia-Pacific Power and Energy Engineering Conference (APPEEC)* (pp. 1–6). http://doi.org/10.1109/APPEEC.2014.7066197.
- **Setiawan, M. A.**, Shahnia, F., Ghosh, A., & Rajakaruna, S. (2014). Developing the ZigBee Based Data Payload Coding for Data Communication in Microgrids. In *IEEE PES Australian Universities Power Engineering Conference (AUPEC)* (pp. 1–6). IEEE Conference Publications. http://doi.org/10.1109/AUPEC.2014.6966516.
- **Setiawan, M. A.**, Shahnia, F., Ghosh, A., & Rajakaruna, S. (2014). Proposing a New Algorithm for Defining the Shortest Distance among ZigBee-Based Communication Devices in Microgrids. In *IEEE PES Australaian Universities Power Engineering Conference (AUPEC)* (pp. 1–6). IEEE Conference Publications. http://doi.org/10.1109/AUPEC.2014.6966517.

Table of Contents

List of Figures

List of Tables

List of Abbreviations

AC	Alternating Current
ACK	Acknowledgment Frame
ADC	Analog-to-Digital Converters
ASCII	American Standard Code for Information Interchange
BPSK	Binary Phase-Shift Keying
CB	Circuit Breaker
DC	Direct Current
DG	Distributed Generations
ESS	Energy Storage Systems
EV	Electric Vehicles
FFD	Full Function Device
GPIO	General Purpose Input-Output
GSM	Global System for Mobile Communications
IEEE	Institute of Electrical and Electronics Engineers
MAC	Medium Access Control
MG	Microgrid
PAN	Personal Area Network
PLC	Power Line Communication
pu	Per Unit
PQ	Power Quality
QPSK	Quadrature Phase-Shift Keying
RFD	Reduced Function Device
RMS	Root Mean Square
SoC	State of Charge
TODR	Time Occupation Duty Ratio
VSC	Voltage Source Converters

List of Symbols

I_{L}	the current in the loads
I_{T}	the total of DG output current
n_{dev}^{CID}	the number of ZigBee devices in the same cluster
N	the number of active DGs in the MG
$P_{\mathrm{DG}k}$	the output power of the DG$_k$
P_{L}	the total power consumed by the loads plus the power losses in the lines
P_{T}	the output power of all DGs
R_{C} and L_{C}	the resistance and inductance of the line impedance
R_{DG}	the weighting factor of the generated power from each DG
$R_{\mathrm{DG}k}^{*}$	the updated ratio of the DG amended to compensate for the unmatched current caused by line impedances
R_{i} and L_{i}	the internal resistance and inductance of the converter's filter
s_{DG}	the DG status
T_{Bit}	the ZigBee time to transfer each bit
T_{c}	the processing delay time
T_{CL}	the controller delay
T_{Cen}	the total time delay in the centralised data communication scheme
T_{DF}	the processing time for the other sections of the Data Frame
$T_{\mathrm{DataFrame}}$	the total processing time for transferring the Data Frame
T_{DC}	the DC-DC converter processing delay
T_{Den}	the total time delay in the distributed data communication scheme
$T_{\mathrm{DataPayload}}$	the total processing time for the data payload
T_{IF}	the data latency affected by communication infrastructure
T_{P}	the predefined time delay
T_{PG}	the propagation delay
T_{Symbol}	the required time to transfer a symbol
V_{DGk}	the output voltage of DG-*k*
V_{L}	the voltage load demand
$V_{\mathrm{L}}^{\mathrm{ref}}$	the voltage load nominated level

$V_{\mathrm{L}}^{\mathrm{fb}}$	the feedback load voltage
Z_{Ck}	the impedance of line-*k* connecting DG-*k* to the load
Z_{L}	the equivalent impedance of the load
ΔI_k^{CS}	the deviation ratio of the DG output current — from the desired value versus the total load current
ΔP_k^{CS}	the deviation ratio of the DG output power — from the desired value versus the total load power

Chapter 1: Introduction

In this Chapter, the background and motivation, research objectives, and significances, and the outline of the thesis are presented. Each of them is further discussed, developed and explained more detail below:

1.1. Background and Motivation

In this subchapter, the backgrounds of this thesis are presented. They are divided into four sections: the required data communication, the voltage regulation and power/current sharing method, various circuit configurations, and the data communication infrastructure and schemes.

1.1.1. Future Microgrid and Required Data Communication

An increasing number of renewable energy resources, such as photovoltaic, wind and micro-hydro, causes a substantial amount of electric energy to be generated — in the form of Distributed Generations (DGs) — within the electric networks. The integration of DGs will benefit the existing electricity grids through the reduction of network expansion costs, minimisation of power losses in long feeders, and an increase in the reliability of the network [1], [2]. It may also be helpful in achieving faster recovery following a fault in the network [3].

A Microgrid (MG) is a DG cluster with several loads and Energy Storage Systems (ESSs), interconnected by a localised network of lines [4]–[6]. An MG can act as an independent power supply and a distribution system (islanded mode), and operate in a grid-connected mode when required [6], [7]. In a grid-connected mode, the network voltage and frequency are dictated by the grid; hence the DGs are controlled so that the desired amount of power (based on maximum power point tracking or economic power dispatch) is supplied by each DG [8]. Any power mismatch, between the power generated by the DGs and the load requirement, is met by the grid [9].

In autonomous mode, on the other hand, the DGs are not only required to supply the MG load demand but also to regulate the feeder voltage and frequency within acceptable limits [2], [9]. Therefore, for DG proper operation and control,

within an MG, each DG should be updated with the information about the MG operating mode [10]. This requires real-time power measurement of the grid, loads, and DGs as well as the State of Charge (SoC) of the available ESSs [11]. The RMS value, phase angle, frequency of voltage and the active/reactive power at specific points in the MG are required to be monitored and given as inputs to the DG control systems [12]. Furthermore, instantaneous values of voltages at the DG terminals and the feeder are needed for synchronising all DGs within an MG [13].

It is expected that in the near future all the operations in an MG will be fully automated [14], [15]. The automation system of future MGs will fetch data from the sensors, pass the data to the controllers, and finally pass the control commands to the actuators. Therefore, MGs need a fast and accurate data transmission system to transfer the measured data and command signals, and hence the use of reliable communication technology is essential [16]–[18]. A comparison of the characteristics of present and future MG systems is presented in Table 1.1.

Table 1.1 Characteristics of present and future MGs [14].

Present	Future
Centralised control	Centralised/distributed control
Little monitoring	Self/automated monitoring
Few sensors	A lot of sensors and actuators
Limited information for customer	Full information for customer
Electromechanical equipment	Digital equipment
Unidirectional communication	Bidirectional communication
Data accessed centrally	Data accessed in multiple centres
Manual restoration	Semi/fully automated restoration
Manual data prediction	Real-time data prediction
Fixed-setting protection systems	Adaptive protection systems

Implementing communication technology into MGs calls for several considerations; these include the compression of data to avoid long communication delay [19], [20], the adoption of a hierarchical communication network to reduce the number of data traffics [21]–[23], and the improvement of

the data exchange format among DGs, ESSs, Electric Vehicles (EVs), and loads and sensors [24]. To date, no attention has been given to these parameters when designing data communication for MG operations. Therefore, this thesis proposes a suitable data payload code and a data management scheme, which can be applied to the MG for proper operational. The effect of the communication delay on MG dynamic performance is also investigated.

1.1.2. Voltage Regulation and Power Sharing in Microgrids

MGs are categorised into two groups: AC MGs and DC MGs [25], [26]. Although electricity is traditionally produced and consumed in AC form, DC MGs are now gaining more traction. The recent global trend is to employ renewable energy resources that generate DC electricity, and an increase in the number of day-by-day loads that can function with a DC voltage [25]–[29]. Power losses in DC MGs are significantly reduced as the number of AC-DC conversions are eliminated [30]–[32]. Introducing more than one DG source into the same network can be easily realized in DC form, rather than in AC form [7], [33]. Several studies, comparing the performance and application of DC and AC MGs, can be found in the literature [34], [35].

Both voltage regulation and proper power/current sharing among DGs are considered as the main dynamic control issue of MGs [16], [36]–[43]. In this context, several techniques have been proposed in the literature to realize either proper voltage regulation or power/current sharing among DGs. However, developing a technique which can:

a. simultaneously regulate the voltage at load points and realize a desired power/load current sharing among DGs,
b. take into account the unequal and unknown line impedances between the DGs and loads,
c. be applied for DC MGs, involving multiple loads at various network locations and circuit configurations, and,
d. provide faster response and consider a big communication delay,

is the main research gap addressed in this thesis.

1.1.3. Various Circuit Configurations of the DC Microgrid

The DC MG circuit configuration (i.e. the connection topology of the sources and loads) directly influences the voltage, current, and power load demand, regardless of the number and types of ESSs, EVs, DGs in the MG. The design of the circuit configuration is based on the system's power demand, the location of the loads and DGs, and also the distance between them, all of which can impact operational cost or energy production [7], [44], [45]. Each configuration has a specific and unique presentation that influences MG operation.

The most commonly used circuit is composed of two DGs and one load [30], [40], [43], [46]–[49]. However, a DC MG can be consisted of multiple loads and multiple sources. Combinations of loads and sources in the MGs can be varied, and each circuit combination (configuration) has a unique characteristic. Moreover, also various configurations of loads and sources in the DC MGs have not yet been explicitly studied in the literature.

Maintaining all load voltages within acceptable limits and sharing the load demand among the DGs are the main challenging issues. Voltage deviation between loads is also inevitable due to the different line impedances [50] and spreading locations. A suitable voltage regulation and power-sharing technique for the MG is a method that can be applied to various configurations and that which is not affected by reconfigurable DGs, loads, ESSs and EVs. The suitable technique — which can be applied to various circuit configurations, taking into account the plug-and-play characteristics of renewable energy sources — is the main research gap addressed in this thesis.

1.1.4. Data Communication Infrastructure and Schemes for Microgrid Application

The communication technology for MG applications should be capable of covering the scattered locations of the DGs, ESSs and loads, handling numerous

sensors/meters, and managing a large geographical area [51]–[53]. However, establishing data communication infrastructure in the MG can lead to a significant installation cost [51], [54], [55]. This is because each communication technology (i.e. wire and wireless technology) has a specific coverage area, meaning that MGs with units scattered over a larger geographical area require repeaters for improving data transmission power, quality, and strength of signals are required but this will be on the account of cost [51], [54], [55]. Therefore identifying short distance for data communication infrastructure without compromising its reliability to reduce installation costs is vital.

While several papers presenting various techniques for DC MG voltage regulation and power/current sharing can be found in the literature, The communication infrastructure was not the main focus [17], [40], [45], [56], [57]. Communication infrastructure has a significant impact on communication delay, data transmission method, and the installation costs [51], [54], [55], [58]. This thesis proposes a new algorithm for establishing cost-effective communication infrastructure in the MG.

Data exchange and communication among the DGs, loads, and ESSs is essential when performing a proper control for voltage regulation and power/current sharing and also when updating and synchronising the outputs via established communication infrastructure. There are two types of data exchange/ communication schemes, which are proposed and discussed in this thesis: centralised and distributed [16], [40], [42].

Most of the papers in the literature, which discuss voltage regulation and power/current sharing in the MG, did not investigate the effects of the data communication scheme on their proposed methods. The data payload, data transmission method, and communication delay have also not been discussed in any detail in the literature. In this thesis, data payload construction, the data transmission method, and their impacts on the MG's performance are proposed, discussed, and simulated.

1.2. Research Objectives

The key aim of this thesis is to propose, develop and verify a proper control scheme and also the required data communication/management for simultaneous voltage regulation and proper power/current sharing among the DGs in the MG. To achieve this goal, the objectives of the research are identified as:

- Developing hierarchical and management data communication in the MG.
- Developing a technique for voltage regulation and power/current sharing in the DC MG.
- Developing a feedback method for various DC MG circuit configurations.
- Developing a short distance algorithm for establishing data communication infrastructure in the DC MG.
- Developing a data communication scheme for DC MGs.

The proposed methods are evaluated through extensive simulation analyses using PSCAD/EMTDC and MATLAB/Simulink.

1.3. Significance of Research

It is expected that in the future, operation of a MG will be fully automated through voltage regulation, re-adjustable generated power from the DGs, fetching data from sensors, the plug-and-play characteristics of sources and loads (such as renewable energy, energy storage, and electric vehicles), various types of load with variable locations, and the potential integration of neighboring MGs. This research aims to introduce new techniques to facilitate some of the above automated operations and simultaneously regulate the load voltages in DC MGs. This thesis also aims to achieve proper power/current sharing among the DGs, and provide cost-effective solutions for data communication schemes and infrastructures.

1.4. Thesis Outline

This thesis is organised into seven chapters. The research aim and its objectives, along with the need and justification for the research topic, are outlined in **Chapter 1**. An extensive literature review is presented in **Chapter 2**. The proposed hierarchical and data communication for the MG is presented in

Chapter 3. A new proposed technique for voltage regulation and power/current load sharing with various types of loads in the MG is proposed in **Chapter 4**. In **Chapter 5**, various MG circuit configurations and their operational characteristics are presented. The new shortest distance algorithm for establishing MG data communication is presented in **Chapter 6.** This chapter also discusses the data communication scheme that will facilitate the possibility of various data communication MG infrastructures**.** Conclusions drawn from this research and recommendations for future research are given in **Chapter 7.**

Chapter 2: Literature Review

In this Chapter, the literature of data communications, voltage regulation and power-sharing methods, various circuit configurations, and data communication schemes in the MGs are presented and discussed.

2.1. Data Communication for Microgrids

The distance between the DGs, loads, and ESSs within a MG may be considerable; hence the use of communication technology for transmitting and exchanging data and information is essential [16]–[18], [56], [59], [60]. The types of communication technology that can be employed for data transmittal and exchange in the MG can be both wired and wireless. The wired technologies have a higher data transfer bandwidth and are more reliable; however, their installation cost is relatively high. Wireless technologies have lower installation costs and are therefore more suitable for remote areas. At the same time, they are more flexible for future expansion [61]. However, it is to be noted that wireless technologies have a lower data transmission rate and may be vulnerable to interference from other signals [55]. That said, due to the growing number of meters, sensors, and actuators, which need to be monitored and controlled continuously within an MG, the use of wired technologies are more significantly more costly to install. Therefore, overall, the wireless technologies are a better candidate for MG applications.

The most popular wired technologies used in power systems are: Serial communication RS-232/422/485; Bus technology (e.g. ModBus, ProfiBus, CANBus) [43], [62]; Power-line communication (e.g. DLC, PLC, BPLC) [63]; and Ethernet/Internet of Things (IoT) (e.g. LAN, optical cable) [62], [64]. The most popular wireless technologies used in power systems are: Cellular (e.g. GSM, CDMA) [5]; Wi-Fi [54], [55], [12]; WiMax [65]; ZigBee [66], [67]; Z-Wave [68]; Bluetooth [61]; Insteon [69]; Radio frequency [61]; and Microwave [69].

A comparison between different wireless technologies that can be considered for MG applications is presented in Table 2.1. [70]

Table 2.1 Technical comparison of different wireless technologies applicable for MGs [52], [70].

Technology	Range	Rate	Frequency	Routing	Security	Suitable for	Modulation	Initial Costs
Cellular	Several km	270 kbps	900, 1800 MHz (2G), 2.1 GHz (3G)	Direct	64 bit A5/1, KASUMI cipher (3G)	Backbone	GMSK	Costly
Wi-Fi	100 m	54 Mbps	2.4 GHz	More than 70 protocols	WPA	Backbone	QPSK, BPSK, 16/64 QAM.	moderate
WiMax	Several km	30-40 Mbps	2.3, 2.5, 3.5 GHz	AODV, DSR, OLSR, ZRP	AES and 3DES	Backbone	BPSK, QPSK, 16/64QAM, OFDMA-PHY	moderate
ZigBee	100-1500 m	250 kbps	2,4 GHz, 868, 915 MHz	AODV, HERA	AES	End devices	OQPSK, BPSK	low
Z-Wave	30 m	100 kbps	900 MHz	Source-routed mesh network	Unique ID	End devices	GFSK	low
Insteon	50 m	38 kbps	900 MHz	Send and receive	Unique ID	End devices, backbone	BPSK	low
Bluetooth	100 m	24 Mbps	2.4 GHz	A master-slave structure	Encryption key	End devices, backbone	GFSK, DQPSK and 8DPSK	low

ZigBee is an emerging technology that has several advantages over other communication technologies. These include: low-cost device compared to others [71]; less complex to use [23], [72]; flexibility for expansion in future [4], [73]; multi-point interconnections [21], [22]; direct connection to any sensor, meter and actuator in the MG [24], [73]; encryption codes for enhancing system security [66]; possibility of developing codes to prevent interference from other wireless communication signals [74]; low consumption device [67], [71]; covers up to 300-1500m [75], further expandable by using repeaters.

ZigBee has been widely considered for data transmission in power systems. In [76], ZigBee is used for data monitoring of all subsystems of a DC MG system. It is also used for real-time measurement and data transfer in power system applications as proposed in [19], [20], which presents an algorithm for data compression. For these reasons, in this thesis, a ZigBee-based communication technology is proposed for data communication in the MG.

A further comparison between existing wireless communication technologies and the characteristics mentioned above is presented in Table 2.2. From this table, it can be seen that ZigBee is the most preferred technology for future MGs.

Table 2.2 Comparison of existing wireless communication technologies.

Specifications	ZigBee	Wi-Fi	WiMax	Bluetooth	Cellular
Low-cost device	✓			✓	
Less complexity	✓			✓	
Point-to-multi-point connections	✓	✓	✓		✓
Direct connection to sensor/meter	✓			✓	
Low consumption	✓			✓	
Flexible for expansion	✓	✓		✓	
Encryption code	✓	✓	✓		
Latency	✓		✓	✓	✓
Bandwidth	low	high	medium	medium	low

The reliability of ZigBee technology in power system applications is evaluated in [71], including the number of good and bad data packets transmitted under impulsive high power transients. In addition, an encryption code is developed for ZigBee in [66] to increase the security of the transmitted data. Since the data transfer rate for ZigBee is low, to reduce the need for high data transfer by such a device, a data traffic scheduling scheme is proposed in [77] where the data traffics are prioritised into three classifications, each with smaller packet sizes. The need for a high data bandwidth can be reduced by using a distributed algorithm in a ZigBee cluster-tree network [21], a multi-interface management framework [22], or by coordinating data traffic diffusion [23]. Implementation of ZigBee as a wireless sensor network is proposed in [73], in which a Wi-Fi-ZigBee message delivery scheme is developed to reduce the power consumption of the wireless devices. Also, an algorithm is developed in [74] to avoid interference between ZigBee and Wi-Fi signals when both are used in power system applications. In [24], a simple data code is presented for ZigBee, which consists of 1 byte of data format, 2 bytes of data length and variable bytes of the data itself. A limitation of this method is that it is suitable for transferring only one datum. ZigBee data payload coding has not been yet addressed for different MG data transfers.

In [72], the ZigBee processing time is calculated to be about 400-600μs for transmitting three different data; however, there is no statement of the utilised data coding format. In the MG applications, the delay of data transmission is crucial and must be kept within an acceptable limit [78]. This delay depends on the utilised data coding and the length of data code. Since longer data codes have longer transmission delays, defining a suitable and efficient data coding method, which represents all data transactions for MG operations, is crucial. Data transfer in ZigBee can be in the form of a binary code (with a lesser number of bits and hence less delay) or a text code (with more flexibility for future expansion) [52]. To avoid critical communication failure in an MG, various methods are proposed in [40], [41] that use distributed control. A distributed control scheme can be used to maintain the desired MG operation performance by limiting communication and exchange of information between a limited number of DGs [16], [17], [41].

2.2. Voltage Regulation and Power Sharing in the DC Microgrid

The aim of voltage regulation is to maintain the load voltage within pre-defined limits (e.g. ±5%) and following any dynamic changes to the load demand. The aim of load power/current sharing is to realize the desired proportion among the DG output powers/currents [36]–[39], [44], [45].

Droop control is the most popular technique aimed at realizing the desired power sharing among DGs by controlling their output voltages [46], [47]. No communication system is required to implement this technique. The existing conventional droop control algorithm does not consider the difference in line impedances between the DGs and loads, and hence the voltage drop across the lines is not taken into account. Thereby, there is no control over the voltage at the load buses, which is considered the main drawback of this technique [46], [48], [79], [80]. Improved droop control methods have been proposed in several literatures. To control the DG output voltage, many literatures propose virtual resistance of the feedback signal [46], [59], [81]–[85]. An adaptive droop control approach is proposed in [46], [49], [82], [86] to regulate the DG voltages in an MG. However, both of these proposed methods require all DGs to provide the same voltage level; hence proportional power sharing cannot be achieved, especially when the MG comprises of multiple loads and multiple configurations. As proposed in [33], [37], [38], [43], [87], the performance of droop control is enhanced by using load bus voltage as a feedback signal in the DG primary controller. Other studies have proposed the load current as a feedback signal for power-sharing control among DGs [56], [88], [89]. However, the coordination of multiple DGs within a DC MG is still a challenge [60].

A hierarchical control, which consists of two or three levels, is proposed to enhance the precision of desired power sharing between several DGs. Using this method, and as proposed in [25], [38], [42], [56], [90], [91], the reference designated voltage/current value of each DG output is dictated by the MG central controller through low-bandwidth communication. A master-slave control scheme is proposed in [92] for DC MGs, which considers the DGs' voltage controller as the master and their current controllers as the slave. This method requires a supercapacitor bank to be installed at the load, which makes it more suitable for the DC MGs within a small area. Another voltage regulation and power/current

sharing method, which is proposed in [17], [46], [93], [94], requires a very complex of mathematical calculations and costly control system for the fast and precise hardware. Because of the distance between the DGs, ESSs, EVs, and loads, the use of communication technology is unavoidable and also therefore, the introduction of a communication delay [78]. This communication delay is not considered in most of the papers published in the literature [7], [37], [53]; neither is its impact on the proposed MG voltage regulation and power-sharing techniques.

Many of the above-mentioned techniques focus on a DC MG with a single load only. However, their application in an MG with multiple loads, spread over various locations, has not yet been considered. When loads are distributed at various locations, the distribution line impedances are likely to be unequal. This can directly affect DG output currents and also MG power loss. Without a proper compensation method, power/current sharing among DGs cannot be realized precisely. Table 2.3 presents a comparison between existing voltage regulation and the power/current sharing methods from a variety of different perspectives including their precision, speed and scalability, the use of communication technologies, and any implementation difficulties. This thesis proposes a new technique, which has many advantages over existing techniques such as a faster response time and applicability to systems with multiple loads, sources, and configurations.

Table 2.3 Comparison of available voltage regulation and power/current sharing techniques in literature.

Method	Communication	Scalable	Simplicity	Precision	Fast response	Sharing Method
Ref [5]	✗	+	–	–	+	CS
Ref [16]	✓	++	–	+	–	CS
Ref [17]	✓	++	–	+	–	PS
Ref [25]	✗	–	+	–	+	CS
Ref [30]	✗	+	–	–	+	CS
Ref [37]	✓	+	–	+	–	PS
Ref [41]	✓	+	+	–	–	PS
Ref [43]	✓	+	–	–	+	CS
Ref [46]	✗	–	–	+	–	CS
Ref [95]	✗	–	+	–	+	CS
Proposed technique	✓	++	++	++	+	PS, CS

✓ = used, ✗ = not used, ++ = very good, + = good, – = less, PS=power sharing, CS=current sharing.

2.3. Various Circuit Configurations of the DC Microgrid

Renewable energy sources that constitute key assets in the DC MG are intermittent, and their energy output depends on environmental conditions. Thereby, renewable energy sources can act as a plug-and-play DG [50], [96] where they inject power to the MG after being plugged in and are unplugged when there is no energy production. ESSs and EVs can also have the same plug-and-play feature, as they can discharge and inject power to the MG (as a source) in addition to being charged from the MG (as a load) [45], [57], [81], [97]–[99]. Such characteristics will change the circuit configuration of the DC MG and have a significant influence on DC MG operations.

The most commonly used circuit is composed of two DGs and one load [30], [40], [43], [46]–[49]. A multiple load configuration is presented in [41], [83]; one load with parallel DGs is illustrated in [33]; and a system with a few

DGs, each with a local load, has been depicted in [36], [50], [82], [100], [101]. These references discuss their proposed methods on a specific MG configuration only. However, as stated above, various configurations can be considered for a DC MG, assuming that there are one or more DGs and one or more loads (distributed in one or more branches). According to Kirchhoff's Law, each circuit configuration has a unique characteristic, and while power/current sharing among sources can be implemented for several MG configurations, it cannot be applied to others.

The introduction of smart MG in the future will allow continuous changes based on dynamic requirements and the availability/mode of the renewable energy source. The proposed voltage regulation and power/current sharing technique is evaluated using extensive simulation analysis — using MATLAB/Simulink — on various circuit configurations of the DC MG.

2.4. Shortest Distance Algorithm for Microgrid Data Communication Infrastructure

The Dijkstra and Bellman-Ford Algorithms are two well-known conventional algorithms for defining the shortest distance [102], [103] for MG data communication infrastructure. These algorithms are usually used for finding the shortest route between two nodes in the directed and weighted graph for data routing [104]–[107]. All data routing that includes the Dijkstra and Bellman-Ford Algorithms finds the shortest route for transmitting data from the transmitter to the receiver. In addition, these algorithms can be applied while the graph has been weighted and routed.

Another short distance algorithm, which is popular and widely used, is the GPS-based map (e.g., Google Map®). As proposed in [108]–[111], the GPS-based map algorithm finds the shortest or fastest route to the destination address through established streets, choosing the minimum number of points or streets to be passed. It requires a predefined map (i.e., a weighted graph) and connects the streets, the source address, and the destination address. In the required MG communication infrastructure, however, there is no weighted, routed or predefined graph. Neither must all points be connected. Table 2.4 shows the differences

between data routing, GPS-based map algorithms, and the requirements in the MG applications.

Table 2.4 Differences between data routing, GPS-based map algorithm with the requirements in the MG.

	Data-routing	GPS-based map	Microgrid
Graph	Weighted	Weighted	Not yet established
Unit	Distance, cost, time	Distance, time	Distance
Value	Positive and negative	Positive	Positive
Passed Point	Selected points	Selected points	All points
Direction	Directed	Directed	Undirected
Source point	Starting and destination	Starting and destination	No source or destination points

The comparison results between the required MG short distance algorithm, the data routing, and the GPS-based map algorithms are illustrated in Figure 2.1. Let us consider an MG with i=8 points spread over the location and connected to a communication network in which i represents either DGs, ESSs or loads and named P1, P2, to P8. As illustrated in Figure 2.1(a), each point has a connection with another point, in a certain direction and with a certain path value. The shortest distance communication network, defined by the data routing and GPS-based map algorithm, is presented in Figure 2.1(b), and the required MG communication network is illustrated in Figure 2.1(c). Figure 2.1(b) shows that the data routing and GPS-based map algorithm connects 5 points instead of 8 points in total, leaving 3 points unconnected. As shown in Figure 2.1(c), for the required communication infrastructure in the MG, all of the DGs must be connected to the single network without leaving any single unit point. In this case, the shortest route in the MG is defined by the smallest total distance connection of all points. In the MG application, the shorter distance of communication infrastructure is preferred because of lower installation costs.

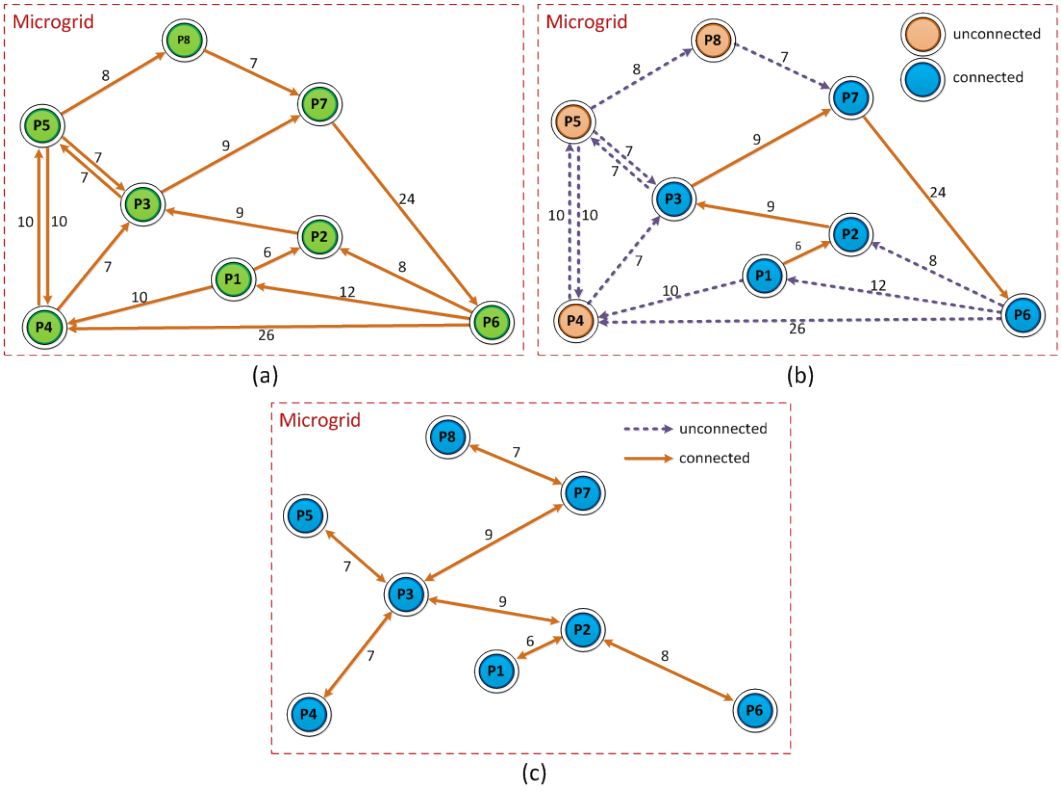

Figure 2.1 Shortest distance for communication infrastructure in the MG: (a) weighted and directed graph, (b) data routing and GPS-based map, and (c) MG required algorithm.

2.5. Centralised and Distributed Data Communication Schemes for Microgrids

In a centralised data communication scheme (which many literatures propose as a hierarchical scheme), all data from DGs, ESSs, and loads are transmitted to the MG central controller. The data are processed by the MG central controller and transmitted back to DGs and ESSs to be executed. Contrary to the centralised scheme, in a distributed data communication scheme, data in the DGs, ESSs, and loads are transmitted to other DGs and ESSs. The data is received, transmitted, and processed among the DGs or ESSs themselves [16], [17]. The centralised scheme is easy to implement and maintain [53], [56]. However, it has a limitation in scalability, requires complex communication networks, and is more prone to communication failure [17]. The distributed scheme offers more flexibility and is more robust to communication failure.

However, it requires a longer processing time, and there is less precision, a higher possibility of data collision, and a complex algorithm [7], [37], [53], [90].

Both wireless and wired communication technology can be employed for centralised and distributed data communication schemes. [30], [112]. Figure 2.2 shows a simplified illustration for centralised and distributed data communication schemes in the MG.

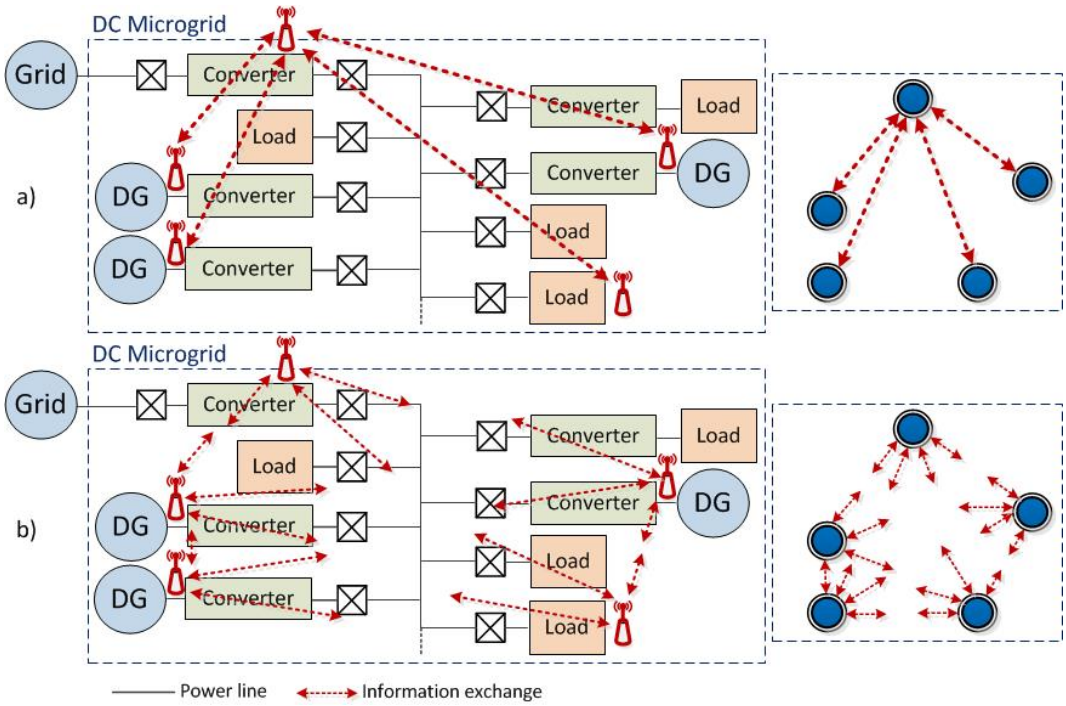

Figure 2.2 Data communication schemes in the MG (a) centralised (b) distributed.

A hierarchical control, which involves three levels of controller (primary, secondary, and tertiary), is discussed in [25], [38], [40]–[43], [56], [90], [113]. In these papers, the reference setpoint is calculated by the MG central controller sends signals to the controller of each DG for updating their outputs. Another centralised scheme is proposed in [40], [41]. A distributed data communication scheme is proposed in [16], [17], [40], in which each DG sends data to all other DGs (within the same DC MG), and also from one DC MG to another. However, the effects of the data communication scheme on the performance of both the proposed voltage regulation and the power-sharing technique have not yet been discussed or evaluated in detail.

The most suitable data communication scheme is determined by the established communication infrastructure, therefore affecting the communication

delay and influencing the power flow among the DGs and interconnected lines [37], [53]. Although a certain type of communication infrastructure might be suitable for one type of data communication scheme (and have a smaller communication delay), it might not be suitable for any other.

The type of communication technology employed for transmitting and exchanging data in the MG also determines which data communication scheme can be used.

Power Line Communication (PLC) technology does not require a new connection line between all DGs, ESSs, and loads, and the MG central controller. Instead, this technology uses power lines for data communication, which reduces the cost considerably. PLC technology, however, does have several challenges when applied to the MG, including a problem with disconnection or distortion in the switch breaker, the step-up/down, or the converter [63], [114], [115]. Transmission data in PLC technology can be established from one controller and communicated to all others; therefore, it is applicable to both centralised and distributed data communication schemes.

For both wired and wireless Ethernet/IoT, a new connection must be established, which can be costly. Ethernet/IoT technology, however, offers a mature, faster and more reliable data communication [54]. Mostly this technology is applied to a centralised data scheme, because a distributed scheme requires additional communication devices for each communication point, such as a router and controller, and this leads to further costs [116].

Global System for Mobile (GSM) Communication and Wi-Max have similar characteristics to a centralised scheme. Here, the data from local DGs, ESSs, and loads are transmitted to central devices before being transmitted back again. This technique offers more flexibility for expansion, easy installation, and reliable communication. On the other hand, it requires more bandwidth, is less robust in communication failure, and impractical for implementation in rural areas [64], [117].

ZigBee and Bluetooth are low power devices, both powered by a smaller battery, and hence suitable for rural areas. However, Bluetooth communication is limited; it can only be established between two active Bluetooth devices and

hence applied to a distributed scheme only [118]. ZigBee has the ability to transmit and receive data among many other ZigBee-based communication devices; therefore, it can be used for both centralised and distributed data communication schemes [52]. However, ZigBee has low bandwidth and is not suitable for a huge number of data to be transmitted.

Radio Frequency (RF) based communication can be used for point-to-point communication and can also reach long distance; it is therefore suitable for a centralised data communication scheme [70]. However, it too has a lower bandwidth, and it is also less precise in data communication [119].

The comparison between various data communication technologies, and their potential applicability in a centralised or distributed data communication scheme, is presented in Table 2.5.

Table 2.5 The potential of data communication technologies in various data communication schemes

Technology	New Infrastructure	Type	Scheme	
			Centralised	Distributed
PLC	×	Point-to-multi-points	✓	✓
Ethernet/IoT	✓	Point-to-point	✓	×
GSM-based	✓	Point-to-point	✓	×
Wi-Max	✓	Point-to-point	✓	×
ZigBee	✓	Point-to-multi-points	✓	✓
Bluetooth	✓	Point-to-point	×	✓
Radio frequency	✓	Point-to-point	✓	×

✓ = possible, × = not-available.

2.6. Summary

In future smart MGs, the data communication is essential. Both wired and wireless communication technology can be used in MGs applications. Due to lower installation costs, more suitable for the rural area and more flexible for expansion, the wireless communication technology is a better candidate for MGs applications. There are many types of wireless communication technologies can be employed for data communication in MGs. Each wireless communication technology has different coverage range, data rate, frequency, data routing and security, modulation and installation costs. ZigBee is an emerging wireless communication technology which has low-cost, less complexity, multi-point interconnection, direct connection to sensors/meters, and low-consumption device. However, this technology has mainly disadvantages such low-bandwidth; and thus not suitable for fast data communication. To employ this low-cost communication device in power applications, several methods are proposed in literature including data traffic scheduling, cluster-tree network, multi-interface framework, data traffic diffusion and data packet compression. The data communication implementation for small and rural MG which requires low-cost, low-consumption, direct connection to sensors/meters, and also as controller device; is still required to be further designed, developed and evaluated.

By increasing the number of sources in the network caused by employing renewable energy sources; voltage regulation and power sharing among sources are considered as the main dynamic control issue of MGs. A droop control is the most popular technique aimed at realizing the desired voltage loads. However, this technique still has several issues to be solved for the real implementation; such unprecise power-sharing and voltage in several points of load. Many developments of this technique have been conducted including virtual resistance, adaptive method, feedbacks voltage and current signals, and also hierarchical control. On the other hand, the renewable energy sources are intermittent source, and an electric vehicle can act as loads or sources; thereby the suitable voltage regulation and power-sharing technique for the future smart MGs is the technique which has faster response, easily coordination among sources, less mathematical calculation, and easily modification for multiple loads and sources configurations. These requirements are still a challenge.

Establishing the communication infrastructure in the MG leads to significant installation costs. To reduce the required installation costs, defining a shorter communication infrastructure distance among communication devices in MG is required to be developed. The required communication infrastructure in the MG has specific requirement and differences with the popular shortest distance methods such there is no source and destination points, units are in the distance (meter), and no weighted graph. Thereby, a new algorithm for determining shorter total communication infrastructure distance in MG will have a big impact on MG implementation in the future. The established communication infrastructure will influence the data routing in the MG. Several types of communication technologies can be applied in specific communication infrastructure only. A data routing (data communication scheme) will influence a communication delay, and thus the MG operational performance. The centralised and distributed data communication schemes according to various communication infrastructures and their effects on the MG operational performance are required to be designed and evaluated.

Chapter 3: ZigBee-Based Communication System for Data Transfer within Future Microgrids

In this Chapter, the ZigBee based communication technology for data communication in the MG is proposed, developed and discussed. Since the ZigBee based communication technology is low-bandwidth, the communication data in the MG requires furthermore development to prevent the negative effects on the system, which is discussed below:

3.1. Communication Layers in Microgrids

A hierarchical control system is required for proper MG operation and control [113], [120], [121], as discussed below:

a) The Local (Primary) Controller:

   This controller is the lowest control block within the hierarchical control system and is located within every DG. This controller mainly controls the operation of a DG, based on its local measurements. It fetches data from the local sensors/meters using small sampling time steps and produces the required outputs for the DGs. During a grid-connected mode of MG operation, the DGs operate in constant PQ mode and generate their rated power. In autonomous mode, the DGs need to operate in droop control or use other techniques.

b) The MG Central Controller:

   This is the main controller for the MG and is responsible for controlling both its voltage magnitude and voltage frequency. It receives the voltage magnitude, angle and frequency data from the voltage sensor installed at the MG feeder and sends back the proper references of the voltage magnitude, angled to each DG. This controller has a larger time step, compared to the local controllers, and operates discontinuously (in steps of a few minutes). The transfer of the MG main CB status to the MG central controller also falls within this control level.

c) The Tertiary Controller:

This controller is the highest control level in the hierarchical control system and is responsible for general control of the power network. This controller may have several modules, such as load/weather forecast, electricity market, self-healing, unit commitment, economic dispatch, etc. This controller also defines how MG should be operating in grid-connected or autonomous mode, the output power of each DG, and the interconnection/isolation of two neighbouring MGs, etc.

To provide a proper data transmission among the above-mentioned three controllers, a communication network and infrastructure is required [115]. The main data to be transferred from the local controllers of each DG to the MG central controller are the voltage magnitude/angle, the output active/reactive power, and the DG CB status. The MG main CB status, the voltage magnitude, and frequency within the MG (measured at one or more locations), need to be transferred to the MG central controller. To transfer these data to the MG Central Controller, several parameters should be considered when selecting and designing the communication technology. These are:

- the size of the area in which the MG is distributed,
- the installation, operational and maintenance costs,
- the number of sensors, actuators, meters or devices,
- the minimum data transmission rate requirement,
- the data precision requirement,
- the maximum data packet error requirement,
- the flexibility for future expansion, and
- the availability of different techniques to access data.

Based on the location of the communication devices, as well as the characteristics of the data to be transferred, the communication technologies in the MG are classified in three layers, as shown schematically in Figure 3.1. The first communication layer provides data transfer capability from the local controller of each DG to the DG sensors, meters and actuators. Also falling within this layer is the transfer of data to the local controllers from any meters/sensors installed along the power distribution lines or CBs. The second communication layer provides data transfer capability between the local DG controllers and the MG central

controller. This layer is the main communication layer of the MG. The third communication layer is used to provide data transfer within a group of neighbouring MGs [4], [40], [113]. This layer transfers data between the MG central controller and the electrical network tertiary controller. This thesis focuses on the MG second communication layer only.

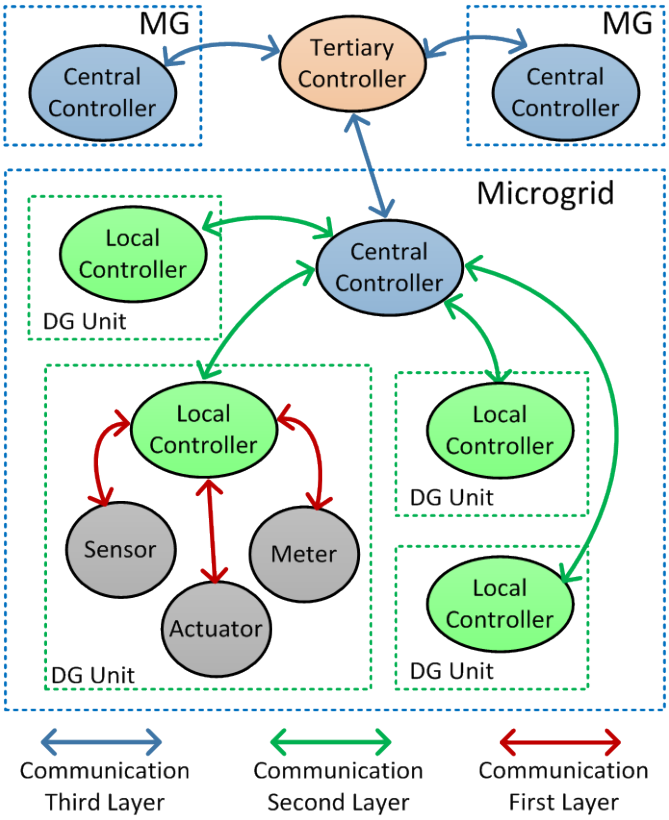

Figure 3.1 Proposed MG hierarchical communication layer.

It is to be noted that distributed control of an MG is also possible. However, the hierarchical control system discussed in this thesis broadens the network operating capabilities.

On the other hand, implementation of this hierarchical control system and the required communication infrastructure increases the complexity of the system control and also the investment costs. A techno-economic analysis can be carried out to define the balance between the imposed costs and complexity and the gained benefits. This is beyond the scope of this research and is not considered in this thesis.

3.2. ZigBee Communication in Microgrids

In terms of communication capabilities, there are two types of ZigBee device: a Full Function Device (FFD) and a Reduced Function Device (RFD) [122]. An RFD has the capability to connect to sensors, actuators and meters; however, it does not have the capability to communicate with other RFDs. An FFD can communicate with all other FFDs as well as the sensors, actuators and meters [122]. The RFD acts as a ZigBee end-device, while the FFD acts as a router or coordinator. The router is used for data routing, or communication with other routers or coordinators, and extending covers the required area as well as strengthening the transmitted signals [67]. The coordinator is used to establish and manage the network.

The sensors/meters/actuators in one DG can be connected directly to the local controller through either Analog-to-Digital Converters (ADC), General Purpose Input-Output (GPIO), or serial communication [24]. The received data and any processed outputs can then be transmitted by the RFD, which is connected to the local controller. The transmitted data by the local controller of the DG will be received by the MG central controller through the FFD. This is shown in Figure 3.2(a). Alternatively, the sensors/meters/actuators can be connected directly to an RFD, which transmits the data to the MG central controller. This is applicable for measurements from the CB and power distribution feeders where no significant computation and control process is required. This is shown in Figure 3.2(b).

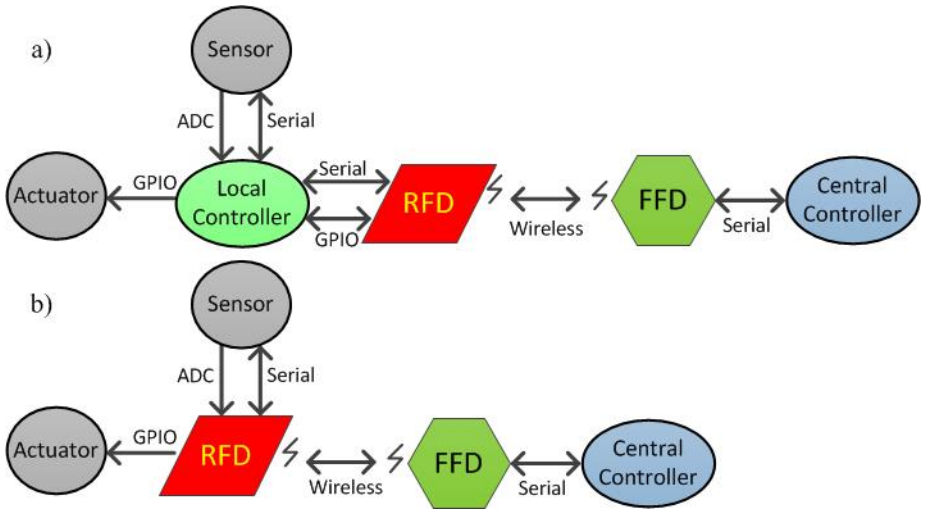

Figure 3.2 FFD and RFD utilisation in the MG: a) DG local controller connection to the MG central controller, b) CB status and voltage/frequency data transfer to MG central controller.

The number of sensors, actuators and meters in the MG can be massive and scattered. A network topology is required to handle communication within a large area and where there are numerous end user devices. ZigBee can operate in star, tree, and mesh network topologies as well as any combination of them [122]. In this thesis, a star topology is considered for the network.

Every ZigBee network is characterised by a 64-bit unique address, referred to as a Personal Area Network (PAN) and managed by the coordinator [122]. In ZigBee technology, communication network clusters are permitted in the same PAN network, and this is a potential solution for when one DG is composed of numerous smaller DGs, distributed over a vast area. An example of this is when wind turbines are distributed within a wind farm, or numerous photovoltaic cells are distributed over a photovoltaic farm. The main advantage of a multi-cluster topology is the expansion of the coverage area, while its main disadvantage is the increase of data latency [69]. Figure 3.3 schematically shows an example of a ZigBee-based multi-cluster communication network for the MG.

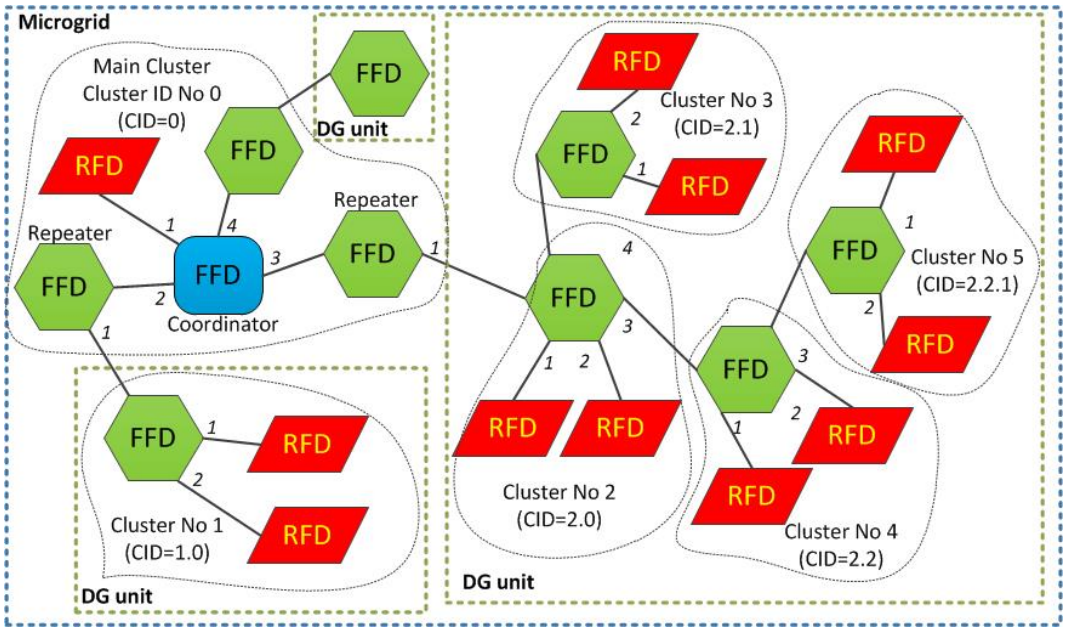

Figure 3.3 ZigBee-based multi-cluster communication network for the MG.

An important parameter to be considered in multi-cluster communication networks is the time occupation duty ratio (TODR); that is the amount of time each ZigBee device can take to transmit data to the coordinator. The TODR depends on the number of ZigBee-based clusters within the MG. Since the time allocated for each ZigBee device within the MG is equal, for the network in Figure 3.3, TODR is calculated from:

$$\mathrm{TODR}(\%) = \frac{100}{n_{dev}^{CID} \times n_{dev}^{CID-1} \times n_{dev}^{CID-2} \times \cdots \times n_{dev}^{0}} \tag{3.1}$$

where n_{dev}^{CID} is the number of ZigBee devices in the same cluster, while the n_{dev}^{CID-1} represents the number of ZigBee devices in its upper cluster, and n_{dev}^{0} is the number of ZigBee devices in the coordinator's cluster (main cluster).

As an example, based on (3.1), for each device in the main cluster (*CID*=0) of Figure 3.3, the TODR for transferring data is:

$$\mathrm{TODR}(\%) = \frac{100}{n_{dev}^{0}} = \frac{100}{4} = 25\%$$

while the TODR for each device in the cluster with *CID*=1.0 and *CID*=2.2.1 is respectively:

$$\mathrm{TODR}(\%) = \frac{100}{n_{dev}^{CID=1.0} \times n_{dev}^{0}} = 12.5\%$$

$$\mathrm{TODR}(\%) = \frac{100}{n_{dev}^{CID=2.2.1} \times n_{dev}^{CID=2.2} \times n_{dev}^{CID=2.0} \times n_{dev}^{0}} = 1.04\%$$

From this example, it can be seen that the TODR (for transferring data to the coordinator) for an RFD in the cluster with *CID*=1.0 is 12 times higher than for an RFD in the cluster with *CID*=2.2.1. Therefore, the RFDs should be placed in different clusters, based on the importance and frequency of data transmission to the coordinator. Based on this concept, the RFDs that transfer data with the following characteristics should be placed in the 1st/2nd cluster:

- Data transmitted frequently,
- Data transmitted to the coordinator immediately,
- Data affecting the whole control system of the MG,
- Data utilised for emergency purposes.

Hence, the voltage magnitude, angle and frequency, active/reactive power, and the states of the CBs should be within the 1st/2nd cluster. This thesis focuses only on the data management scheme of these sets of data. However, the data from the RFDs with the following characteristics can be placed in the farther clusters:

- Data sent for monitoring purpose only,
- Data with wide tolerance of data packet error,
- Data with low precision, and
- Data affecting the local controllers only.

If the data, such as weather forecasting information (e.g. the sun's radiation, the ambient temperature, wind speed, etc.), or the SoC of the batteries need to be transferred to the MG central controller, the relevant RFDs can be located in farther clusters.

3.3. Data Management in Microgrids

The number of data to be monitored and transferred in an MG depends on the number of the DGs within the MG. Some DGs might also have a particular set

of data to be monitored and transmitted, such as weather data. Consequently, the number of data to be transferred within the MG can be large. Since the data transfer rate of the ZigBee is only up to 250 kbps, the data transmission in the MG should be carefully managed so that the network bandwidth can handle the data transactions.

The data management scheme proposed in this thesis defines a suitable time interval for transmitting the data and also the proper number of bits for data representation. Some data needs to be transmitted immediately, such as the CB status; however other data — such as the voltage magnitude, angle and frequency, and the active/reactive power — can be transferred in short intervals of ΔT. This interval needs to be defined based on the effect of the data on MG performance and can be within a range of a few minutes.

To further reduce the number of data transmissions, acceptable limits for data variation can be defined such that the data are transmitted instantly, but only if the data exceed the defined limits of ΔL. Usually, the acceptable limits are defined for the MG frequency (e.g. 49.5-50.5 Hz) and the voltage magnitude (e.g. 90-110% of the nominal voltage) only. Based on ΔT and ΔL, the data management flowchart for each FFD is as shown in Figure 3.4.

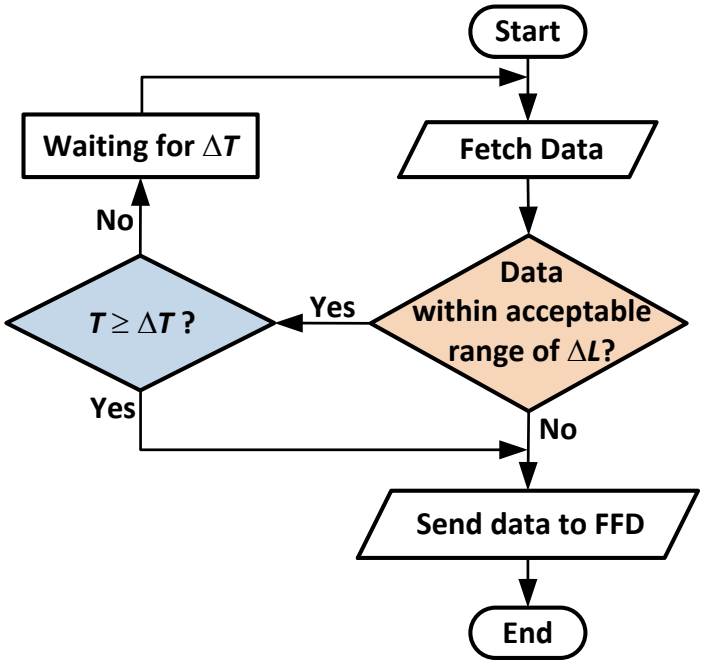

Figure 3.4 Data management flowchart for RFDs.

Based on IEEE Std. 802.15.4, data communication in the ZigBee is formulated in the following four frames [122]:

1. A Beacon Frame is used by a coordinator to transmit beacons. This frame consists of 104+(32 or 80)+k+m+n bits where n is the number of beacon payload bits, m is the pending address field bits, and k is Guarantee Time Slot (GTS) field bits. Note that the (32-80) bits represent the address field.
2. A Data Frame is used for transferring all the data. This frame consists of 88+(32-160)+N bits. The (32-160) bits represent addressing field bits, and N is the number of data payload bits where the maximum data payload is 888 bits.
3. An Acknowledgment Frame (ACK) is used for confirming successful frame reception. This frame consists of 88 bits.
4. The Medium Access Control (MAC) Command Frame is used for handling all MAC peer entity control transfers. This frame consists of 96+(32-160)+u bits where u is the command payload bit.

The communication between the FFD/RFDs and the coordinator (in the non-beacon network) is initiated by the coordinator requesting data from the FFD/RFDs. The RFD/FFDs confirm the request by transmitting an ACK and the requested data. After receiving the data, the coordinator transmits the Acknowledge Frame to the FFD/RFDs. The schematic of this communication sequence is illustrated in Figure 3.5.

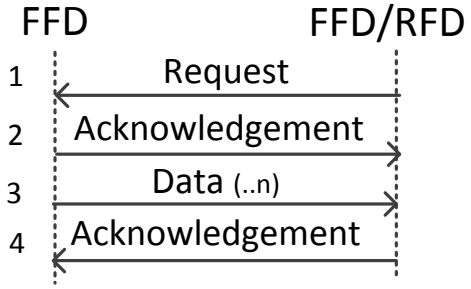

Figure 3.5 Schematic of data request, transfer, and acknowledgment between the FFD/RFD and the coordinator.

Based on IEEE Std. 802.15.4, ZigBee devices are available with 868 MHz, 915 MHz, and 2.45 GHz carrier frequencies. The lower carrier frequency usually has a longer area of coverage, e.g. the 2.45 GHz ZigBee from the XBee-Pro from Digi International Inc. can cover an area up to 1.5 km, while the 868 MHz and 915 MHz ZigBees from the same manufacturer can cover an area of up to 40 km and 14.5 km, respectively [75]. The data modulation technique for both the 868 MHz and 915 MHz ZigBees is Binary Phase-Shift Keying (BPSK), while for the 2.45 GHz ZigBees, it is offset Quadrature Phase-Shift Keying (OQPSK). The data transfer rate for the 868 MHz, 915 MHz and 2.45 GHz ZigBees is 20 Kbps, 40 Kbps and 250 Kbps, respectively [122].

In the 2.45 GHz ZigBee, every 4 data bits need to be mapped into one symbol, and each symbol is then mapped into a 32-bit-chip-PN sequence. In the 868 MHz and 915 MHz ZigBees, each data bit needs to be mapped into a symbol, and each symbol is then mapped into a 15-bit-chip-PN-sequence [122]. As an example, to transmit the voltage magnitude of 220 V — measured in the MG from RFD to FFD using a 2.45 GHz ZigBee — first, the 220 decimal digits need to be coded into a binary digit (i.e. 1101 1100). Next, the binary digit should be mapped into a symbol, and then each symbol is mapped into the chip-PN sequence. Figure 3.6 shows the schematic data modulation process from binary digit to symbol, from symbol to chip-PN sequence, and then finally the spreading into the form of a modulated signal.

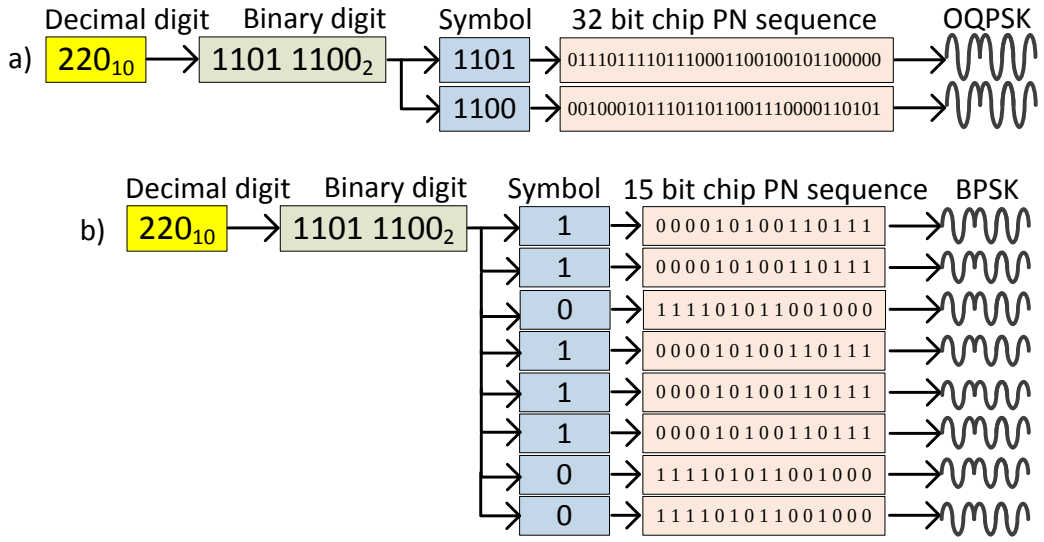

Figure 3.6 An example illustrating the steps of modulating “220 V” in ZigBee with a carrier frequency of (a) 2.45 GHz, (b) 868 MHz or 915 MHz.

The data to be transferred should be coded so that it represents the MG’s data type (i.e. voltage magnitude, voltage angle, active power, reactive power, frequency, and CB status); data dimension (e.g. kilo, mega); data value (e.g. 220); RFD or FFD number; channel number (if there is more than one sensor/actuator/meter connected to a single RFD), and DG number. All these data need to be mapped into a data payload section, which has a maximum 888 bits [122].

The data payload code can be represented in a binary or text format [123]. As an example, the voltage magnitude of 220 V in decimal digits can either be represented by a binary code of 1101 1100, or as text characters of 220. The binary format can be processed faster by digital devices (such as a microcontroller) and has a lesser number of bit representations. However, the text format has more flexibility for expanding the network devices and data transactions in the MG. Also important to note, the binary format can be directly converted into a symbol (and then into the OQPSK or BPSK modulator), while the text format must first be converted into a binary code (using the well-known ASCII code).

Data transactions required in the MG can be classified as:

- Data transfer where RFD sends data to FFD/coordinator,
- A data request transaction, where the coordinator requests a data value or status from the RFD (e.g. the coordinator needs the DG's generated active power data), or
- A command transaction, where the coordinator sends a command to the RFD (e.g. the coordinator requests the RFD to open/close a CB).

To define the transaction type as one of the above three options, a special code must be developed in binary or text format. As an example, the developed code can represent a data value, data request, and command transaction, respectively, by 01, 10 and 11 in binary format, or by "VL", "RQ" and "CM" in text format. Each data type can be defined in binary or text format as shown in Table 3.1. The commonly used dimensions of 10^0, 10^1, 10^2, 10^3, 10^4, 10^5 and 10^6 can be represented as 000, 001, 010, 011, 100, 101 and 110 in binary format or "E", "1", "2", "K", "4", "5" and "M" in text format, respectively.

To measure the 6 required data from each MG (i.e. voltage magnitude, angle and frequency, active/reactive power, and CB status), a maximum of 6 RFDs are required. It is also expected that no more than four sensors/meters/actuators are connected to the same RFD. A maximum of 3 bits are therefore required for the RFD number and 2 bits for the channel number. The number of DGs within an MG establishes the number of bits required to define it. As an example, assuming the number of DGs is less than 15; 4 bits are required to define the number of DGs in the MG. This data payload coding — in binary and text format — is given in Table 3.1, and is then utilised within the data payload section of the standard ZigBee Data Frame.

Table 3.1 Data to be transferred in the MG, the number of bits, and the binary/text format for each data.

Data	Data Value					Data Type	
	Range	Data steps	Step No	Bit No	Text digit	Binary	Text
Voltage Magnitude	0 - 500 V 0.00-20.00 kV	1 0.04	500 500	9 9	3 5	001	“VM”
Voltage Angle (°)	0.0 - 360.0	0.1	3600	12	5	010	“VA”
Frequency (Hz)	0.0 - 60.0	0.1	600	10	4	011	“FR”
CBs	on, off	–	2	1	1	100	“CB”
Active Power	0 - 999 W 0 - 99 kW/MW	1 0.1	999 1000	10 10	3 4	101	“AP”
Reactive Power	0 - 999 W 0.0 - 99.0 kW/MW	1 0.1	999 1000	10 10	3 4	110	“RP”

There are two ways to transmit the data. The first method is based on a fixed number of bits, or characters, for each parameter. This method is more easily recognised by both the system and RFD/FFDs; however, it results in longer data bit lengths. In the second method, as introduced in Table 3.1 and Table 3.2, the number of bits used for each parameter depends on the number of bits or characters defined for each parameter. The main advantage of the second method is that it uses a lesser number of bits, and hence it has a shorter processing delay. Figure 3.7(a) shows the standard Data Frame for the ZigBee, and the two methods are shown schematically in Figure 3.7(b) and Figure 3.7(c). In this research, both of these methods are utilised and their processing delay times compared. As shown in Figure 3.7(a), the period of the Data Frame in the ZigBee is the sum of the period of data payload, and the period of other transmitted parameters such as the preamble sequence, the start of frame delimiter, etc.

Table 3.2 Binary and text format coding, used for defining the number of data for the grid/DGs, and for each RFD/FFD and their channels.

Data	Data Code		Device	Data Code		Channel	Data Code	
	Binary	Text		Binary	Text		Binary	Text
Grid	0000	“Grid”	RFD/ FFD-1	001	“Dev1”	Ch-1	01	“Ch1”
DG-1	0001	“DG01”	RFD/ FFD-2	010	“Dev2”	Ch-2	10	“Ch2”
DG-2	0010	“DG02”	RFD/ FFD-3	011	“Dev3”	Ch-3	11	“Ch3”
DG-3	0011	“DG03”	RFD/ FFD-4	100	“Dev4”	Ch-4	00	“Ch4”
DG-15	1111	“DG15”	RFD/ FFD-8	000	“Dev8”			

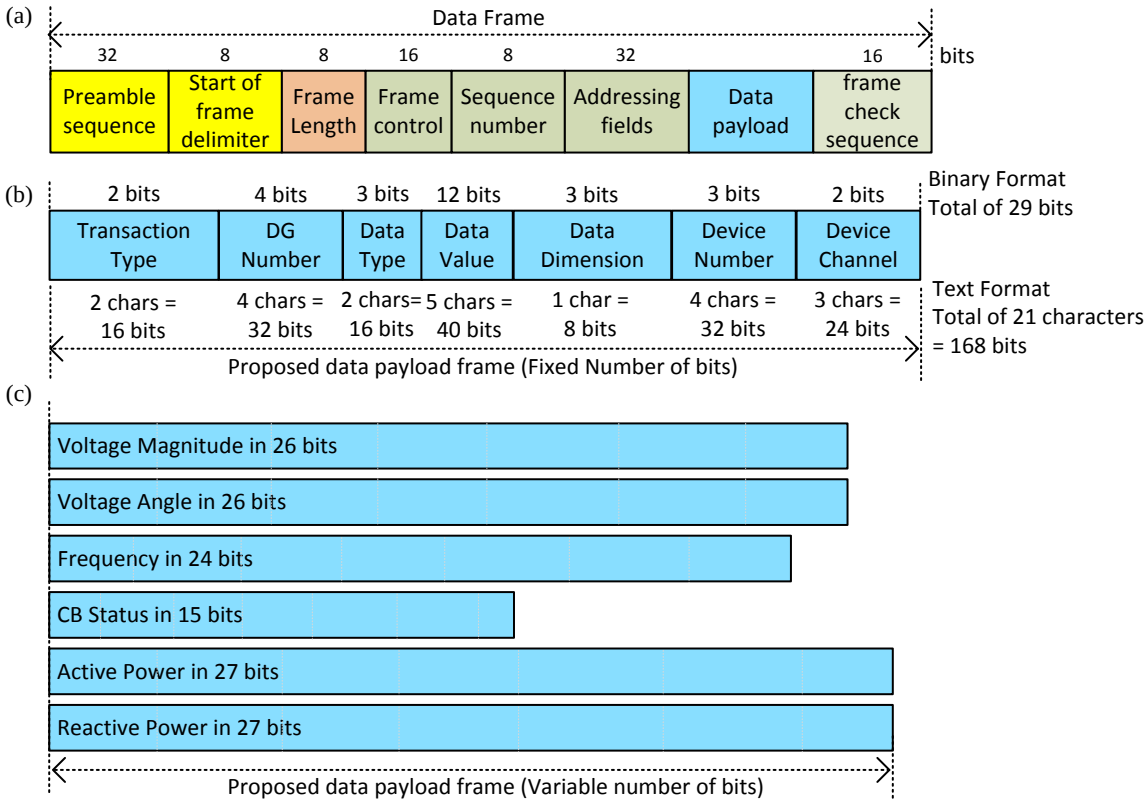

Figure 3.7 (a) Standard Data Frame for the ZigBee, (b) proposed data payload structure, using fixed number of bits for each parameter, (c) proposed data payload structure, using variable number of bits for each parameter.

As an example, let us assume a voltage sensor that is connected to Channel-2 of the RFD-5 in the DG-4 measures a voltage magnitude of 220 V. Figure 3.8 shows how the data to be transmitted is coded, and also how the 220 V measurements can be transmitted by either 26 bits in binary format or by 152 bits in text format.

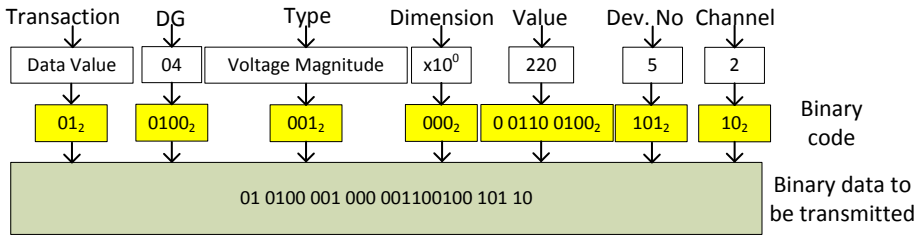

(a)

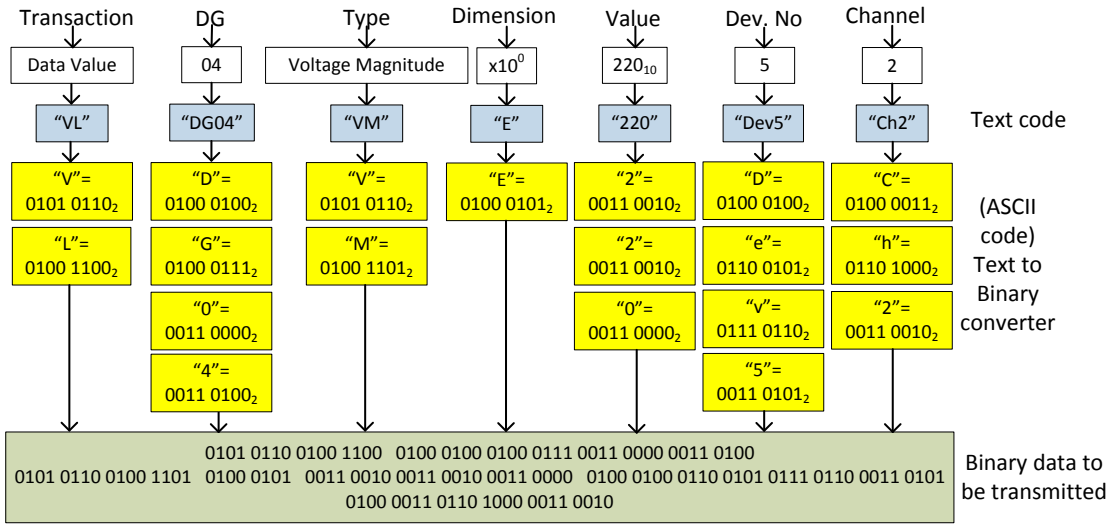

(b)

Figure 3.8 An example illustrating how the output of a voltage sensor is coded within the data payload section of the ZigBee Data Frame, based on (a) the proposed binary format, and (b) the proposed text format.

3.4. Data Transmission Delay

The time taken to transfer each bit from the ZigBee device depends on the data transfer rate. This time can be calculated as $T_{\text{Bit}} = 1/\text{data rate}$. T_{Bit} is equal to 4 μs, 25 μs, and 50 μs for the 2.45 GHz, 915 MHz and 868 MHz ZigBee devices, respectively.

The required time to transfer a symbol (T_{Symbol}) can be calculated as $T_{\text{Symbol}} = T_{\text{Bit}}$ (i.e. number of bits in each symbol). The T_{Symbol} of a 2.45 GHz ZigBee is T_{Bit} = 16 μs; however, the T_{Symbol} when using 915 MHz and 868 MHz ZigBees is T_{Bit} = 25 μs and T_{Bit} = 50 μs, respectively.

The total processing time for the data payload ($T_{\text{DataPayload}}$) is calculated as:

$$T_{\text{DataPayload}} = T_{\text{Symbol}} \times \text{ceiling}\left(\frac{\text{number of binary digits}}{\text{number of bits in each symbol}}\right) \quad (3.2)$$

where the T_{Bit} in the 2.45 GHz ZigBee is 4 bits, and 1 bit in the 868 MHz and 915 MHz ZigBees.

As an example, the processing time for transmitting the data payload of 220V (shown in Figure 3.8) from ZigBee with different carrier frequencies and different formats are listed in Table 3.3.

Table 3.3 Numerical comparison of the data processing time when using ZigBees with different carrier frequencies and different formats.

$T_{\text{DataPayload}}$	Binary Format [ms]	Text Format [ms]
2.45 GHz	16 μs × ceiling (26/4) = 0.112	16 μs × ceiling (152/4) = 0.608
915 MHz	25 μs × 26 bits = 0.65	25 μs × 152 bits = 3.8
868 MHz	50 μs × 26 bits = 1.3	50 μs × 152 bits = 7.6

Assuming the minimum number of bits is used for the address fields (i.e. 32 bits based on [122]), the total processing time for transferring the Data Frame ($T_{\text{DataFrame}}$) is calculated as:

$$T_{\text{DataFrame}} = T_{\text{DataPayload}} + T_{\text{DF}} \quad (3.3)$$

where T_{DF} is the processing time for the other sections of the Data Frame (i.e. preamble sequence, start of frame delimiter, frame length, frame control, sequence number, addressing field, and frame check sequence sections). T_{DF} is 480 μs, 3000 μs, and 6000 μs, respectively, for 2.45 GHz, 915 and 868 MHz ZigBee.

After a successful data transaction, the receiving FFD sends an Acknowledgement Frame. The processing time of an ACK is 352 μs, 2200 μs,

and 4400 µs, respectively, for 2.45 GHz, 915 and 868 MHz ZigBee. The data transmission process in the ZigBee commences with a transmittal of the Data Frame by the transmitter, and is completed with receipt of an Acknowledgement Frame from the receiver. The receiver sends back the Acknowledgement Frame after a period of $12T_{\text{Symbol}}$. The waiting time between when the data is fully transmitted until the receipt of the Acknowledgement Frame is a maximum of $54T_{\text{Symbol}}$ [122]. A successful ZigBee data transfer is illustrated in Figure 3.9(a).

If the transmitter does not receive an Acknowledgement Frame within this period, it resends the Data Frame to the receiver. The transmitter will retry to transmit this data a maximum of three times [122]. If the transmitter still does not receive an Acknowledgement Frame, it generates an MLME-COMM-STATUS indication with a status of NO_ACK [122]. An unsuccessful ZigBee data transmission is illustrated in Figure 3.9(b).

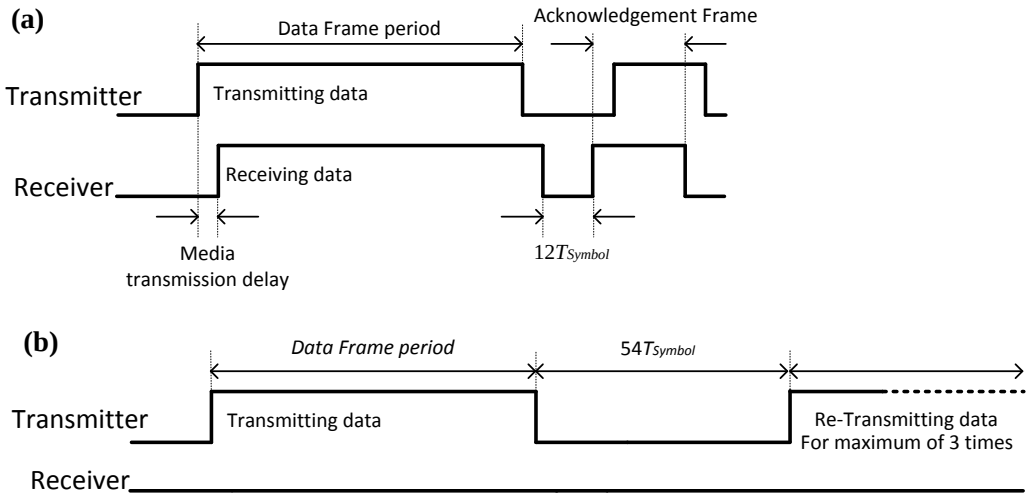

Figure 3.9 Schematic representation of data transmission in the ZigBee: (a) successful data transaction, (b). unsuccessful data transaction.

3.5. Numerical Analysis Results

The time delay for transmitting the numerical values of the measurements from sensors to the MG central controller or the data commands from the central controller to the local controllers of each DG, is of high importance [78]. In this section, the time delay is calculated and presented as the processing time required

for transferring a Data Frame ($T_{\text{DataFrame}}$). The example below presents a numerical analysis of the communication delay. It also shows the number of transmitted symbols (as a function of the number of DGs in an MG), the ZigBee carrier frequencies, and the different proposed formats of the data payload.

Let us consider the MG structure of Figure 3.10 , which includes N converter-interfaced DGs and a few distributed loads. The DGs are connected through Voltage Source Converters (VSCs) and their associated filters. A detailed discussion on the DG type — and the VSCs, their associated filter structure and control system — is presented in [113] and not repeated here. The local controller for each DG transmits the average active and reactive output power of the DG to the MG central controller. The local controller of each DG also receives the voltage and angle set-points from the MG central controller. The MG central controller receives the status of the MG main CB from the CB, and also the voltage magnitude, angle, and frequency from a voltage sensor installed at the MG feeder.

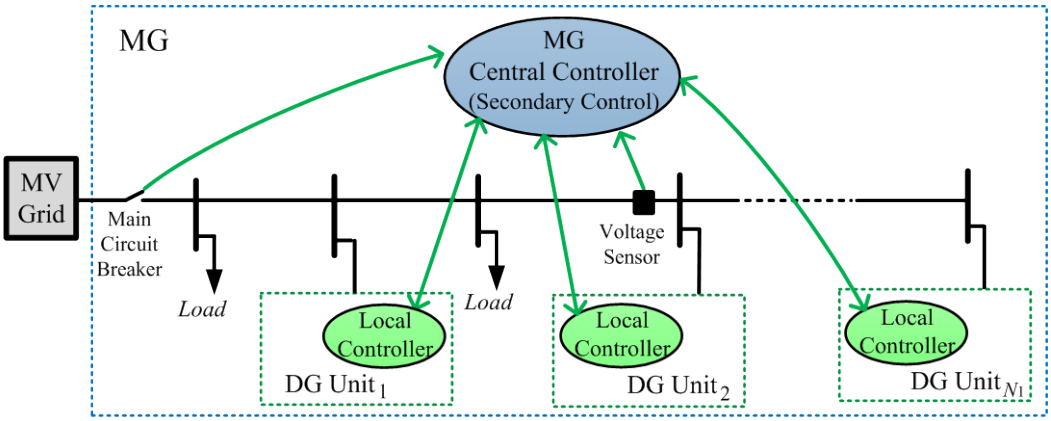

Figure 3.10 Schematic diagram of the MG network under consideration.

Figure 3.11(a) shows a $T_{\text{DataFrame}}$ comparison between 2.45 GHz, 915 and 868 MHz ZigBee when transferring one set of data (i.e. voltage magnitude, voltage angle, frequency, active power, reactive power, or CB status) for each DG in the MG. These results are for a fixed number of data bits in the payload section. The results indicate that the $T_{\text{DataFrame}}$ is around 48 and 86 ms, respectively, when using binary and text formats for a 2.45 GHz ZigBee. However, when using 915 and 868 MHz ZigBee, $T_{\text{DataFrame}}$ becomes 5 and 10 times more than that of

the 2.45 GHz ZigBee. Figure 3.11(a) also shows that transmitting 15 sets of the above-mentioned data takes approximately 48.03 ms when using binary coding with a 2.45 GHz ZigBee.

Figure 3.11(b) shows the $T_{\mathrm{DataFrame}}$ comparison between the variable and fixed number of data bits in the payload section of the Data Frame. The results, using a 2.45 GHz ZigBee, are shown in both binary and text format. The results indicate that in text format, the $T_{\mathrm{DataFrame}}$ is 1.8 times larger in text format than in binary format. However, $T_{\mathrm{DataFrame}}$ is approximately 7% larger when using a fixed number of bits compared to a variable number of bits.

The maximum number of symbols that can be transmitted in a ZigBee network, when using 2.45 GHz, 868 MHz and 915 MHz ZigBees, respectively, is 62.5 kilo Symbols, 40 kilo Symbols and 20 kilo Symbols per second. Figure 3.11(c) shows that using a 2.45 GHz ZigBee, the total number of symbols transmitted in the MG is 1,112 in binary format and almost 3 times more in text format. This result indicates that when transmitting 15 sets of the above-mentioned data, the ZigBee still has the capability to transfer approximately 56 times and 18 times more data in binary and text formats, respectively.

Figure 3.11(d) shows the number of symbols required for transmitting the above-mentioned data when using 2.45 GHz, 915 and 868 MHz ZigBee. From this figure, it can also be seen that when using an 868 MHz ZigBee in a text format, the number of symbols required for transmitting 15 sets of the above-mentioned data is very close to the maximum limit of ZigBee technology. However, when using a 2.45 GHz and 915 MHz ZigBee, the number of symbols in the same format is only 5.5% and 34.8% of the maximum limit, respectively.

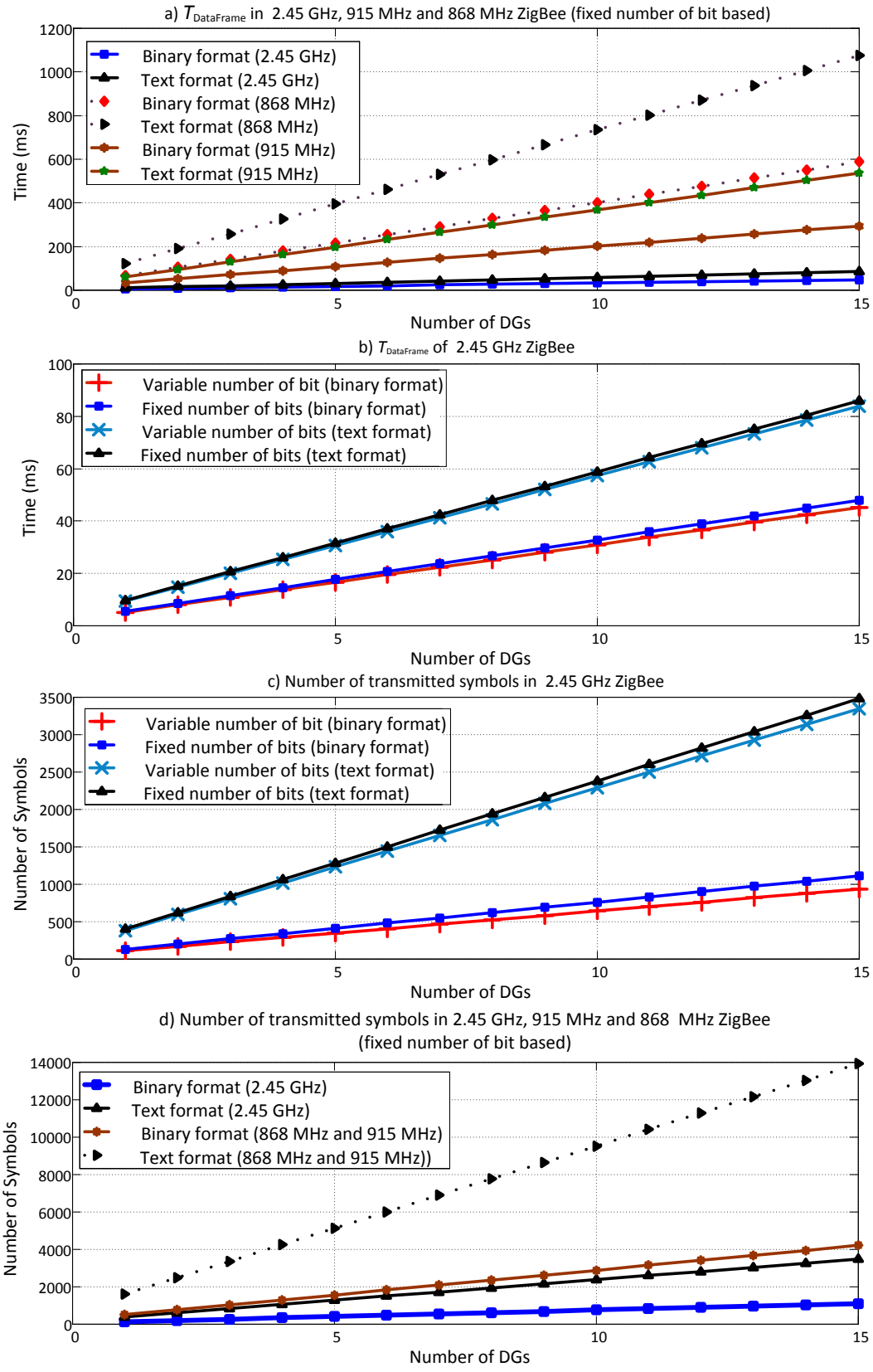

Figure 3.11 Numerical analysis results.

Table 3.4 shows the processing time (i.e. $T_{\text{DataPayload}}$ and $T_{\text{DataFrame}}$) for each data with a variable and fixed number of bits in the data payload section when using a 2.45 GHz ZigBee. This table also shows that when using the fixed number of bits for all data, the $T_{\text{DataFrame}}$ is 0.608 ms in binary format and 1.088 ms in text format. When using a variable number of data bits, the minimum $T_{\text{DataFrame}}$ is 0.544 ms in binary format and 0.992 ms in text format, while its maximum is 0.592 ms in binary format and 1.152 ms in text format.

Table 3.4 Number of bits and characters for each parameter in binary and text formats, the required data payload, and the processing times of the Data Frame.

	Data	Total Number of		$T_{\text{DataPayload}}$ (ms)		$T_{\text{DataFrame}}$ (ms)	
		Bits	Characters	Bits	Characters	Bits	Characters
Variable number of bits	Voltage Magnitude	26	21	0.112	0.672	0.592	1.152
	Voltage Angle	26	20	0.112	0.64	0.592	1.12
	Frequency	24	19	0.096	0.608	0.576	1.088
	Active Power	27	20	0.112	0.64	0.592	1.12
	Reactive Power	27	20	0.112	0.64	0.592	1.12
	CB Status	15	16	0.064	0.512	0.544	0.992
Fixed number of bits		29	21	0.128	0.672	0.608	1.152

3.6. Communication Delay Effect on Microgrid Performance

To evaluate the dynamic performance of an MG — which consists of converter-interfaced DGs, and where communication delay is considered in the MG hierarchical control system — a simulation study is carried out in PSCAD/EMTDC.

Let us consider the MG network of Figure 3.10, which has only two DGs (i.e. DG1 and DG2). Assuming that output power ratio is maintained at 1:2 (DG1 versus DG2) and that the MG is considered initially at a steady-state and autonomous condition — with a total load demand of 0.41 pu, where 1 pu is 6 kVA — the MG load is increased to 1 pu at t = 0.5 s and decreased to 0.53 pu at t = 1 s. At t = 1.5 s, the load is further decreased to 0.17 pu. Following every load change, the DGs update their output powers accordingly, and the voltage magnitude and frequency in the MG feeder are modified. MG dynamic operation and control is summarised in the next sub-chapter, and the technical parameters are listed in Table 3.5.

3.6.1. MG Dynamic Operation and Control

The considered DGs in this thesis are connected to the MG by VSCs, and the VSCs operate within a Voltage Control Strategy (VCS). The VSCs and their associated filter structure, as well as their VCS, are presented in [113] and not repeated here.

When the MG is in a grid-connected mode, the DGs operate at maximum power point (or rated) conditions; however, as the MG falls into autonomous mode, the status of the MG main CB is transferred through the MG central controller to the local controller of each DG. This changes the local controller mode of operation. In autonomous mode, each DG's output power is controlled by P-δ and Q-V droop control equations as [113]:

$$\begin{aligned} |V| &= V_{\text{rated}} + n\,(Q_{\text{rated}} - Q) \\ \delta &= \delta_{\text{rated}} + m\,(P_{\text{rated}} - P) \end{aligned} \tag{3.4}$$

where $|V|$ and δ are the magnitude and angle of the voltage at the output of the DG VSCs, respectively; P and Q are the average active and reactive output power at the DG connection point to the network, respectively; m is the coefficient of the P-δ droop equation; and n is the coefficient of the Q-V droop equation. In (3.4), it is assumed that $P_{\text{rated}} = \frac{P_{\text{max}}}{2}$ and $Q_{\text{rated}} = 0$.

In [113], it is shown that among parallel DGs in an autonomous MG, a proper power sharing ratio control requires satisfaction of the following equations:

$$\frac{P_2}{P_1} = \frac{P_{\text{rated},2}}{P_{\text{rated},1}} = \frac{m_1}{m_2}$$
$$\frac{Q_2}{Q_1} = \frac{Q_{\text{rated},2}}{Q_{\text{rated},1}} = \frac{n_1}{n_2} \quad (3.5)$$

As the network load is varied, the DGs automatically adopt their output power to supply the new load demand of the system. Hence, the voltage and frequency of the network is indirectly regulated by (3.4).

If the network voltage and frequency fall beyond the acceptable pre-defined limits, the MG central controller will take action and adjust the set points of the droop controller for each DG. This process required a data transfer between the feeder's voltage sensor and the MG central controller and between the central controller to the local controllers of each DG. The new set-points can are presented in [124].

3.6.2. Technical Parameters of the Network under Consideration

The technical data of the MG under consideration in Figure 3.10 are listed in Table 3.5.

Table 3.5 Technical data of the network parameters of Figure 3.10.

MG network	400 Vrms L-L, 50 Hz			
MG feeder impedance	R = 0.2 Ω, L =10 mH			
	P_{max} [kW]	L_T [mH]	m [rad/kW]	n [V/kVAr]
DG1	2	2.72	3.1416	18
DG2	4	1.36	1.5708	9

3.6.3. Case-1: Microgrid Performance Without Delay

Firstly, let us assume there is no communication delay ($T_{\text{DataFrame}}$ = 0). The total active power demand of the MG loads is shown in Figure 3.12(a), and in Figure 3.12(b), the active power output ratio between the two DGs is maintained as 1:2. As shown in Figure 3.12(c), the Root Mean Square (RMS) voltage of the MG feeder (V_{MG}) is within the acceptable limits for all load changes.

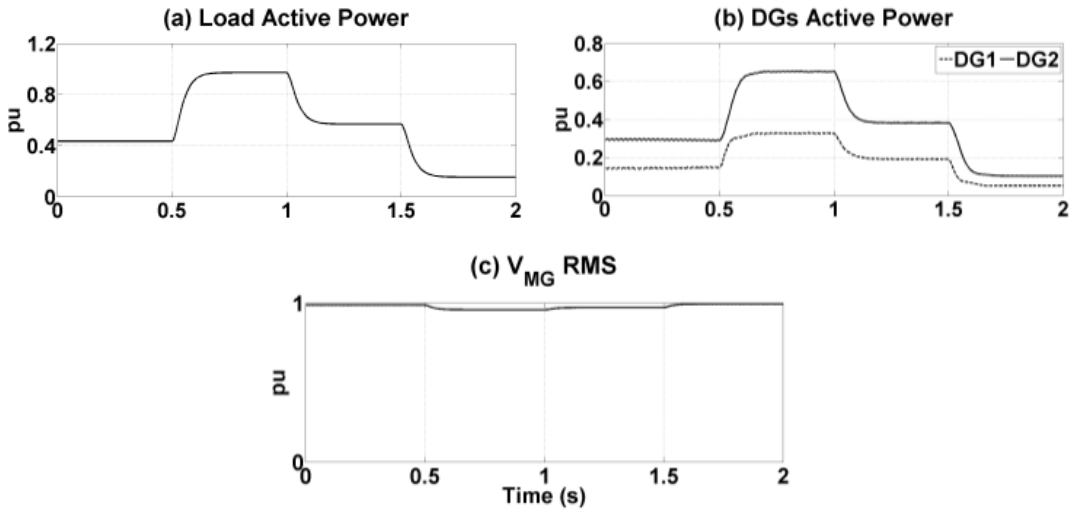

Figure 3.12 MG performance without any communication delay (Case-1).

3.6.4. Case-2: Droop Control within the Microgrid Central Controller

As discussed in Section 3.1, the droop control should be located within the local controller of each DG. If the droop control is considered as a module of the MG central controller (i.e. a centrally managed droop control), the data communication system is required to transfer the active and reactive output power from each DG to the central controller and also return the voltage magnitude and angle instantaneously to the DG local controllers. The ZigBee devices in the central controller and the DG local controllers may transmit and receive only one data at a time. Therefore, for the MG system of Figure 3.10 — which contains two DGs, and where each DG needs to transmit 2 data (i.e. active and reactive power) and receive 2 data (i.e. voltage magnitude and angle) — the total processing time for transmitting and receiving data — using the fastest ZigBee technology (i.e. 2.45 GHz) and assuming a fixed binary format — is calculated as 2 DGs × 4 data × (0.608 + 0.544) ms = 9.216 ms where 0.608 ms is $T_{\text{DataFrame}}$ for a single data (from Table 3.4) and 0.544 ms is the sum of the period of waiting time (i.e. $12T_{\text{Symbol}}$ = 12 × 16 μs = 192 μs) plus the Acknowledgement Frame processing time (i.e. 352 μs from Section 3.4). Thus, 9.216 ms is the minimum communication delay for an MG with only two DGs. It should be noted that in this calculation, the controller processing time and the media transmission delays

(in Figure 3.11) are still ignored. This delay is higher if the number of DGs is increased, or if 868 MHz or 915 MHz ZigBee, or text format is used.

A fixed delay of 0.5 ms is applied to the MG system of Case-1 to transfer the active and reactive power from the local controller of each DG to the MG central controller Another 0.5 ms delay is applied to transfer the voltage magnitude and angle from the MG central controller to the local controller of each DG. The simulations results in Figure 3.13 show that the considered delay time does not lead to dynamic DG mal-operation. However, by increasing the delay time to more than 1 ms, DG dynamic operation is affected. Figure 3.14 and Figure 3.15 show the results of a system with a 4 ms and a 10 ms delay, respectively. For a delay of 4 ms, there is a deviation in DG voltage magnitude and output power; while for a delay of 10 ms, the MG system becomes unstable.

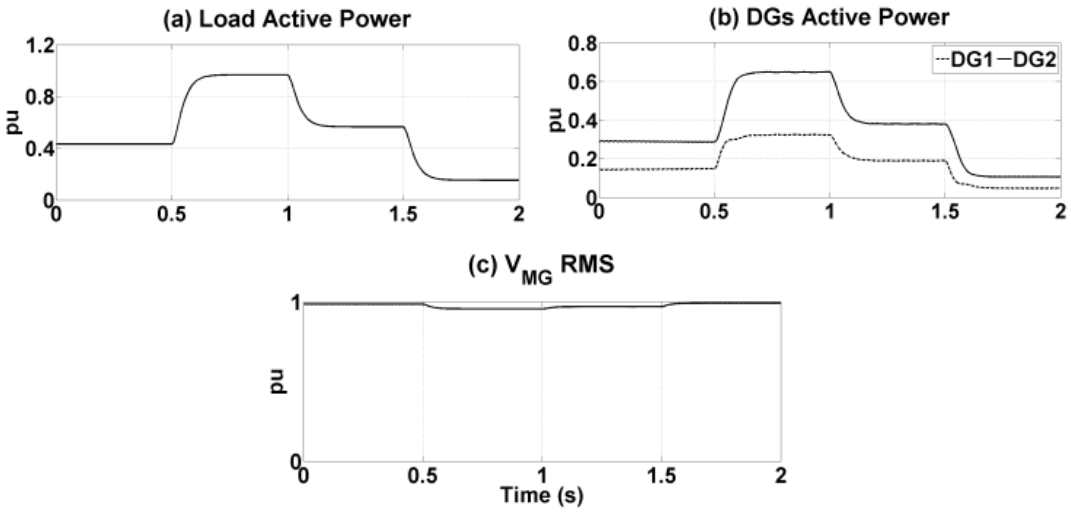

Figure 3.13 MG performance assuming 0.5 ms communication delay (Case-2)

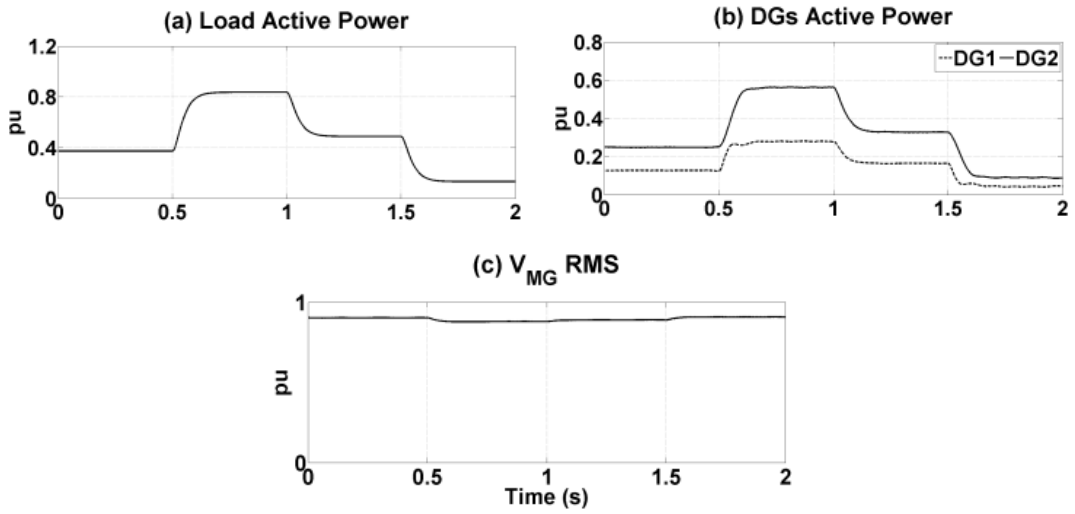

Figure 3.14 MG performance assuming 4 ms communication delay (Case-2).

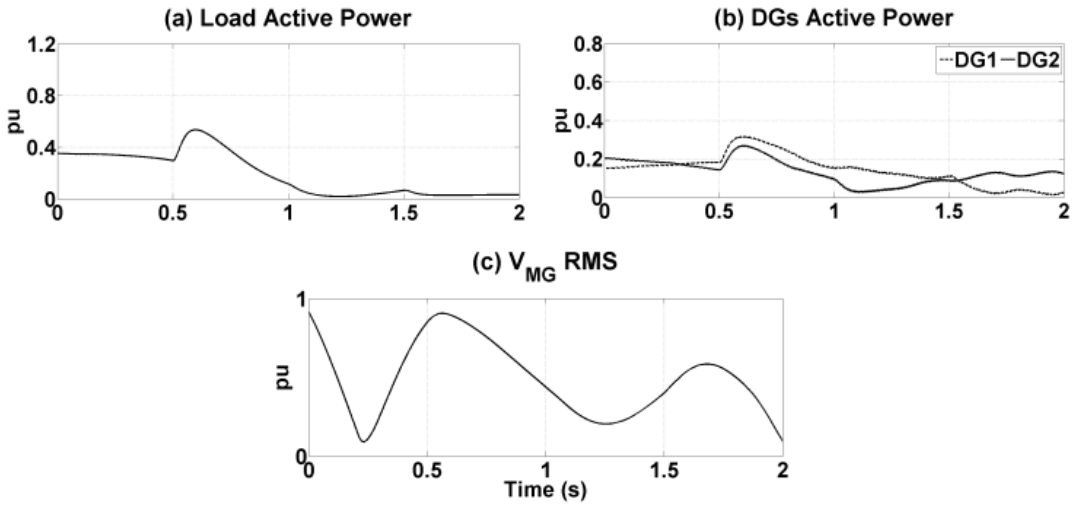

Figure 3.15 MG performance assuming 10 ms communication delay (Case-2).

3.6.5. Case-3: Droop Control within the DG Local Controller

In Case-2, it has been demonstrated that a centrally managed droop control will fail due to a high communication delay. Now, let us assume that the droop control is located within the local controller of each DG, as discussed in Section 3.1, and the MG central controller is only responsible for regulating the network voltage and frequency within the standard limits, and only if they are violated. It is to be noted that this is a discrete process with a sampling time of a few minutes. The voltage magnitude and frequency are monitored in the MG feeder using a voltage sensor. The total communication delay for transferring these 2 data from

the voltage sensor to the MG central controller with the slowest ZigBee technology (i.e. 868 MHz) and in a fixed text format is 2 data × (14.4 + 5) ms = 38.8 ms where 14.4 ms is $T_{\text{DataFrame}}$ for a single data and 5 ms is the sum of the waiting time and an Acknowledgement Frame (i.e. 4400 μs from Section 3.4).

Based on the same processing time for the MG central controller to transfer back the new references for voltage magnitude and angle, the total communication delay is at least 2 × 38.8 ms = 77.6 ms. However, as this process has a discrete operation with a large time step of few minutes, this delay will not affect the system operation.

3.6.6. Case-4: Communication Delay for Transferring Microgrid Main CB Status

As discussed in Section 3.1, the status of the MG main CB should be immediately transferred to the local controller of each DG via the MG central controller. This is so that if the MG operation mode is updated — from grid-connected to autonomous, and vice versa — so can the DG operation mode. In such a case, the total communication delay for the MG system of Figure 3.10 — with two DGs, the slowest ZigBee technology (i.e. 868 MHz), and a fixed text format for one data — is (14.4 + 5) ms = 19.4 ms. The communication delay includes the transmission processing time from the CB controller to the MG central controller, and also the transmission processing time from the MG central controller to the local controller of each DG. This data communication delay is then at least 2 data transfers of × 19.4 ms = 38.8 ms. It is to be noted that this delay will not arise if the total number of MG DGs increases.

Now, let us consider the network of Case-1. It is assumed that the MG is initially in the steady-state condition and grid-connected. At t = 0.4 s, the MG main CB opens, and it falls into the autonomous mode of operation. The system of Case-1 is simulated assuming a zero and 40 ms communication delay for transferral of the MG main CB status to the DG local controller. The network voltage is shown in Figure 3.16. As it can be seen from this figure, the DGs' dynamic operation does not fail even with a 40 ms delay.

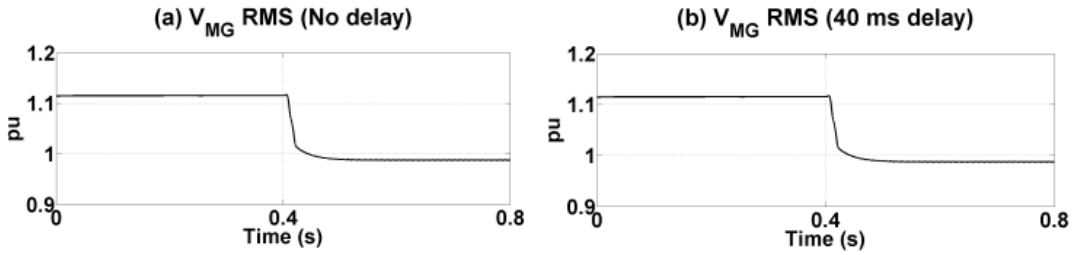

Figure 3.16 MG performance assuming a zero and 40 ms communication delay for transferral of the MG main CB status to the DG local controller (Case-4).

3.7. Summary

A ZigBee-based wireless data communication system is presented in this chapter for future MGs. The proposed communication system is responsible for transmitting several electrical parameters (i.e. voltage magnitude, angle and frequency, active/reactive power, and CB status) from the local controller of each DG to the MG central controller. It must also transmit the reference for voltage magnitude and angle, and CB status, from the MG central controller to the local controller of each DG. The ZigBee standard Data Frame is used to transmit the data.

This thesis also presents a new coding for the data payload section of this frame. The new coding can represent each of the data mentioned above — their values, dimensions, and the origin of the data (sensor, meter, etc.) — in both a binary and text format, while the data payload section can be composed of a fixed number of bits or a variable number of bits. The data transmission delay is affected by the selection of the binary/text format, and the fixed/variable number of bits for the data payload and carrier frequency. Through a series of numerical analyses, the expected data transmission delay, as well as the maximum number of symbols used for the MG data transaction, is compared over several DGs.

These analyses are carried out for the above-mentioned data sets, while the relevant transmission delays are calculated for each format/coding configuration. It can be seen from these analyses, that to cover a vast area, ZigBee with a carrier frequency of 868 MHz or 915 MHz must be used; however, the data transmission delay is increased. For shorter distances, a 2.45 GHz ZigBee can be used, which has a much smaller data transmission delay. Through the PSCAD/EMTDC-based

simulations, it is shown that the droop control system needs to be located within the local controller of each DG; otherwise, due to communication delays, there is a greater possibility of system instability, even for the ZigBee with the fastest processing time. It is also shown that the communication delay — for transferring the set-points of the droop control from the MG central controller and also the MG main CB status to the local controller of each DG — does not affect the dynamic performance of the MG system, even for the ZigBee with the slowest processing time. The average communication delay by employing ZigBee based communication technology is varied in millisecond, and this delay is much larger than the delay in the required processing in the controller based micro-controller which is usually in microsecond. The total delay including the communication delay and the processing delay is then mostly influenced by the communication delay, and in the several cases, the processing delay will not have a big impact on the system.

Chapter 4: A New Technique for Simultaneous Load Power/Current sharing and Voltage Regulation in the DC Microgrid

In this Chapter, the new technique for voltage regulation and power sharing in DC MG is proposed, discussed and simulated. The detail of the proposed technique, required data communication, stability analysis and the simulation in various load demands is presented and discussed below:

4.1. Proposed Technique

Consider the DC MG of Figure 4.1, which consists of two DGs and one load. In this figure, the DG output currents and the voltage at the load point can be expressed mathematically as:

$$I_{\mathrm{L}} = \sum_{\mathrm{k}} I_{\mathrm{DG}k}$$

$$I_{\mathrm{DG}k} = \frac{V_{\mathrm{DG}k} - V_{\mathrm{L}}}{Z_{\mathrm{C}k}} \tag{4.1}$$

$$V_{\mathrm{L}} = Z_{\mathrm{L}} I_{\mathrm{L}}$$

where $Z_{\mathrm{C}k}$ is the impedance of line-*k* connecting DG-*k* to the load, Z_{L} is the equivalent impedance of the load, and V_{DGk} is the output voltage of DG-*k*.

It has been stated in [46], [57], [92], [125] that a circulating current (i.e. negative I_{DGk}) may take place among the DGs following a mismatch between their generated voltages or currents, and only if the configuration and type of the DGs and their dc-dc converters allow for this negative current. As an example, a circulating current may be observed within the dc-dc converter of a photovoltaic-based DG, but it will not occur when the output voltage of a rotating machine, such as an induction generator, is converted to a DC voltage through a diode-based rectifier. From (4.1), a circulating current may occur only if $V_{\mathrm{L}} > V_{\mathrm{DGk}}$. Consequently, the DGs can produce unequal voltages at their outputs without resulting in a circulating current if $V_{\mathrm{L}} < V_{\mathrm{DGk}}$. Table 4.1 summarises various operating conditions for this MG, along with the possibility of circulating current, voltage regulation at the load point, and also power sharing.

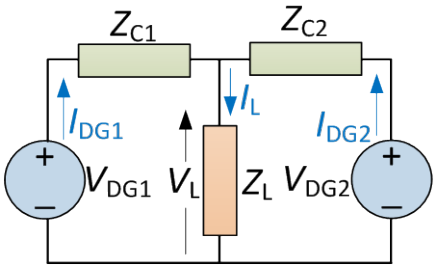

Figure 4.1 Considered DC MG configuration.

Table 4.1 Summary of conditions under which current circulation and power sharing among DGs, and also load voltage regulation, is possible for the MG of Figure 4.1.

DGs voltage	V_L condition	CC*		VR#	PS$
		into DG_1	into DG_2		
$V_{DG1} = V_{DG2}$	$V_{DG1} > V_L, V_{DG2} > V_L$	×	×	✓	×
	$V_{DG1} \geq V_L, V_{DG2} \geq V_L$	×	×	✓	✓
$V_{DG1} \neq V_{DG2}$	$V_{DG1} \geq V_L, V_{DG2} < V_L$	×	✓	✓	✓
	$V_{DG1} < V_L, V_{DG2} \geq V_L$	✓	×	✓	✓

*CC = Current Circulation, #VR= Voltage Regulation, $PS = Power Sharing

✓ = possible, × = unacceptable

According to (4.1), for voltage regulation at the load point, V_{DGk} has to be controlled; while for power/current sharing among DGs, coordination for V_{DGk} of both DGs is required. Thus, the proposed technique consists of two controllers: local and central. Within the local controller, a feedback signal is transmitted from the voltage of the closest load to a DG to its controller, to regulate the load voltage following any fluctuations in the load demand. The output current and voltage of each DG needs to be transmitted to the MG central controller to facilitate power/current sharing. The local and central controllers are discussed in detail below:

4.1.1. Proposed Technique for Local Controller

It can be seen from (4.1) that Z_{Ck}, and Z_L influence both the voltage at the load point and the DG output currents. However, due to their dynamic changes, it is impractical to measure Z_{Ck} and hard to consider Z_L. Following a change in the

load demand, the load point voltage changes by $\Delta V_{\mathrm{L}} = V_{\mathrm{L}}^{\mathrm{ref}} - V_{\mathrm{L}}$. To restore the voltage back to the desired level, a control technique should be employed to continuously change the output voltage of each DG until V_{L} retains its nominated level $V_{\mathrm{L}}^{\mathrm{ref}}$. To realize this, the reference output voltage of each DG can be calculated as:

$$V_{\mathrm{DG}k}^{\mathrm{ref}} = V_{\mathrm{DG}k} + \Delta V_{\mathrm{L}} \tag{4.2}$$

$V_{\mathrm{DG}k}^{\mathrm{ref}}$ needs to be updated discretely to prevent instability in the electronics-based dc-dc converters, which is caused by continuous variation of their references. This process continues until ΔV_{L} falls within an acceptable bandwidth of $\pm\alpha V_{\mathrm{L}}^{\mathrm{ref}}$ where α (a positive number, e.g. 0.05) is defined by the MG operator. A predefined time delay of T_{P}, shown in fixed intervals of a few seconds/minutes, is suggested and presented in Figure 4.2. This delay is longer than the total required time for the dc-dc converters and other related delay such communication delay, and so generates a settled output voltage (i.e. 95% of desired value), a measurement delay in sensors, and also a delay in the transmittal of V_{L} from the sensor to the DG controller. According to the Nyquist theorem, T_{P} should be more than twice the controller's settling time; otherwise, the MG may exhibit oscillations or instability [31], [126], [127].

4.1.2. Proposed Technique for Microgrid Central Controller

Due to the physical differences and ratings of MG DGs, it is possible to have a mismatch in power generation, which can in turn lead to a DG supplying different voltages and currents. It is essential however that DGs within an MG share the load according to a designated ratio, e.g. proportional to their respective capacity (if the cost to generate electricity for each DG is equal), or proportional to the cost of DG electricity generation. The total power consumed by the loads plus the power losses in the lines (P_{L}) is equal to the sum of the power generated by DGs ($P_{\mathrm{DG1}}, P_{\mathrm{DG2}}, \ldots P_{\mathrm{DG}N}$). Therefore, any change in the load demand, plus the power losses (ΔP_{L}), corresponds to a change in the DG generated power (ΔP_{DGk}):

$$\Delta P_{\mathrm{L}} = \sum_{k=1}^{N} \Delta P_{\mathrm{DG}k} \tag{4.3}$$

where N is the number of active DGs in the MG.

The proposed technique needs to be updated with DG status (s_{DG}), so that the appropriate mode of operation can be determined for those renewable energy sources with intermittent characteristics or plug-and-play sources such as energy storage. The s_{DG} of a source or energy storage, capable of generating power, will be 1; otherwise, it will be 0. Thereby, N is defined as:

$$N = \sum_{k=1}^{N} \mathrm{s}_{\mathrm{DG}k} \tag{4.4}$$

Power sharing among DGs can be achieved by multiplying the generated power of each source by R_{DG}, $0 \leq R_{\mathrm{DG}} \leq 1$, which is a weighting factor of the generated power from each DG. Therefore, (4.2) can be re-written as:

$$V_{\mathrm{DG}k}^{\mathrm{ref}} = V_{\mathrm{DG}k} + R_{\mathrm{DG}k}\, N\, \Delta V_{\mathrm{L}} \tag{4.5}$$

R_{DG} of each DG is determined by the MG central controller based on the DG's capacity and operational cost. The renewable energy sources have an intermittent character and an energy output dependent on environmental conditions. Hence, their generated power can be less than their capacity. The power most recently generated by each renewable energy-based DG should be considered when determining a new R_{DG}. The algorithm for determining the value of R_{DG} for each DG is beyond the scope of this research and not discussed here.

In reality, measuring all load currents is both impractical and costly, because the number of loads can be varied, and they can be spread at different locations within the MG. Load current sharing among DGs in the MG can instead be achieved by adjusting each DG output current ($I_{\mathrm{DG1}}, \cdots I_{\mathrm{DG}N}$) in proportion to the sum of the DG output current (I_{T}):

$$I_{\mathrm{T}} = \sum_{k=1}^{N} I_{\mathrm{DG}k} \tag{4.6}$$

According to (4.1), the output current of a DG can be adjusted by controlling the DG output voltage, and as seen in (4.5), the $V_{\mathrm{DG}}^{\mathrm{ref}}$ can be adjusted by modifying R_{DG}. Hence, the deviation ratio of the DG output current — from the desired value versus the total load current — can be formulated as:

$$\Delta I_k^{\mathrm{CS}} = \frac{R_{\mathrm{DG}k}\, I_{\mathrm{T}} - I_{\mathrm{DG}k}}{I_{\mathrm{T}}} \tag{4.7}$$

Consequently, the new DG ratio can be defined as:

$$R^{*}_{\mathrm{DG}k} = R_{\mathrm{DG}k} + \Delta I^{\mathrm{CS}}_{k} \tag{4.8}$$

where $R^{*}_{\mathrm{DG}k}$ is the updated ratio of the $\mathrm{DG}_{k,}$ amended to compensate for the unmatched current caused by line impedances.

For the power sharing method, Equations (4.6) through (4.8) can be rewritten as:

$$P_{\mathrm{T}} = \sum_{k=1}^{N} P_{\mathrm{DG}k} \tag{4.9}$$

$$\Delta P^{\mathrm{CS}}_{k} = \frac{R_{\mathrm{DG}k}\, P_{\mathrm{T}} - P_{\mathrm{DG}k}}{P_{\mathrm{T}}} \tag{4.10}$$

$$R^{*}_{\mathrm{DG}k} = R_{\mathrm{DG}k} + \Delta P^{\mathrm{CS}}_{k} \tag{4.11}$$

where P_{T}, $P_{\mathrm{DG}k}$, and $\Delta P^{\mathrm{CS}}_{k}$ represent the output power of all DGs, the output power of the DG_{k}, and the deviation ratio of the DG output power, respectively.

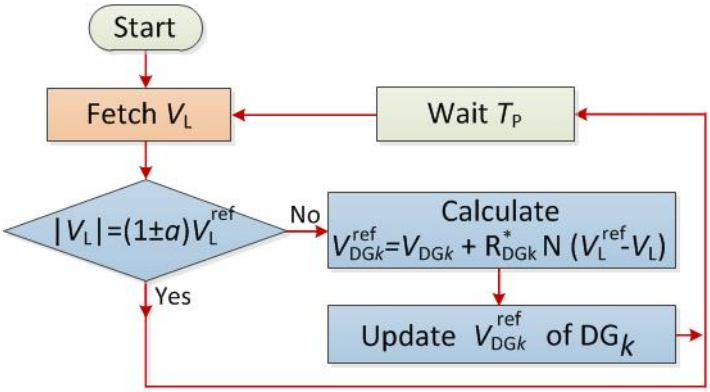

Figure 4.2 Flow chart for the proposed load voltage regulation and load power/current sharing method.

The proposed method in (4.5)-(4.8) requires voltage and current information from all DGs that need to be transmitted to the MG central controller. The MG central controller then calculates and obtains a suitable value for power/current load sharing for each DG. The proposed method is illustrated schematically in the flowchart of Figure 4.2, while Figure 4.3 shows a schematic illustration of an MG using the proposed approach, which simultaneously regulates the voltage at the load points and facilitates load power/current sharing among DGs. In this figure,

V_{L} represents the load point voltage, which shows communication delays with the voltage measured at the load point. In this thesis, the dc-dc converter of a DG is assumed to be an ideal converter, which has the ability to produce in a short interval (represented by processing delay time T_{c}) a voltage at its output (V_{DGk}) that is equal to its reference ($V_{\mathrm{DGk}}^{\mathrm{ref}}$). V_{DG} is considered as a local measurement for the converter control and thus it is not required to be transmitted elsewhere. In Figure 4.3, R_{i} and L_{i} represent the internal resistance and inductance of the converter's filter [47], [48], [53] while R_{C} and L_{C} represent the resistance and inductance of Z_{C}. The load can be represented as single-load, multiple parallel loads, or multi-parallel loads in multiple branches.

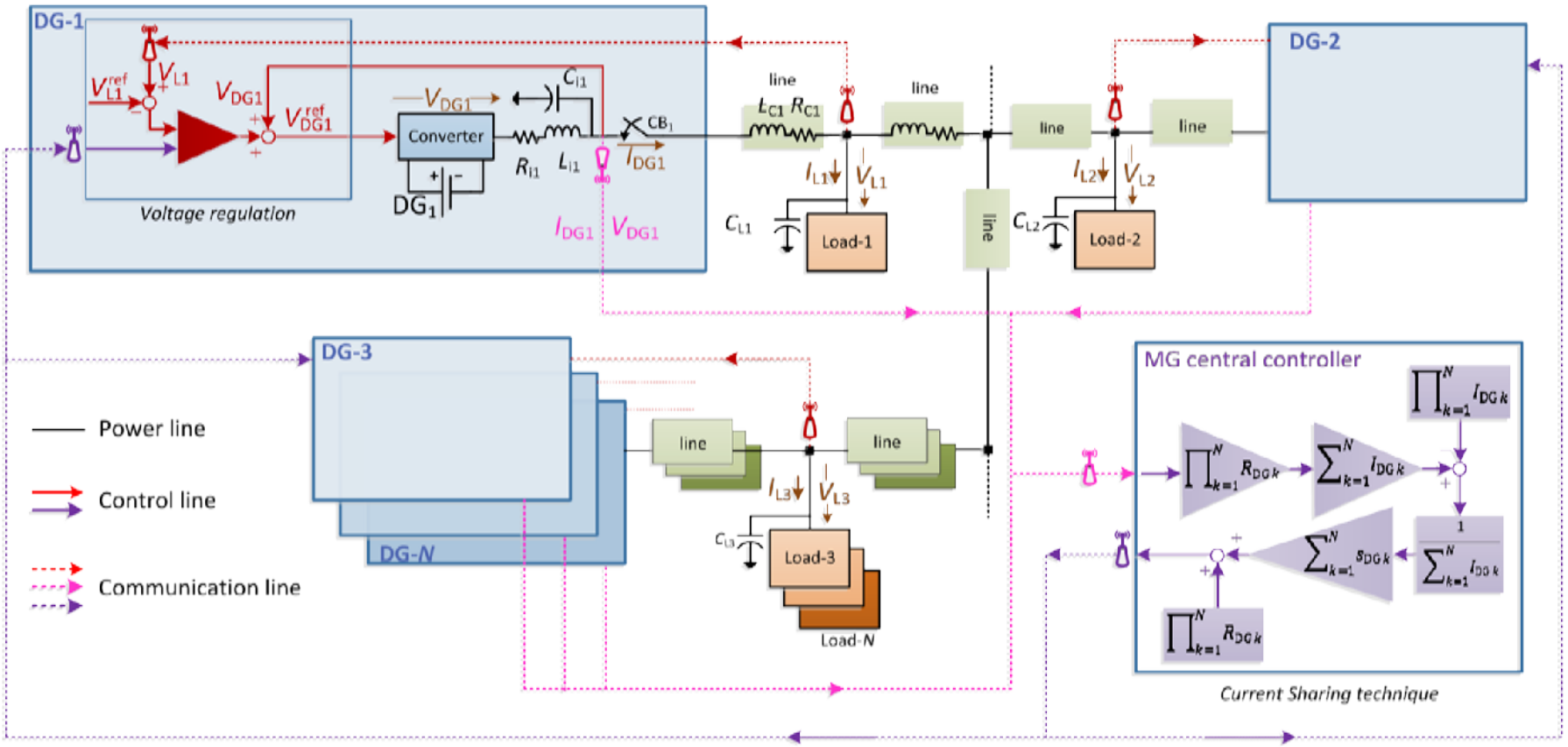

Figure 4.3 Schematic diagram of an MG, using the proposed technique for simultaneous load current sharing and load point voltage regulation.

4.2. Required Data Communication

The data required to be transmitted using the proposed technique are the load point voltage; the output current and voltage; DG status and their desired power ratios; and the number of active DGs. V_{L}, R_{DG}, and N are required for voltage regulation at the load point, while $I_{\mathrm{T}}, P_{\mathrm{T}}$ and $I_{\mathrm{DG}}, P_{\mathrm{DG}}$ are required for load power/current sharing among DGs. Data should be transmitted as soon as any change takes place in the status of a DG. The rest of the data needs to be transmitted periodically. V_{L} is transmitted to the DG controllers as soon as it exhibits a change larger than the pre-defined voltage fluctuation limit (e.g. ±5%).

The above data transfer management can reduce the required communication bandwidth without any negative effects to MG dynamic operation [52].

To determine $R^{*}_{\mathrm{DG}k}$, I_{DG} is transmitted to the MG central controller from each DG controller, and to calculate N, s_{DG} is transmitted. N, and R^{*}_{DG} are then transmitted from the MG central controller to the DG controllers. This data communication process is designed, evaluated and simulated in a centralised data communication scheme as illustrated in Figure 4.4. The possibility of another data communication scheme, which can be used as an alternative, is discussed, evaluated and simulated in Chapter 6.

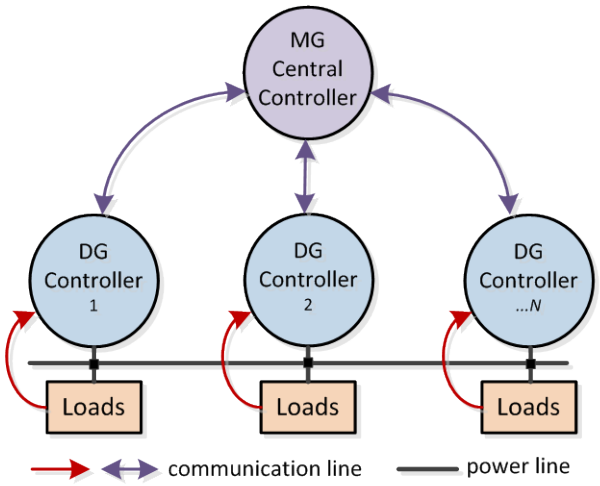

Figure 4.4 Proposed data communication flow.

In the proposed technique, all received data are saved in the DG controllers and in the MG central controller and are used in the calculations until a new value is received. In the event of a failure in the communication system, the proposed control technique continues to function using the stored data.

When employing communication technologies for information exchange in the MG, the communication delay for transmitting data must be considered [128], [129]. The communication delay is affected by several factors, including data bandwidth, communication topology, protocol, frequency, infrastructure, security and modulation, landscape, data queue, packet loss and collision, signal strength, number of hops and routes, transmitted data, communication devices, and clusters [53], [58], [79], [130], [131]. Each communication technology, such as Ethernet/IoT and ZigBee, has a built-in protocol to avoid and eliminate problems such as the re-transmittal of the confirmation code to the transmitter [122]. This thesis does not intend to evaluate the impact of each and every factor mentioned above on MG applications, but will consider the accumulated impact of such factors, i.e. communication delay.

To reduce the lengthy data transmissions, which affect the communication delay, the required data in this thesis is classified based on the data code, the device number, and the range of data value. This data classification is presented in Table 4.2. To evaluate the performance of the proposed method, low bandwidth communication (instead of high bandwidth) is used. As discussed in Chapter 3, this thesis uses the low bandwidth 2.4GHz ZigBee (250 kbps) for basic calculation of the communication delay. According to the calculations in Chapter 3, the period for transmittal of 1 data is presented in Table 4.2. This period becomes smaller when using higher bandwidth (i.e. Ethernet/IoT-based) communication technology.

To evaluate the performance and reliability of the proposed method, a relatively large value has been considered for T_{P}. Assuming the number of devices is 20-40, the time processing speed in the dc-dc converters is 1.5-20 ms, and the probability of receiving the transmitted data completely is 1-3x the transmission [122], the T_{P} is assumed to be 200 ms in all studies of this chapter. As demonstrated through simulation studies below, the dynamic operation of an MG with the proposed technique and such a large communication delay can be

realized successfully; thereby, any other communication technology with a smaller delay is also acceptable.

Table 4.2 Proposed data in the communication code.

Type	Code	bit	Number	bit	Value	Step	bit	Total bit	Period [μs]
V_L	001	3	$V_{L1} \cdots V_{L100}$	7	0 … 400 V	0.1	12	22	576
N	010	3	-	0	1 … 20	1	5	8	528
R_{DG}	011	3	$R_{DG1} \cdots R_{DG20}$	5	0 … 1	0.05	5	13	544
s_{DG}	100	3	$s_{DG1} \cdots s_{DG20}$	5	0, 1	-	1	9	528
V_{DG}	101	3	$V_{DG1} \cdots V_{DG20}$	5	0 … 400 V	0.1	12	20	576
I_{DG}	110	3	$I_{DG1} \cdots I_{DG20}$	5	–200…200 A	0.1	12	20	576
P_T	111	3	-	0	0 … 400 kW	0.1	12	15	544
I_T	000	3	-	0	0 … 400 A	0.1	12	15	544

4.3. Stability Analysis

Using the proposed technique, Figure 4.5 presents the closed-loop block diagram of the considered DC MG in Figure 4.4. In this diagram, the internal dynamics of the dc-dc converters are simplified as a first order system with a unity gain and a time delay of T_c. As illustrated in Figure 4.2, the V_{DGk} in (4.5) is assumed to be the output of the converter at $t - T_P$. Thus, the system transfer function can be represented as:

$$\frac{V_L(s)}{V_L^{ref}(s)} = \frac{(R_L + sL_L)\sum_{i=1}^{N} A(s,i)}{B(s,i) + (R_L + sL_L)\sum_{i=1}^{N} A(s,i)} \tag{4.12}$$

Where:

$A(s,i) = \frac{R_{DGi}N}{(s^2 L_i C_i + sR_i C_i + 1)(1 + sTc) - e^{-sTp}} \prod_{j=1, j\neq i}^{N} (R_j + sL_j)$, and

$$B(s,i) = \prod_{i=1}^{N} (R_i + sL_i)$$

Delays of T_C and T_P in the transfer function of (4.12) are then modelled by a Padé approximation of order 5 in the form of:

$$e^{x} = \frac{1 + \frac{x}{2} + \frac{x^2}{9} + \frac{x^3}{72} + \frac{x^4}{1008} + \frac{x^5}{30240}}{1 - \frac{x}{2} + \frac{x^2}{9} - \frac{x^3}{72} + \frac{x^4}{1008} - \frac{x^5}{30240}} \tag{4.13}$$

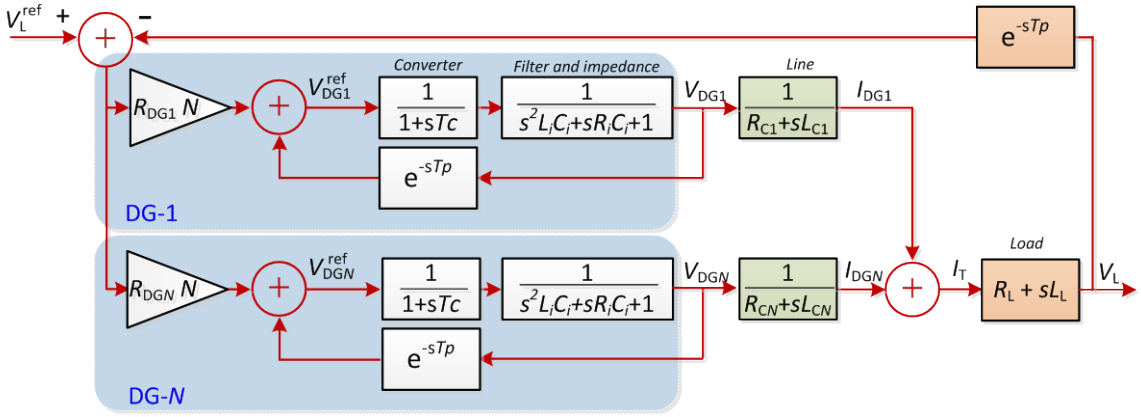

Figure 4.5 Closed-loop block diagram of the considered MG.

It should be noted that a higher order of Pade approximation will increase the precision of the delay value. As delays in this thesis are considered to be 1-200 ms, a precision of 0.001 ms is assumed. By employing Pade approximation of order 5, the desired precision of delay can be achieved.

Considering the parameters of Table 4.3, the step response of this system to a different number of active DGs (assuming all are supplying the load with the same ratio) is illustrated in Figure 4.6. By increasing the number of DGs, while at the same time maintaining equal ratios, the system will exhibit overshooting and also oscillations around the steady-state level. The stability of the system is also analysed with respect to the variations in the MG demand (by varying the load impedance), the impedance of the network lines, and DG ratio. The results are shown in Figure 4.7(a), Figure 4.7(b), and Figure 4.7(c), respectively. Figure 4.7(a) reveals that an MG with a smaller demand (higher load resistance) is more prone to oscillations, and its stability margin decreases with the decrease of its load demand. On the other hand, Figure 4.7(b) shows that larger line impedances decrease the stability margin. In Figure 4.7(c) it can be seen that to maintain system stability, DG ratios should be decreased at the same time as the number of active DGs is increased in the MG. It is worth mentioning that the selected order of Pade approximation does not impact the defined stability margins. Repeating

the analysis of Figure 4.7, by assuming a Pade approximation of order-3 to 10, shows that the stability margin remains constant.

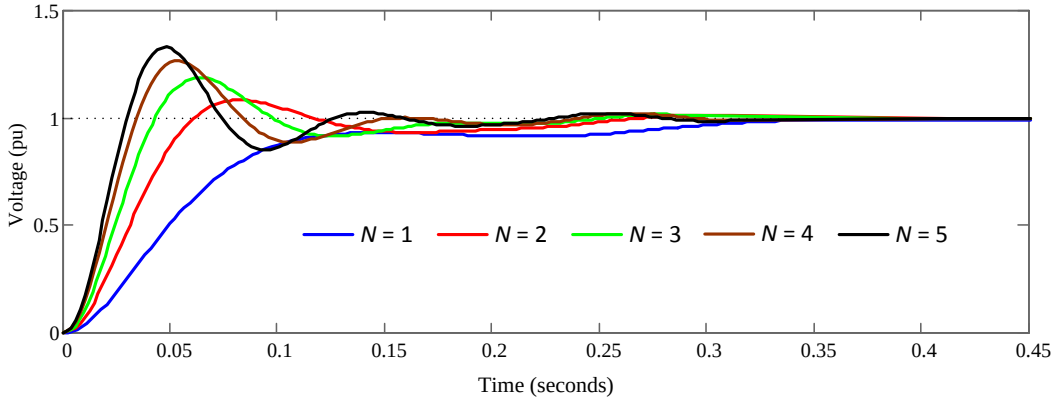

Figure 4.6 Step response of the block diagram of Figure 4.5, showing a different number of active DGs with equal generation ratios.

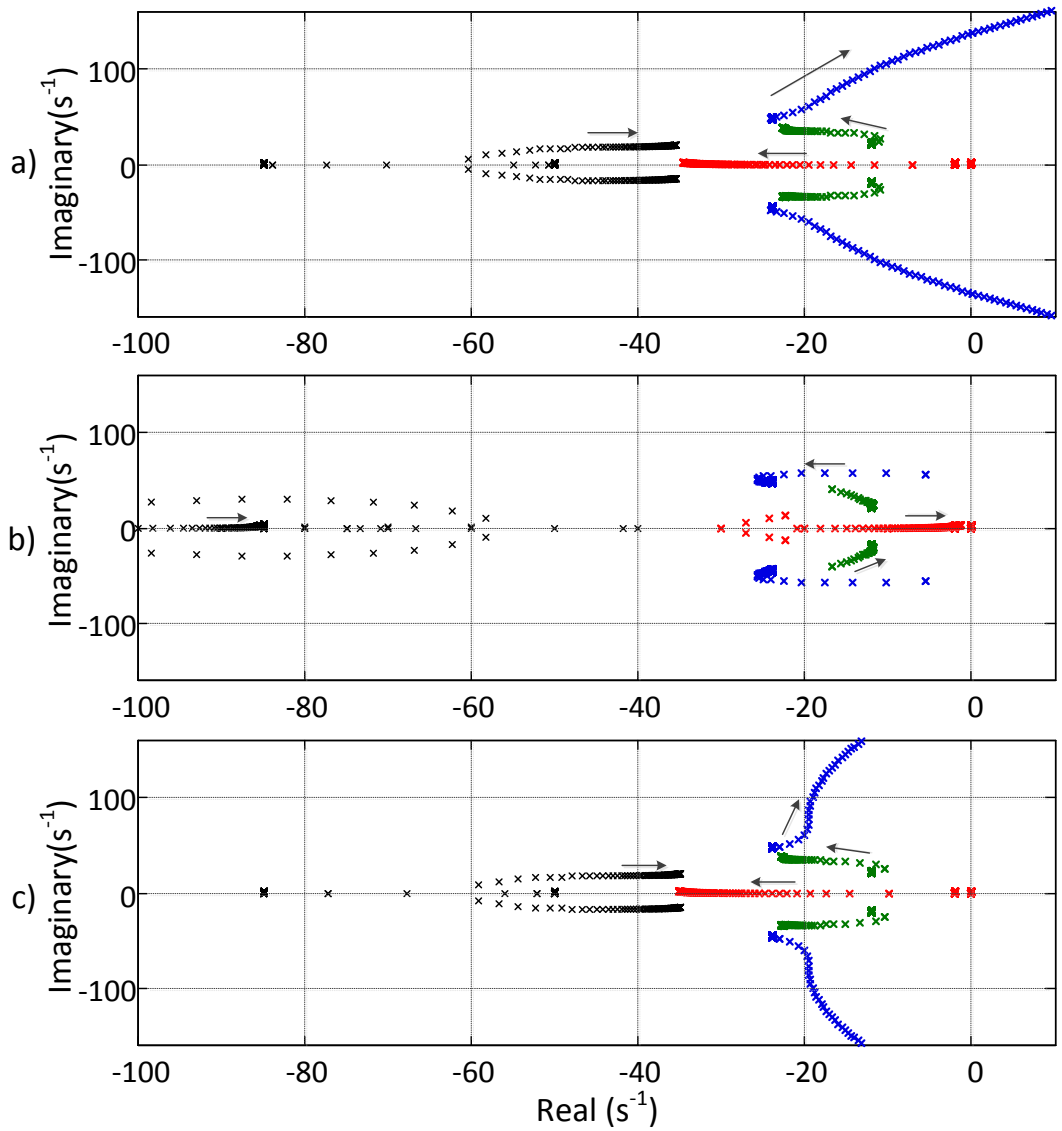

Figure 4.7 Root locus of the block diagram of Figure 4.5, showing (a) a decreasing load demand (increasing load resistance), (b) an increasing network line resistance, and (c) increasing DG ratios.

Table 4.3 Technical parameters for stability analysis.

Line	$R_{\mathrm{C}} = 0.5\ \Omega$, $L_{\mathrm{C}} = 10$ mH
Load	$R_{\mathrm{L}} = 5\ \Omega$, $L_{\mathrm{L}} = 10$ mH,
DG	$L_{\mathrm{i}} = 10$ mH, $C_{\mathrm{i}} = 100$ mF, $R_{\mathrm{i}} = 5\ \Omega$
Delays	$T_{\mathrm{P}} = 200$ ms, $T_{\mathrm{C}} = 1.5$ ms

4.4. Dynamic Performance Evaluation

To examine the dynamic performance of the investigated system with the proposed technique, the DC MG configuration of Figure 4.3 is modelled using MATLAB/Simulink under different operating conditions, a few of which are discussed below:

4.4.1. Case-A: Voltage Regulation at the Load Point

The technical parameters of Table 4.4 are used to simulate the DC MG of Figure 4.3 with one DG. The MG is initially assumed to be in a steady-state condition, and the voltage at the load point is assumed to be 1 pu. At t = 3s, the load demand is increased by 33.3%, which results in a voltage drop of 10% across the load as shown in Figure 4.8 (a). With the proposed algorithm, the output voltage of the DG is regulated to a new and higher level (within the capacity limits of the DG) to retain the load voltage at the desired level of 1 pu, which is realized at t = 3.6 s with only three updates of the V_{DG}. Figure 4.8 (b) shows that in order to push the load voltage to the desired level, the output voltage of the DG is increased to 1.36 pu. The load demand is then decreased by 50% at t = 5s, which causes the voltage across the load to increase by 22%. As can be observed in Figure 4.8, the proposed technique acts to regulate the load voltage at the desired level of 1 pu, which is realized at t = 5.8s. In this case, the output voltage of the DG decreases to 1.12 pu as can be seen in the zooming plot of Figure 4.8 (c).

To evaluate the performance of the proposed method, a noise generator is also added in the DC MG system generated by a Gaussian Noise with 2 volt peak-to-peak amplitude and 10 kHz frequency. The simulation result is presented in Fig. 4.8 (d). The result reveals that the performance of the MG system during the increasing, decreasing, and fluctuations of the load demands is still stable as expected responses.

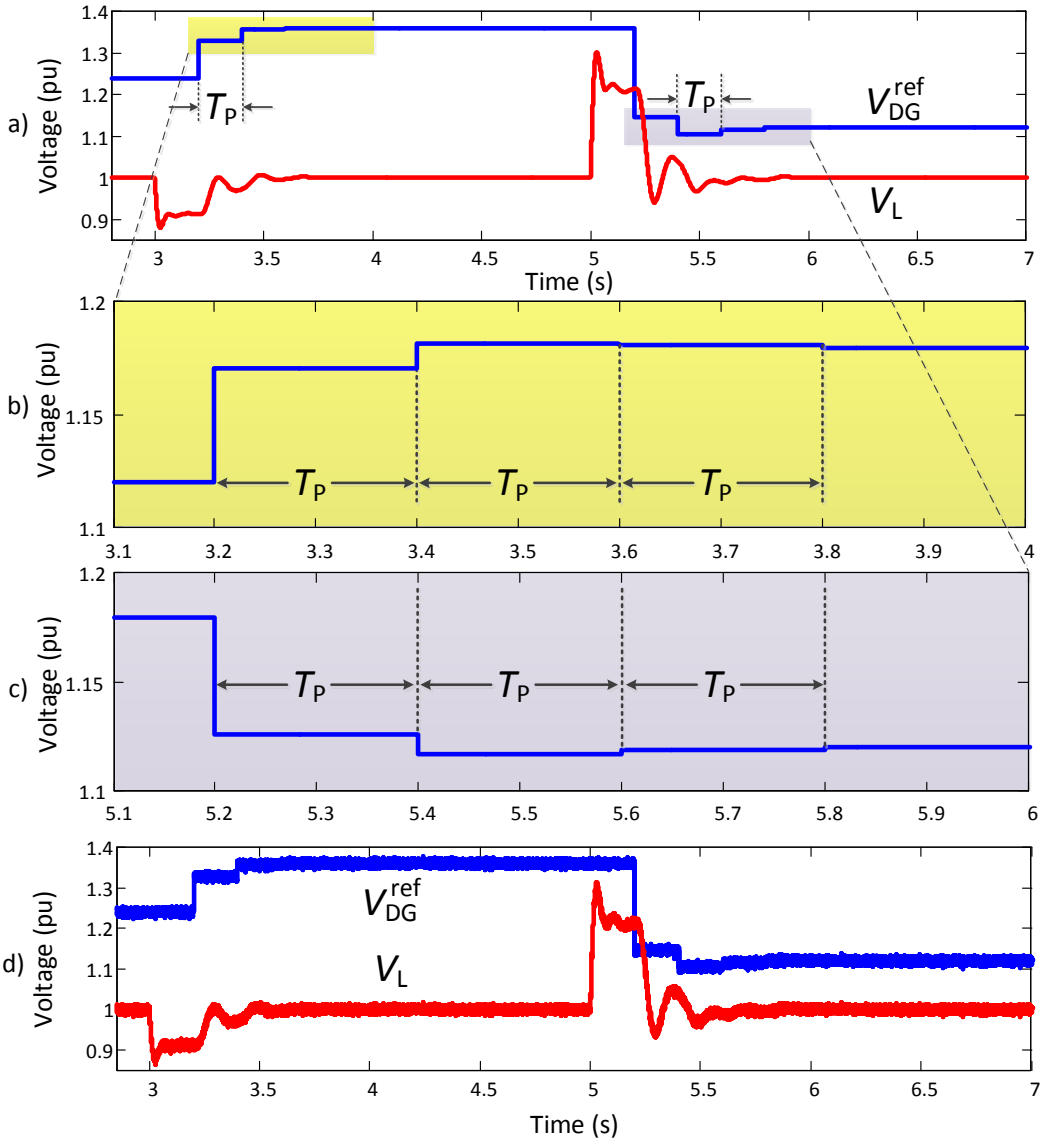

Figure 4.8 Regulation of the load point voltage after load demand changes in an MG with the proposed technique: a) increasing and decreasing load demand, b) zooming plot of increasing load demand, c) zooming plot of decreasing load demand, d) the response of the DC MG with noise.

Table 4.4 Considered parameters for Case-A.

Base parameters	220 V, 70 A, 15 kW, $T_P = 200$ ms
Line	$R_C = 1.1\ \Omega$, $L_C = 10$ mH
Load	$R_L = 5\ \Omega$, $L_L = 10$ mH, $C_L = 1$ mF
DG	$L_i = 4$ mH, $C_i = 1.5$ mF, $R_i = 0.1\ \Omega$

4.4.2. Case-B: Load Current Sharing among DGs

The technical parameters of Table 4.5 are used to simulate the MG of Figure 4.3 with two DGs. The MG is assumed to be at steady-state condition initially, and a load demand increase of 33.3% applies at t = 3s. Figure 4.9 shows the load current and DG output currents, while Figure 4.10 depicts the load voltage and the DG output voltages. When only the voltage regulation technique is adopted, Figure 4.10(a) shows that the voltage at the load can be effectively regulated to the desired level, regardless of any variation in demand. However, Figure 4.9(a) reveals that the DG output currents do not comply with the desired ratio.

On the other hand, when the proposed simultaneous voltage regulation and current sharing technique is applied, not only do the DG output currents satisfy the desired ratio (see Figure 4.9(b-c)), but also the voltage across the load is retained at the desired level (see Figure 4.10(b-c)), regardless of demand variations. It is worth mentioning that while results are presented for an MG with two DGs, the proposed method is general, and similar results can be achieved when the MG comprises of multiple DGs at various locations.

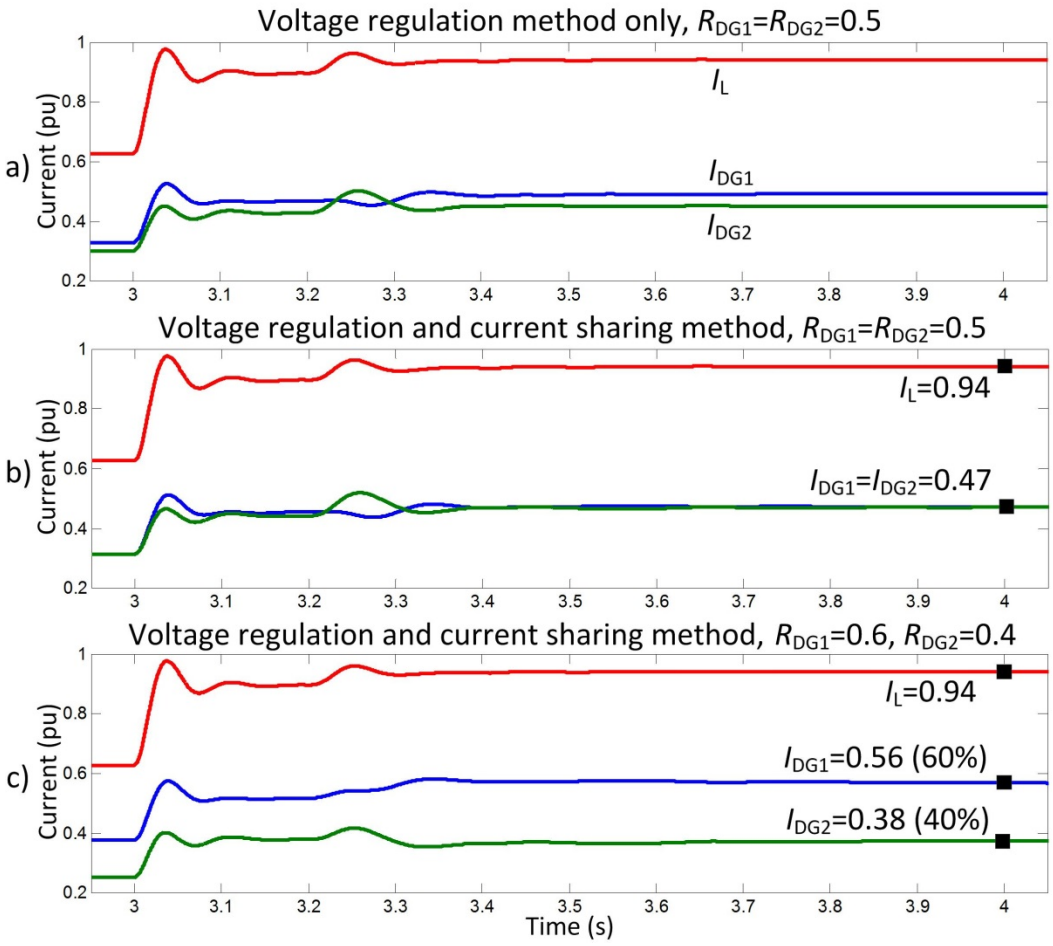

Figure 4.9 Variations in load current and the DG output currents after an increase in the load demand: (a) when only the voltage regulation technique is in operation, (b) using the proposed technique when all DGs have the same ratio, and (c) using the proposed technique when DGs have different ratios.

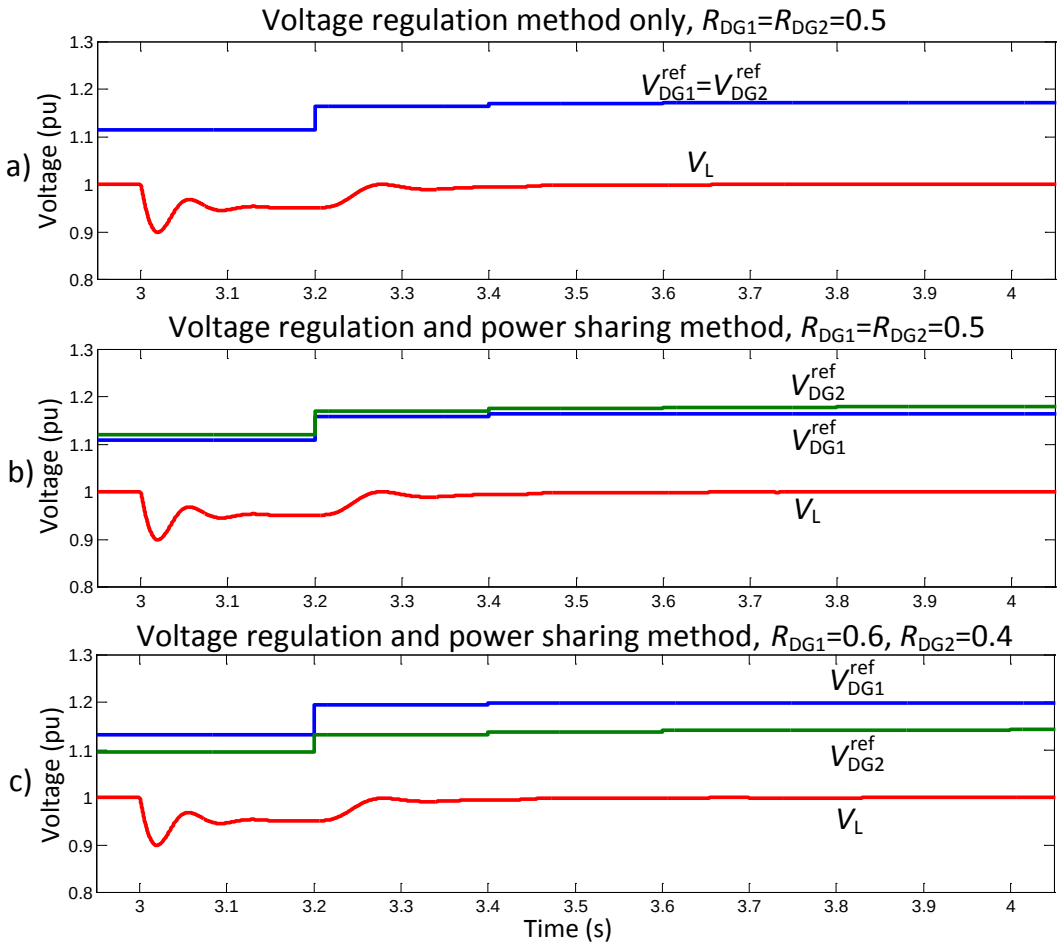

Figure 4.10 Variations in load point voltage and DG output voltages after an increase in load demand: (a) when only the voltage regulation technique is in operation, (b) using the proposed technique when all DGs have the same ratio, and (c) using the proposed technique when DGs have different ratios.

Table 4.5 Considered parameters for Case-B-D.

DG_1	$L_i = 4\text{mH}$, $C_i = 150\text{mF}$, $R_i = 0.3\Omega$, $R_C = 0.8\Omega$, $L_C = 10\text{mH}$
DG_2	$L_i = 4\text{mH}$, $C_i = 100\text{mF}$, $R_i = 0.1\Omega$, $R_C = 1.1\Omega$, $L_C = 10\text{mH}$
Load	$R_L = 5\Omega$, $L_L = 10\text{mH}$, $C_L = 1\text{mF}$

4.4.3. Case-C: Power Sharing among DGs

The simulation in Case-B is repeated in Case-C to assess the proposed power sharing technique. Case-B uses the proposed load current sharing technique of (4.6) – (4.8), while Case-C uses the proposed power sharing technique presented in (4.9) – (4.11). The DC MG of Figure 4.3 is simulated using the

technical parameters of Table 4.5, assuming equal ratios for the DGs ($R_{\mathrm{DG1}} = R_{\mathrm{DG1}} = 0.5$). The performance of the proposed power sharing technique is evaluated under the same demand variation investigated in Case-B.

The MG is assumed to be at steady-state condition when a load demand increase of 33.3% is applied at t = 3s. Figure 4.11 shows the simulation results of the proposed load current sharing technique, while Figure 4.12 depicts the simulation results of the proposed power sharing technique. It can be seen that both proposed methods are successful in maintaining the load voltage within acceptable limits during loading variations. In addition, the proposed techniques are also successful in forcing DGs to generate current and power proportionally to their designated ratio.

The generated voltage of each DG is unequal ($V_{\mathrm{DG1}} \neq V_{\mathrm{DG2}}$); this is to compensate for the unequal line resistance as presented in Figure 4.10 (b). However, as shown in Figure 4.11 (a) and Figure 4.12 (b), both the current and power generated by the DGs are proportional to their designated ratio. Figure 4.11 (b) shows a slight difference in generated power between DG_1 and DG_2, whereas Figure 4.11 (a) shows that the generated DG currents — using the same R_{DG} ratio, and with the proposed current load sharing — are equal. When the proposed power sharing method is applied, as shown in Figure 4.12 (b), the generated powers are equal. However, when there are unequal line resistances, as can be seen in Figure 4.12 (a), the generated currents become unequal. These results also show that there are no circulating currents among the DGs, even though they are not working at the same voltage level.

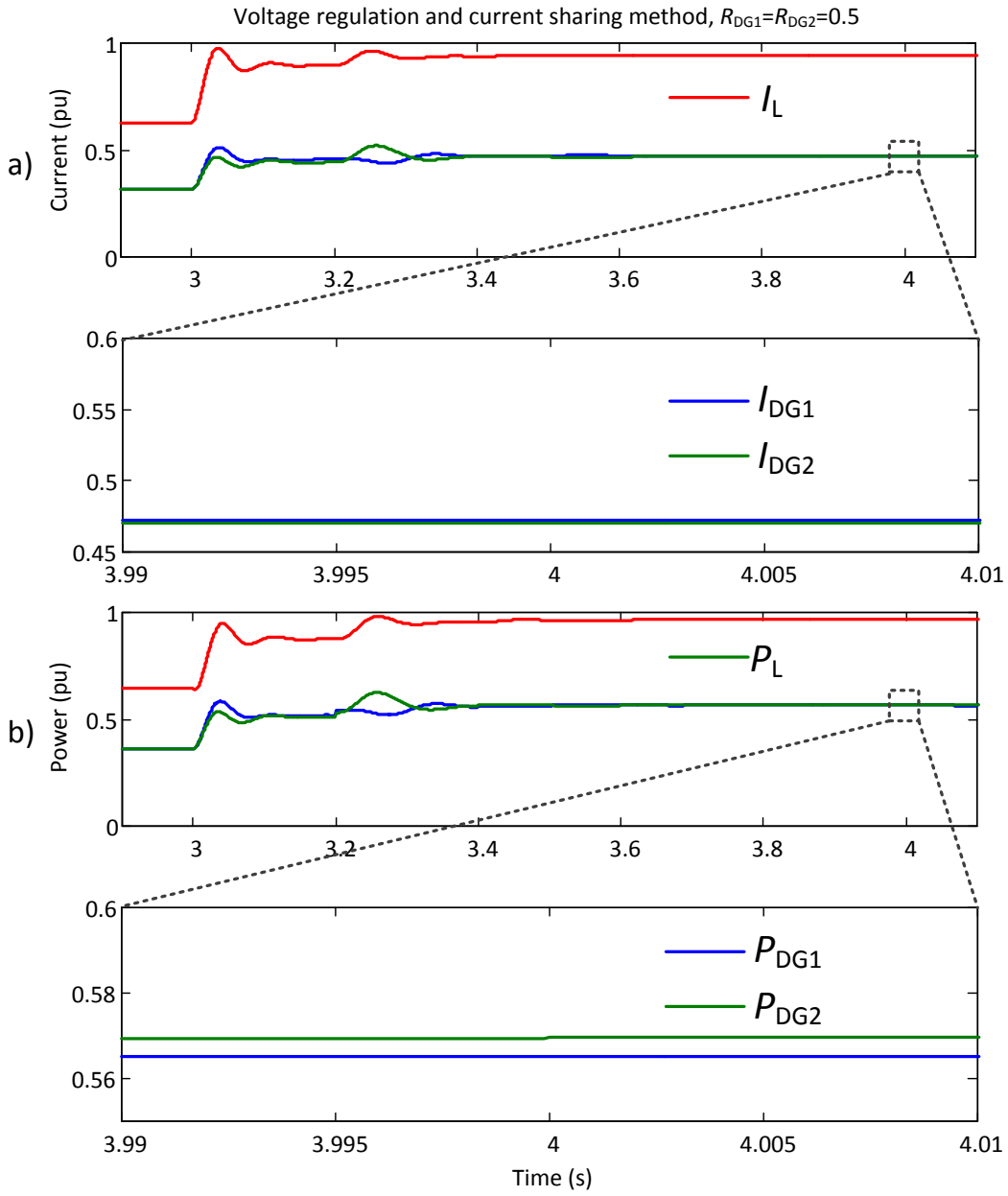

Figure 4.11 Simulation results of the proposed load current sharing technique: (a) DGs output currents, (b) DGs output powers when DGs have equal ratios.

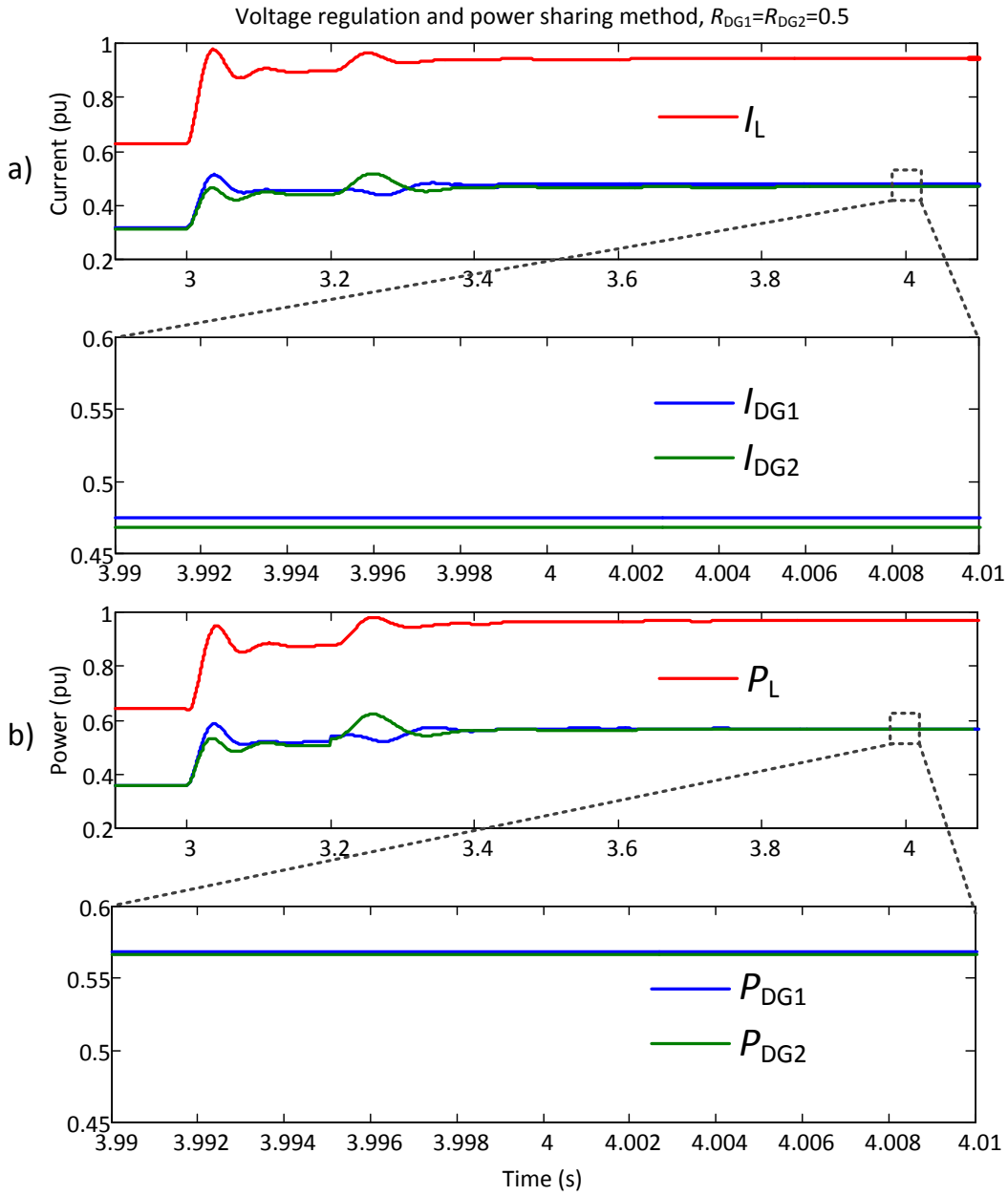

Figure 4.12 Simulation results of the proposed power sharing technique: (a) DGs output currents, (b) DGs output powers when DGs have equal ratios.

4.4.4. Case-D: Impact of DGs with Plug-and-Play Characteristics

Renewable energy resources have an intermittent nature and can function as plug-and-play DGs, depending on the environmental conditions. Also, while energy storage is considered a DG in a discharging mode, it acts as a load when being charged. To evaluate the performance of the proposed technique when plugging in and out of a DG, and assuming that DG_1 has a plug-and-play

characteristic, the MG configuration of Figure 4.3 is simulated with the technical parameters of Table 4.5. DG_1 is assumed to be unplugged from the MG at t = 3s and re-plugged at t = 7s. Both the current and voltage profiles of the considered MG are presented in Figure 4.13. It can be seen that during the plugging in and out periods of the DG, which causes a transient for a few cycles, the proposed algorithm is capable of regulating the load point voltage at the designated level. For $3 < t < 7$, the output current of DG_1 is equal to zero and only DG_2 supplies the load; its output voltage increases to 1.12 pu to compensate for the absence of DG_1. When DG_1 is re-plugged, the DG output currents display proper sharing of the demand (equal DG ratios are assumed in this case study), while the output voltage of DG_2 decreases to 1.06 pu.

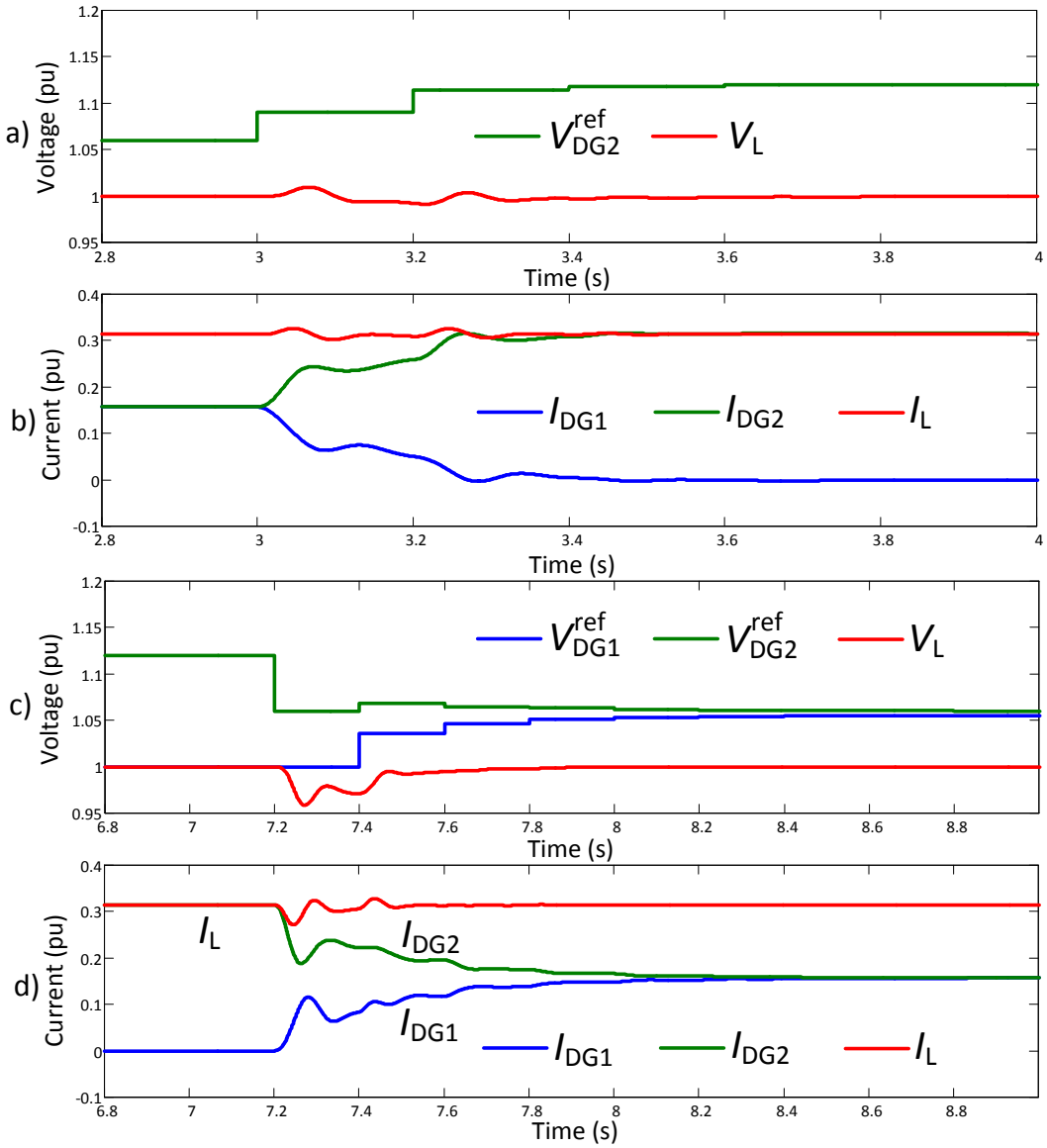

Figure 4.13 MG voltage and current profiles during (a)-(b): unplugging a DG, (c)-(d): re-plugging the DG.

4.4.5. Case-E: Presence of Multiple Loads

This case study considers the MG of Figure 4.14, which consists of two DGs, each with an equal desired output current/power ratio ($R_{DG1} = R_{DG1} = 0.5$), and 4 distributed loads (L1 to L4) with the technical parameters in Table 4.6. In this configuration, the dissimilarity between load voltages is inevitable due to the nature of the system; however, the voltages should not exceed the acceptable limit during fluctuation of the load demands. Also, the change in demand across any of the loads will lead to a change in the MG voltage profile. To evaluate the

performance of the proposed technique for such a configuration, the demand of L1 is increased by 50% at t = 2s, followed by a 50% increase in demand of L3 at t = 6s. Under this scenario, Figure 4.15 shows the load voltages, output voltages, and DG currents. The figure also reveals that the proposed technique can retain all load voltages at the desired level (within ±5%) while maintaining DG generated currents at the desired ratio and regardless of the load dynamics. As shown in Figure 4.15(b), and to achieve the designated current ratio, the DG output voltages are different; this is due to the unbalanced load demand.

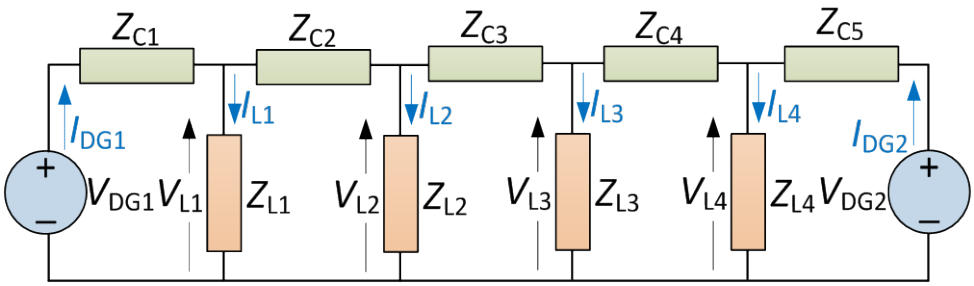

Figure 4.14 A DC MG with multiple loads.

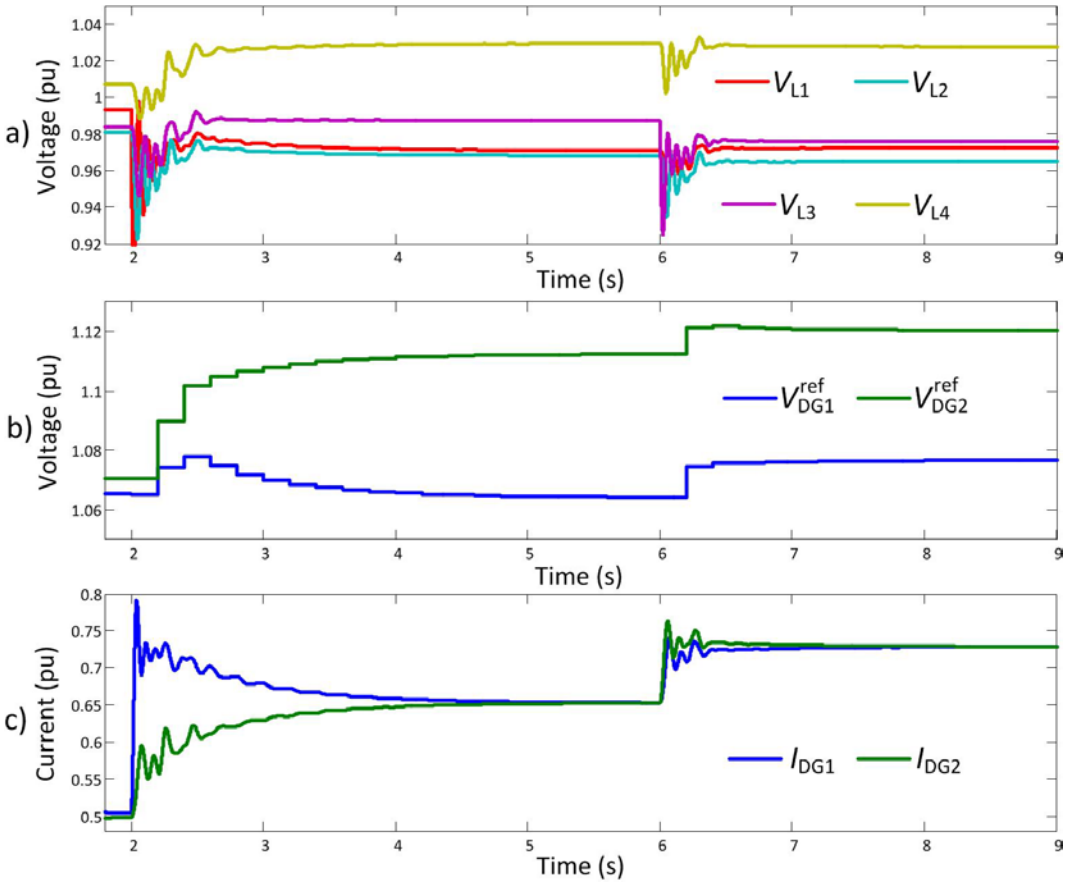

Figure 4.15 Voltage and current profiles of DC MG with multiple load points.

Table 4.6 Considered parameters for Case-E.

DG_1	$L_i = 4\text{mH}, C_i = 150\text{mF}, R_i = 0.15\Omega$
DG_2	$L_i = 4\text{mH}, C_i = 100\text{mF}, R_i = 0.1\Omega$
Load	$R_{L1} = 10\Omega,\ L_{L1} = 10\text{mH},\ C_{L1} = 1\text{mF},\ R_{L2} = 14\Omega,\ L_{L2} = 10\text{mH},\ C_{L2} = 1\text{mF},\ R_{L3} = 20\Omega,\ L_{L3} = 10\text{mH},\ C_{L3} = 1\text{mF},\ R_{L4} = 10\Omega,\ L_{L4} = 10\text{mH}, C_{L4} = 1\text{mF},$
Line	$R_{C1} = 0.3\Omega,\ L_{C1} = 10\text{mH},\ R_{C2} = 0.2\Omega,\ L_{C2} = 10\text{mH},\ R_{C3} = 0.35\Omega,\ L_{C3} = 10\text{mH}, R_{C4} = 0.4\Omega, L_{C4} = 10\text{mH}, R_{C5} = 0.3\Omega, L_{C5} = 10\text{mH},$

4.4.6. Case-F: Impact of Different Time Delays

To investigate the impact of time delays on the proposed technique, the DC MG of Case-A is simulated with time delays of $T_P = 50$ ms and 200 ms, and the results are depicted in Figure 4.16. It can be seen from this figure that if the time delay is less than the required processing time of the converter, as shown in Figure 4.16(a), the voltages of the system will experience substantial oscillations. A better dynamic response is achieved for a delay time larger than the processing time of the converter, as seen in Figure 4.16(b).

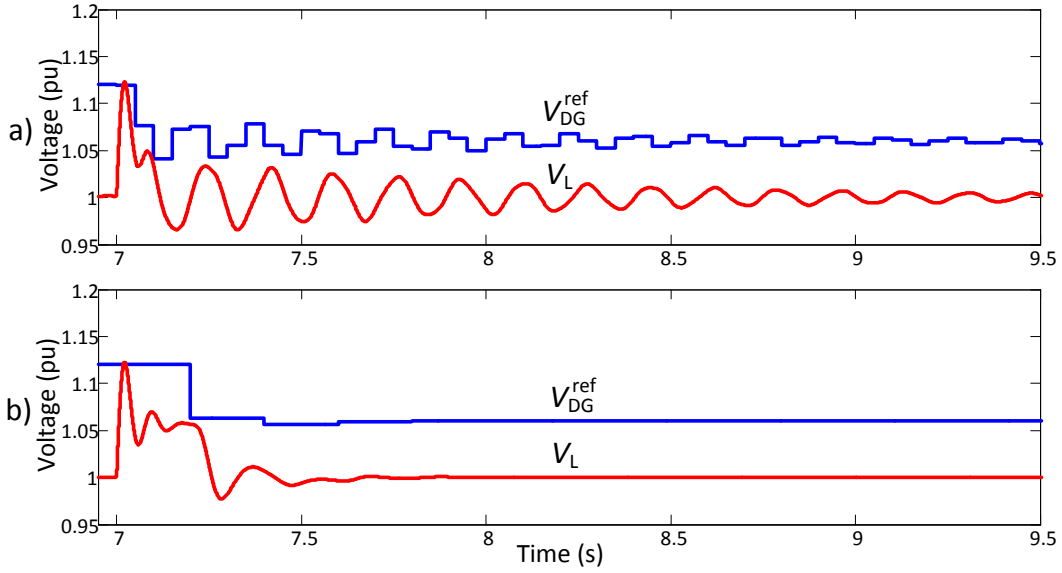

Figure 4.16 Variations in DG output voltage and reference, as well as the voltage of the load point, assuming a) $T_P < T_C$, b) $T_P > T_C$.

4.4.7. Case-G: Impact of Communication Failure

Operating under the proposed technique, a simulation of communication failure on the system of Case-B assesses the impact on MG performance. During 2.8s < t < 6.5s, data packet transmission is missed between load and DG_2, and as a consequence, in this period, V_L is not received by the DG_2 controller. In the proposed technique, all received data are saved in the MG central controller and DG controllers, and are used in the calculations until a new updated value is received. Upon failure in the communication system, the proposed control technique continues to function using the previously stored data. Figure 4.17 presents the MG voltage and current profiles during a communication failure. The results of this figure show that the proposed technique can not only retain the load voltage at a desired level, but also maintain the DG generated currents in a proportional ratio. The load voltage is healed at t = 4.5s, and the currents are retained at t = 5.8s. It can be seen that compared to a system with a healthy communication link, the required times are longer here. Also, even though the proposed technique is discussed and proposed in a centralised communication scheme, it does not rely on a single communication and can therefore be implemented in real application.

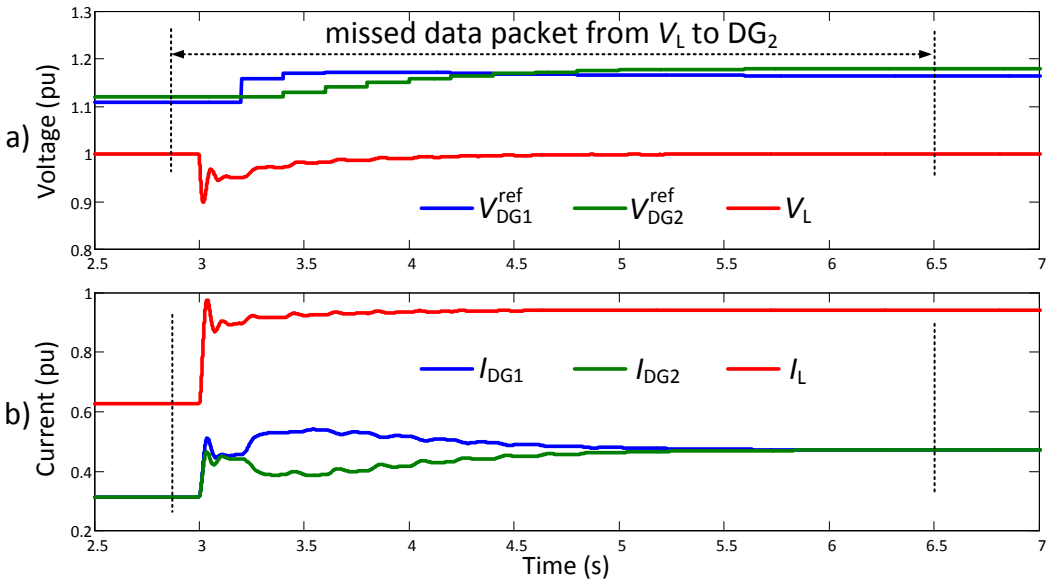

Figure 4.17 Voltage and current profiles of the considered MG during data communication failure (missed data packet).

4.5. Summary

This chapter proposes a new technique, which simultaneously facilitates voltage regulation at DC MG load points and achieves proper power/current sharing among the existing active DGs. Results indicate that the technique can retain MG voltage within acceptable limits while adjusting the DG output currents/powers to realize the desired ratio; this is irrespective of load demand variations and the unequal and unknown impedances of the MG lines. The chapter also proposes a data communication scheme for deployment of the technique, verifying the successful dynamic operation of the system and considering the maximum processing delay time imposed by the communication system. Using the proposed technique, the studies also illustrate successful MG dynamic operation under different loading conditions, various load types, failures in the data communication system, and in the presence of DGs with plug-and-play characteristics. The proposed technique considers for practically implementations, and can be adopted for any DC MG configuration regardless of the number and locations of the DGs and MG loads. The proposed results also reveal that the larger communication delay does not effect on the stability of the DC MG system.

Chapter 5: Voltage Regulation and Power Sharing for Various Circuit Configurations of the DC Microgrid

In this Chapter, the proposed technique for voltage regulation and power sharing in DC MG which is discussed in Chapter 4 is further analysed in various possibility of DC configurations. Each configuration has special characteristic which has big impact on the voltage regulation and power sharing; and is discussed and simulated in this Chapter.

5.1. Various DC Microgrid Configurations

The types of connection between MG loads and DGs can vary greatly. However, in this thesis, only the main configurations are presented, simulated and discussed — those which have big impacts and unique characteristics for voltage regulation and power/current sharing. By introducing renewable energies, ESSs, or EVs — which can act as plug-and-play sources or loads in the MG — MG configuration is subject to dynamic change based on the status of those devices. More complex configurations can be achieved by combining two or more configurations. The DC MG configurations that are under consideration in this thesis are briefly described below.

5.1.1. Configuration-A

The simplest configuration of a DC MG, which consists of one DG and one load only, is illustrated schematically in Figure 5.1. In this configuration, voltage at the load point and DG output current are influenced by output voltage and DG current, respectively. All load demand is supplied by the source, while fetched voltage, to be processed by the DG controller, is equal to the voltage of the load point. In Figure 5.1, R_{i}, L_{i} and C_{i} represent the internal impedance of the converter filter, while R_{C} and L_{C} represent the impedance of the MG feeder.

In this chapter, the proposed voltage regulation and power/current sharing technique of (4.5) (discussed further in Chapter 4) can be rewritten as:

$$V_{\mathrm{DG}k}^{\mathrm{ref}} = V_{\mathrm{DG}k} + R_{\mathrm{DG}k}\, N\, \Delta V_{\mathrm{L}}^{\mathrm{fb}} \tag{5.1}$$

where $\Delta V_{\mathrm{L}}^{\mathrm{fb}} = \Delta V_{\mathrm{L1}}$

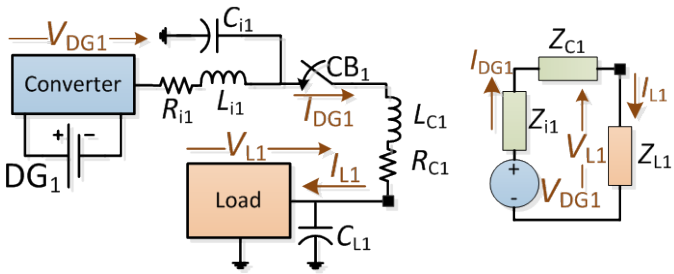

Figure 5.1 Configuration-A: DC MG circuit under consideration with single load point, and simplified circuit.

5.1.2. Configuration-B

In the configuration shown in Figure 5.2, a DG supplies multiple (*J*) parallel-connected loads. Due to the nature of the radial system, voltage deviation between load points is inevitable during fluctuation of load demands; however, it should not exceed the acceptable limit (e.g. ±5%). In this configuration, a change of demand in one of the loads will lead to a change in the voltage profile across the MG network.

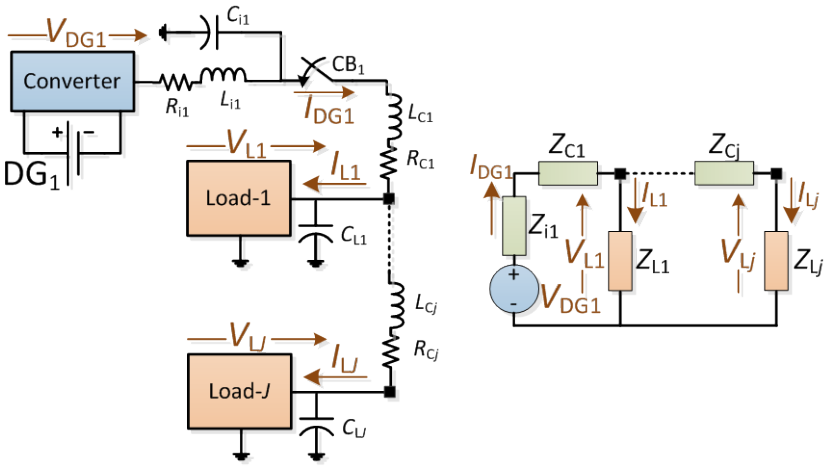

Figure 5.2 Configuration-B: DC MG with parallel load points, and simplified circuit.

To prevent over- or under-voltage violation at any of the load points, a

single load voltage feedback is required to be processed by the DG controller. The feedback load voltage ($V_{\mathrm{L}}^{\mathrm{fb}}$) can be used for increasing or decreasing the output voltage of the DG, and thus affecting its output power. The voltage value of $V_{\mathrm{L}}^{\mathrm{fb}}$can be equal to the closest load to the DG (Method-1), the farthest load to the DG (Method-2), the middle-point load (Method-3), the average of all loads (Method-4), or the average of the closest and farthest loads (Method-5). This is because — when there are multiple loads, each with a different voltage of ($V_{\mathrm{L}1}.V_{\mathrm{L}j}$) — only one $V_{\mathrm{L}}^{\mathrm{fb}}$ can be processed by the DGs. In this configuration, the $V_{\mathrm{L}}^{\mathrm{fb}}$ of the proposed voltage regulation and power/current sharing in (5.1) can be summarised as below:

$$V_{\mathrm{L}}^{\mathrm{fb}} = \begin{cases} V_{\mathrm{L}1} & \mathrm{Method}-1 \\ V_{\mathrm{L}j} & \mathrm{Method}-2 \\ V_{\mathrm{L}j/2} & \mathrm{Method}-3 \\ \mathrm{avg}\left(V_{\mathrm{L}y}\right) \quad \forall y \in \{1, \cdots j\} & \mathrm{Method}-4 \\ \mathrm{avg}\left(V_{\mathrm{L}1}, V_{\mathrm{L}j}\right) & \mathrm{Method}-5 \end{cases} \tag{5.2}$$

It is noted that a larger number of feedback signals will be more accurate. However, this increases the cost and number of required sensors, and can also complicate the proposed control and communication systems. In (5.2), Methods-1 to -3 require only one voltage sensor, Method-5 requires two voltage sensors (regardless the number of loads in the MG), and Method-4 requires a voltage sensor for each load (as proposed in [41], [46], [56], [113]); thus, Method-4 is the most expensive technique.

5.1.3. Configuration-C

This configuration is an expansion of Configuration-B, in which loads are distributed in Branch-1 (B_1) to Branch-M (B_M), and where $M \geq 2$ (as shown in Figure 5.3). Similar to Configuration-B, the voltage deviation among branches in this configuration is unavoidable. Any changes in the load demand can lead to changes in the voltage profile across the MG network; however, the biggest impact of changes in the load demand is within the same branch network. Small and internal DG impedance leads to a bigger independency for each branch, so when this internal impedance is neglected, changes in the load demand affect its own branch only and not the loads of others.

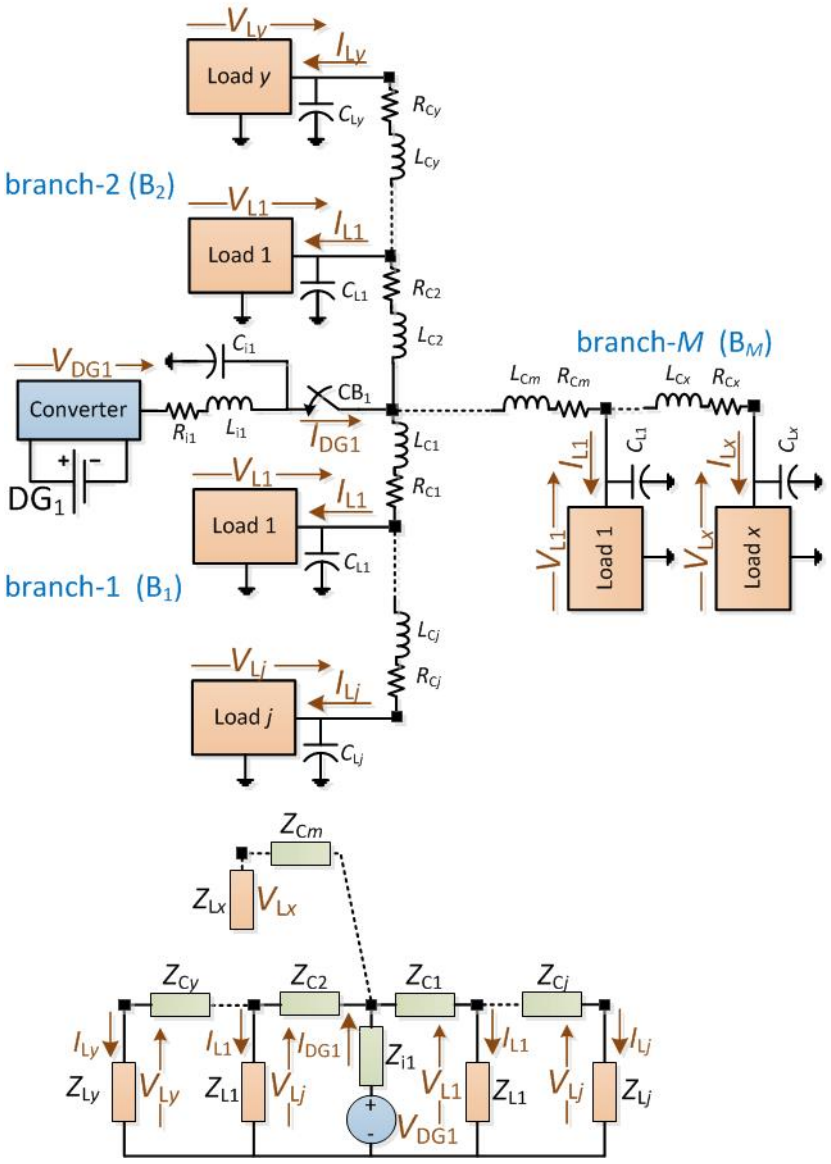

Figure 5.3 Configuration-C: DC MG with branch load points, and simplified circuit.

To minimise over- or under-voltage variation in the MG, feedback load voltage ($V_{\mathrm{L}}^{\mathrm{fb}}$) in (5.1) is calculated using one of the methods below:

$$V_{\mathrm{L}}^{\mathrm{fb}} = \begin{cases} \mathrm{avg}(V_{\mathrm{L}j}) \quad \forall j \in \{1, \cdots M\} & \mathrm{Method}-6 \\ \mathrm{avg}(V_{\mathrm{L}}^{\min}, V_{\mathrm{L}}^{\max}) & \mathrm{Method}-7 \end{cases} \tag{5.3}$$

where $V_{\mathrm{L}j}$ is the average load voltage feedback from all branches.

The load voltage feedback from each branch can be determined from (5.2), and $V_{\mathrm{L}}^{\min}$ and $V_{\mathrm{L}}^{\max}$ are the minimum and maximum values of MG load voltage, respectively.

5.1.4. Configuration-D

In this configuration, the MG comprises of N DGs ($N \geq 2$) that supply the load. As discussed in Configuration-A, -B and -C, the load can either be a single load, multiple parallel loads, or multiple branches of loads. The load is physically located between all DGs; thus, it is in parallel with every DG.

Figure 5.4 illustrates schematically an MG with this configuration, when multiple DGs and a single load point are used. Figure 5.5 shows a schematic diagram of when multiple load points are used. In the presence of ESSs during charging mode, the Configuration-D becomes identical to Configuration-B. Also in Configuration-D, the feedback load voltage ($V_{\mathrm{L}}^{\mathrm{fb}}$) in (5.1) can be formed either as a single load system, a closest load voltage, the average of all load voltages, or as an average of maximum and minimum load voltages for multiple loads, as described below:

$$V_{\mathrm{L}}^{\mathrm{fb}} = \begin{cases} V_{\mathrm{L}} & \mathrm{Method}-8 \\ V_{\mathrm{L}j} \quad \forall j \in \text{load in } \mathrm{DG}_j & \mathrm{Method}-9 \\ \mathrm{avg}\left(V_{\mathrm{L}j}\right) \quad \forall j \in \{1, \cdots n\} & \mathrm{Method}-10 \\ \mathrm{avg}(V_{\mathrm{L}}^{\min}, V_{\mathrm{L}}^{\max}) & \mathrm{Method}-11 \end{cases} \tag{5.4}$$

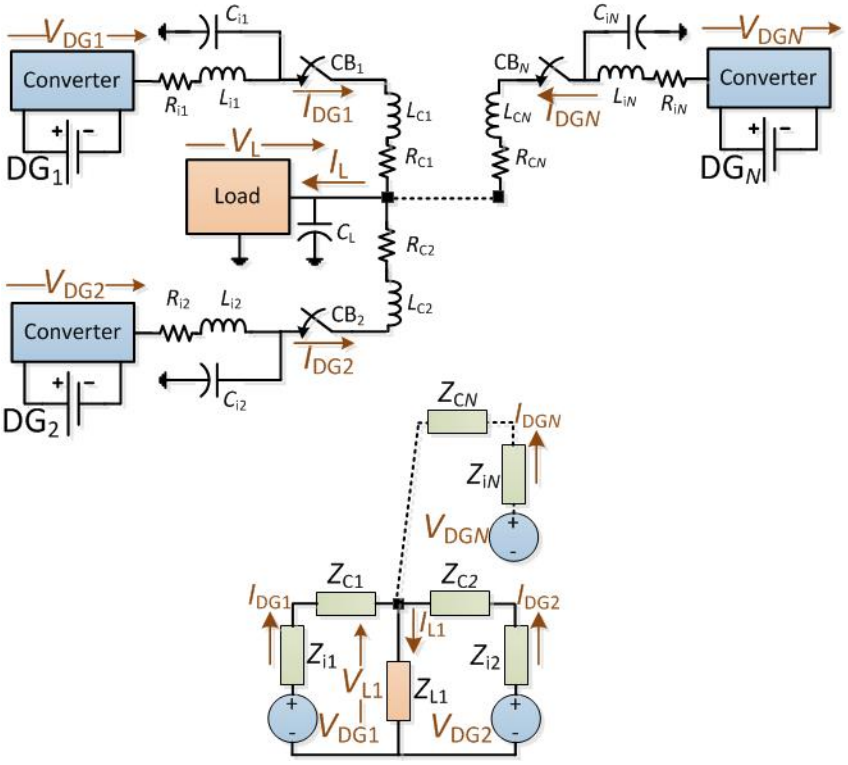

Figure 5.4 Configuration-D: DC MG with multiple DGs, a single load point between DGs and simplified circuit.

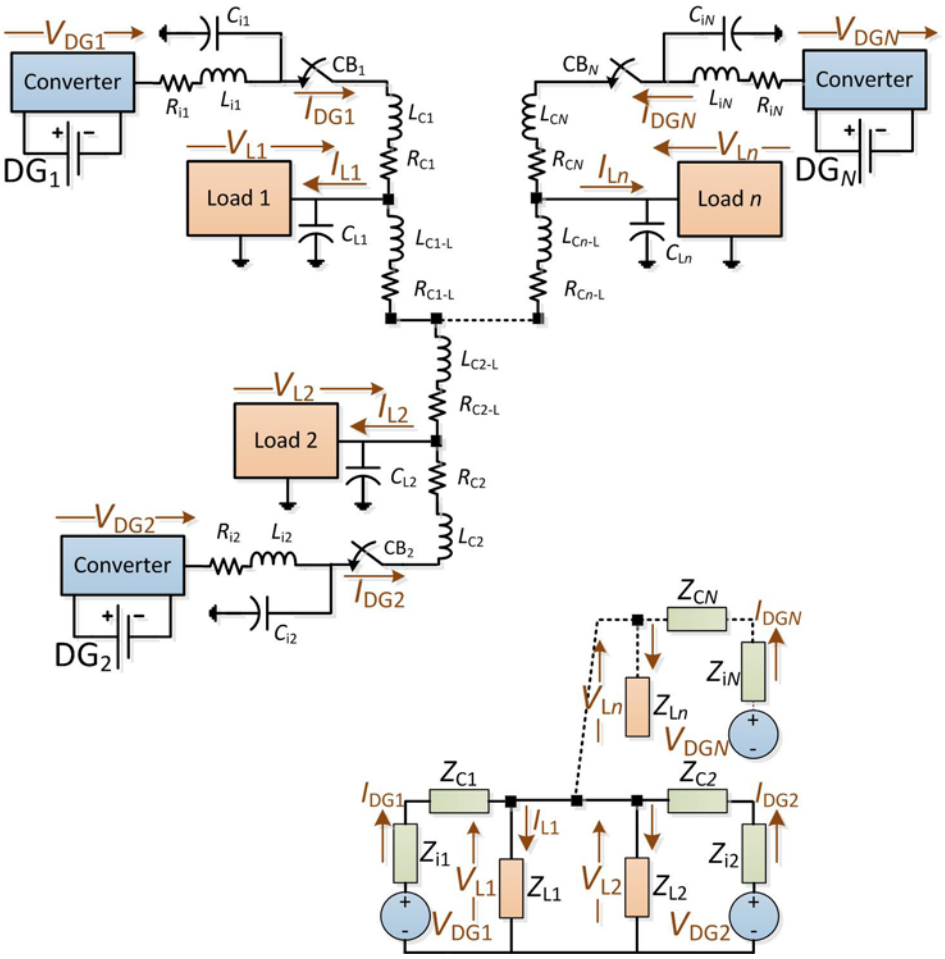

Figure 5.5 Configuration-D: DC MG with multiple DGs, multiple load points between DGs, and simplified circuit.

For a steady-state condition, the voltage and current shown in Figure 5.4 can be expressed as:

$$I_{\mathrm{DG}k} = \frac{V_{\mathrm{DG}k} - V_{\mathrm{L}}}{Z_{\mathrm{DG}k}} \tag{5.5}$$

$$V_{\mathrm{L}} = \sum_{i=1}^{N} \frac{V_{\mathrm{DG}i} \prod_{j=1, j\neq i}^{N} Z_{\mathrm{DG}j}}{\prod_{j=1}^{N} Z_{\mathrm{DG}j}} Z_{\mathrm{L}} \tag{5.6}$$

where $Z_{\mathrm{DG}} = \sum Z_{\mathrm{i}}$, Z_{C} is the impedance of the line connecting the DG to the load, and Z_{i} is the equivalent impedance of the filter and converter.

According to (5.5), a circulating current occurs when $I_{\mathrm{DG}k} < 0$, which will only take place if $V_{\mathrm{L}} > V_{\mathrm{DG}k}$; otherwise, there is no circulating current in the DG_k. This configuration can then adopt a power sharing mechanism in which the DGs

can generate unequal voltage magnitude without producing circulating current.

Similar to Figure 5.4, in the multiple load system of Figure 5.5, DGs can generate unequal voltage magnitude and share the total load currents. However, a circulating current occurs only when $V_{\mathrm{L}k} > V_{\mathrm{DG}k}$ and the power flows from the higher V_{L} to the lower one.

Table 5.1 summarises various operating conditions for the *N* DGs shown in Figure 5.4 and Figure 5.5, along with the possibilities of circulating current generation, voltage regulation, and also power sharing capabilities.

Table 5.1 DC MGs Configuration-D, showing possibility of current circulation (CC), voltage regulation (VR) at the load point(s), and power sharing (PS) among DGs.

DGs voltage	V_{L} condition	CC	VR	PS
$\bigcup_{j,k=1,j\neq k}^{N} V_{\mathrm{DGj}} = V_{\mathrm{DGk}}$	$\bigcup_{k=1}^{N} V_{\mathrm{DG}k} > V_{\mathrm{Lk}}$	×	✓	✓
$\bigcap_{j,k=1,j\neq k}^{N} V_{\mathrm{DGj}} \neq V_{\mathrm{DGk}}$	$\bigcup_{k=1}^{N} V_{\mathrm{DG}k} > V_{\mathrm{Lk}}$	×	✓	✓
	$\bigcup_{k=1}^{N} V_{\mathrm{DG}k} < V_{\mathrm{Lk}}$	✓	✓	✓

× : No, ✓ : Yes.

5.1.5. Configuration-E

In this configuration, similar to Configuration-D, the MG is composed of $N \geq 2$ DGs, and one or multiple loads in one or more branches (as discussed in Configuration-A, -B and -C). However, unlike in Configuration-D, the load in Configuration-E is located in the external area of the DGs with a single DG load-side and multiple DGs load-side; this is shown in in Figure 5.6 and Figure 5.7, respectively. The load is in parallel with the closest DG, and the closest DG is in parallel with the rest of the MG DGs. This configuration can be expressed as:

$$I_{\mathrm{L}k} = I_{\mathrm{DG}k} + \sum_{j,k=1,j\neq k}^{N} \frac{V_{\mathrm{DG}j}^{\mathrm{Bus}} - V_{\mathrm{DG}k}^{\mathrm{Bus}}}{Z_C} \tag{5.7}$$

where $V_{\mathrm{DG}k}^{\mathrm{Bus}} = V_{\mathrm{DG}k} - I_{\mathrm{DG}k}\, Z_{\mathrm{i}k}$, and Z_{C} are the total impedances of the lines connecting the DG to other DGs.

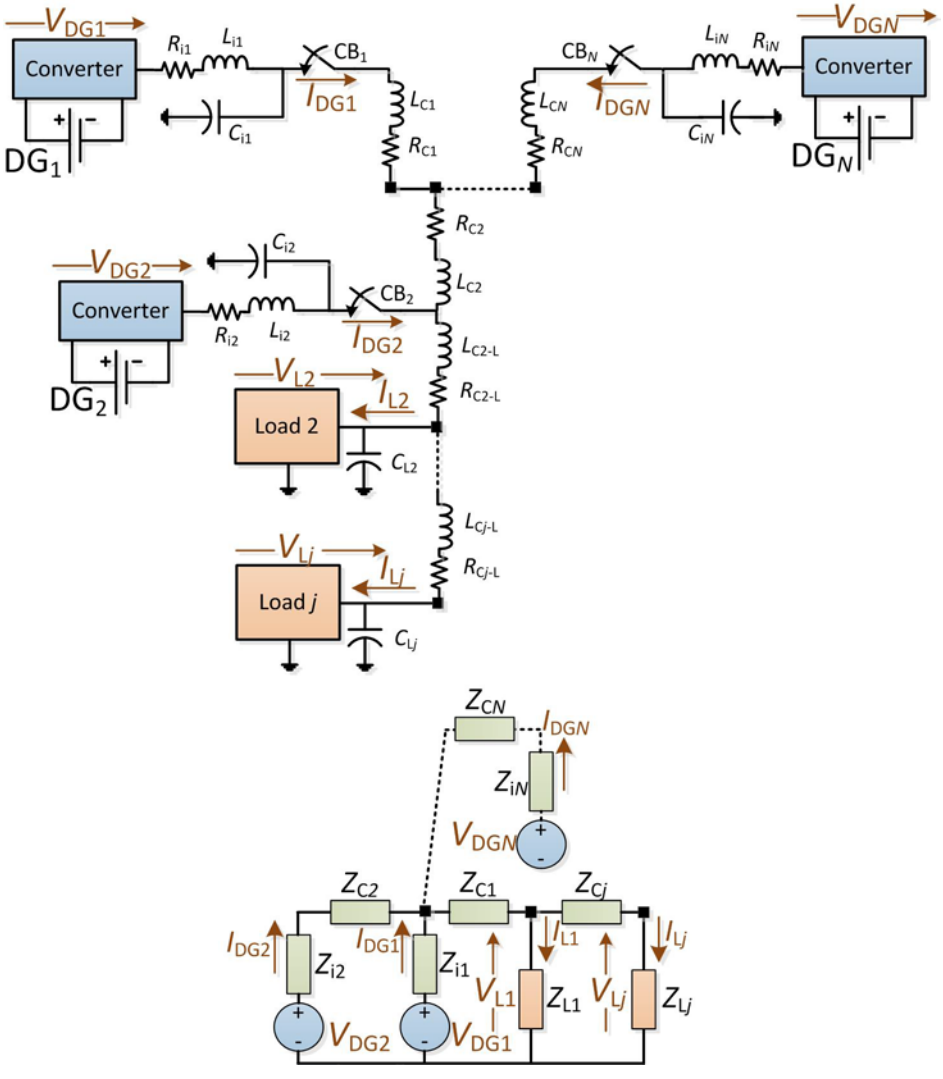

Figure 5.6 Configuration-E: DC MG with parallel multiple DGs, single-side loads, and simplified circuit.

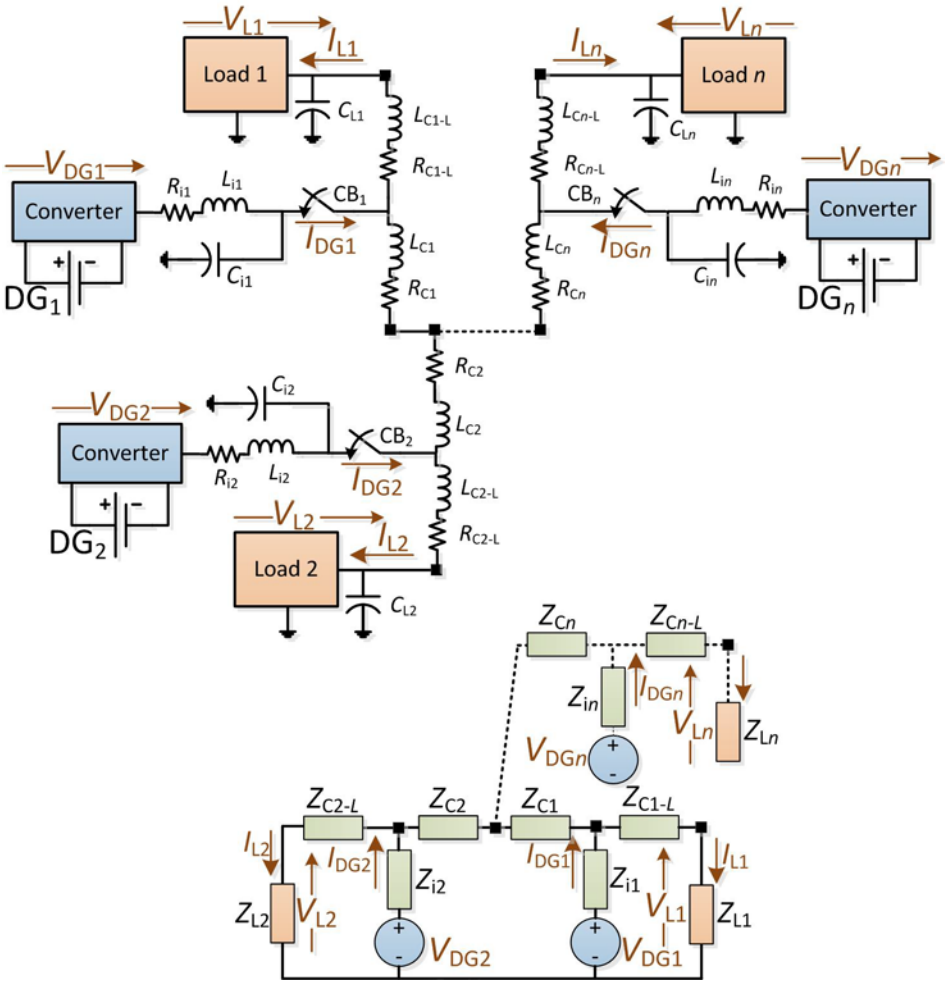

Figure 5.7 Configuration-E: DC MG with parallel multiple DGs, multiple load points, and simplified circuit.

According to (5.7), the current at each load point is supplied by the current of the closest DG, and also the loop current between the DGs. The loop current is caused by unequal voltage among DGs, and a higher loop current leads to an increased possibility of circulating current in the DG and thus a lower output voltage magnitude. In this configuration, power sharing can take place; however, as presented in Table 5.2, there is a higher possibility of circulating current when compared to Configuration-D.

The feedback voltage methods ($V_{\mathrm{L}}^{\mathrm{fb}}$) in (5.1) that can be applied in this configuration are:

$$V_{\mathrm{L}}^{\mathrm{fb}} = \begin{cases} V_{\mathrm{L}j} & \forall j \in \text{load in } \mathrm{DG}_j \quad \text{Method} - 12 \\ \mathrm{avg}\left(V_{\mathrm{L}j}\right) & \forall j \in \{1, \cdots n\} \quad \text{Method} - 13 \end{cases} \tag{5.8}$$

Table 5.2 DC MGs Configuration-E, showing current circulation, voltage regulation at the load point(s), and power sharing among DGs.

DGs voltage	V_{L} condition	CC	VR	PS
$\bigcup_{j,k=1,j\neq k}^{N} V_{\mathrm{DGj}} = V_{\mathrm{DGk}}$	$\bigcup_{k=1}^{N} V_{\mathrm{DG}k} > V_{\mathrm{Lk}}$	×	✓	×
$\bigcap_{j,k=1,j\neq k}^{N} V_{\mathrm{DGj}} \neq V_{\mathrm{DGk}}$	$\bigcup_{k=1}^{N} V_{\mathrm{DG}k} > V_{\mathrm{Lk}}$	✓	✓	✓
	$\bigcup_{k=1}^{N} V_{\mathrm{DG}k} < V_{\mathrm{Lk}}$	✓	✓	✓

× : No, ✓ : Yes.

5.1.6. Combination of Several Configurations

The DC MG can be formed by combining several configurations, depending on MG capacity and size. As an example, consider a DC MG with four DGs and several load points, with the simplified schematic circuit presented in Figure 5.8. Connecting several DC MGs into the same network will transform and combine many configurations into a single larger DC MG [50], [101], [132].

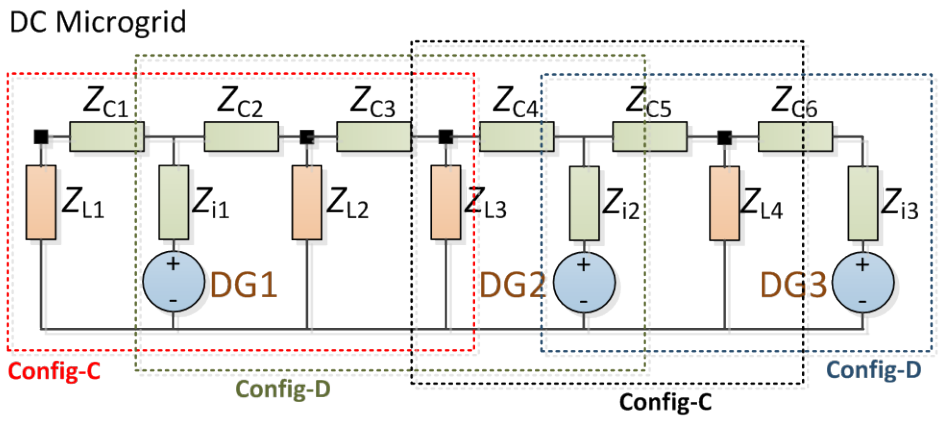

Figure 5.8 Simplified circuit of combination configurations in a DC MG.

Figure 5.8 shows that several configurations can be combined in a DC MG. In this case, Method-1 to Method-13 can be applied and combined. The proposed voltage regulation and power/current sharing in (5.1) for the DC MG described in Figure 5.8 can be illustrated as:

$$V_{\mathrm{DG1}}^{\mathrm{ref}} = V_{\mathrm{DG1}} + R_{\mathrm{DG1}}\, N\, \Delta\mathrm{avg}\left(V_{\mathrm{L}}^{\min}, V_{\mathrm{L}}^{\max}, \forall V_{\mathrm{L}} \in \{V_{\mathrm{L1}} \cdots V_{\mathrm{L3}}\}\right)$$

$$V_{\mathrm{DG2}}^{\mathrm{ref}} = V_{\mathrm{DG2}} + R_{\mathrm{DG2}}\, N\, \Delta\mathrm{avg}\left(V_{\mathrm{L}}^{\min}, V_{\mathrm{L}}^{\max}, \forall V_{\mathrm{L}} \in \{V_{\mathrm{L2}} \cdots V_{\mathrm{L4}}\}\right) \quad (5.9)$$

$$V_{\mathrm{DG3}}^{\mathrm{ref}} = V_{\mathrm{DG3}} + R_{\mathrm{DG3}}\, N\, \Delta\mathrm{avg}\left(V_{\mathrm{L}j}, \forall V_{\mathrm{L}j} \in \{V_{\mathrm{L4}}\}\right)$$

$$V_{\mathrm{DG}k}^{\mathrm{ref}} = V_{\mathrm{DG}k} + R_{\mathrm{DG}k}\, N\, \Delta\mathrm{avg}\left(V_{\mathrm{L}}^{\min}, V_{\mathrm{L}}^{\max}, \forall V_{\mathrm{L}} \in \{V_{\mathrm{L1}} \cdots V_{\mathrm{L4}}\}\right) \quad (5.10)$$

5.2. Performance Evaluation

To evaluate the performance of the proposed technique for voltage regulation and power sharing in a DC MG, the configurations of Section 5.1 are modelled using MATLAB/ Simulink as discussed below. All simulation results are presented as per-unit (pu).

5.2.1. Voltage Regulation in Configuration-A

Consider the network of Figure 5.1 with the technical parameters of Table 5.3. The MG is assumed to be initially at steady-state condition and the voltage of the load point is 1 pu. At t = 2 s, the load demand is assumed to increase by 33.3%, which as shown in Figure 5.9, results in a drop to the load point voltage to 0.908 pu. The load voltage will remain at this level if no voltage regulation technique is adopted. However, when the proposed voltage regulation technique is applied, the output voltage of the DG is controlled and regulated to a new and higher level (within the capacity limits of the DG), and thus the voltage of the load point can be retained at the desired level of 1 pu at t = 2.8 s. As expected, the output voltage of the DG increases to 1.18 pu to push the load point voltage to the desired level. The load demand is returned back to the previous value (i.e. there is a decrease in load demand) after t = 5 s. Figure 5.9 also reveals that after fluctuation, the load demand is only required to regulate the voltage load three times; therefore, the proposed voltage regulation technique is a very fast response method.

Table 5.3 Technical parameters of the network of Figure 5.1.

System base parameters	220 V, 70 A, 15 kW
MG line impedance	$R_{\mathrm{C}} = 0.5\ \Omega$, $L_{\mathrm{C}} = 10$ mH
MG load	$R_{\mathrm{L}} = 5\ \Omega$, $L_{\mathrm{L}} = 10$ mH, $C_{\mathrm{L}} = 1$ mF
dc/dc converter	$L_{\mathrm{i}} = 4$ mH, $C_{\mathrm{i}} = 1.5$ mF, $R_{\mathrm{i}} = 0.1\ \Omega$
T_{P}	200 ms

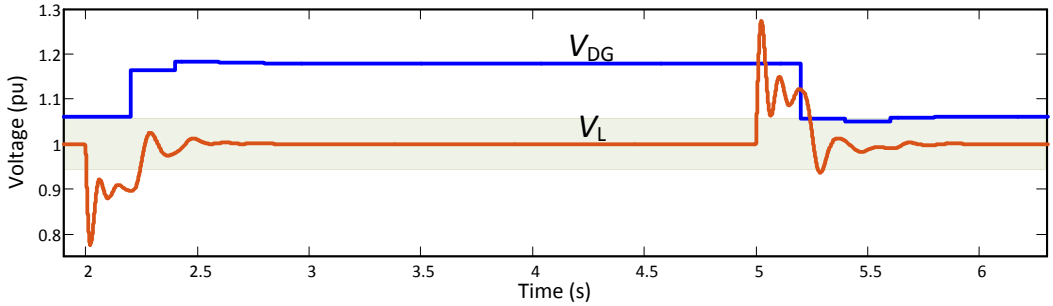

Figure 5.9 Voltage profiles in Configuration-A after an increase and decrease in load demand.

5.2.2. Voltage Regulation in Configuration-B

Assume the network of Figure 5.2 with three loads is at steady-state condition. Table 5.4 represents the technical parameters while line and load impedance is unequal. Using the voltage regulation technique from the proposed Method-1 to Method-5 in (5.2), the performance of the steady-state system is simulated and analysed. The network is analysed under eight different loading scenarios, each derived from a combinations of loads, as shown in Table 5.4. The symbols “L” and “H” represent low and high load demand, respectively, and the high load demand is three times higher than the low load demand. Figure 5.5 also shows that the maximum and minimum voltage profiles across all loads are measured to determine the voltage outside the limits. The graphical signal of the steady-state load voltage profiles is presented in Figure 5.10.

Table 5.4 Technical parameters of the network of Configuration-B.

MG line impedance	$R_{C1} = 0.7\ \Omega$, $L_{C1,2,3} = 10$ mH, $R_{C2} = 0.3\ \Omega$, $R_{C3} = 0.4\ \Omega$
MG load	$R_{L1} = 30\ \Omega$, $R_{L2} = 25\ \Omega$,$R_{L3} = 35\ \Omega$, $L_{L1,2,3} = 10$ mH, $C_{L1,2,3} = 1$ mF
dc/dc converter	$L_i = 4$ mH, $C_i = 1.5$ mF, $R_i = 0.1\ \Omega$

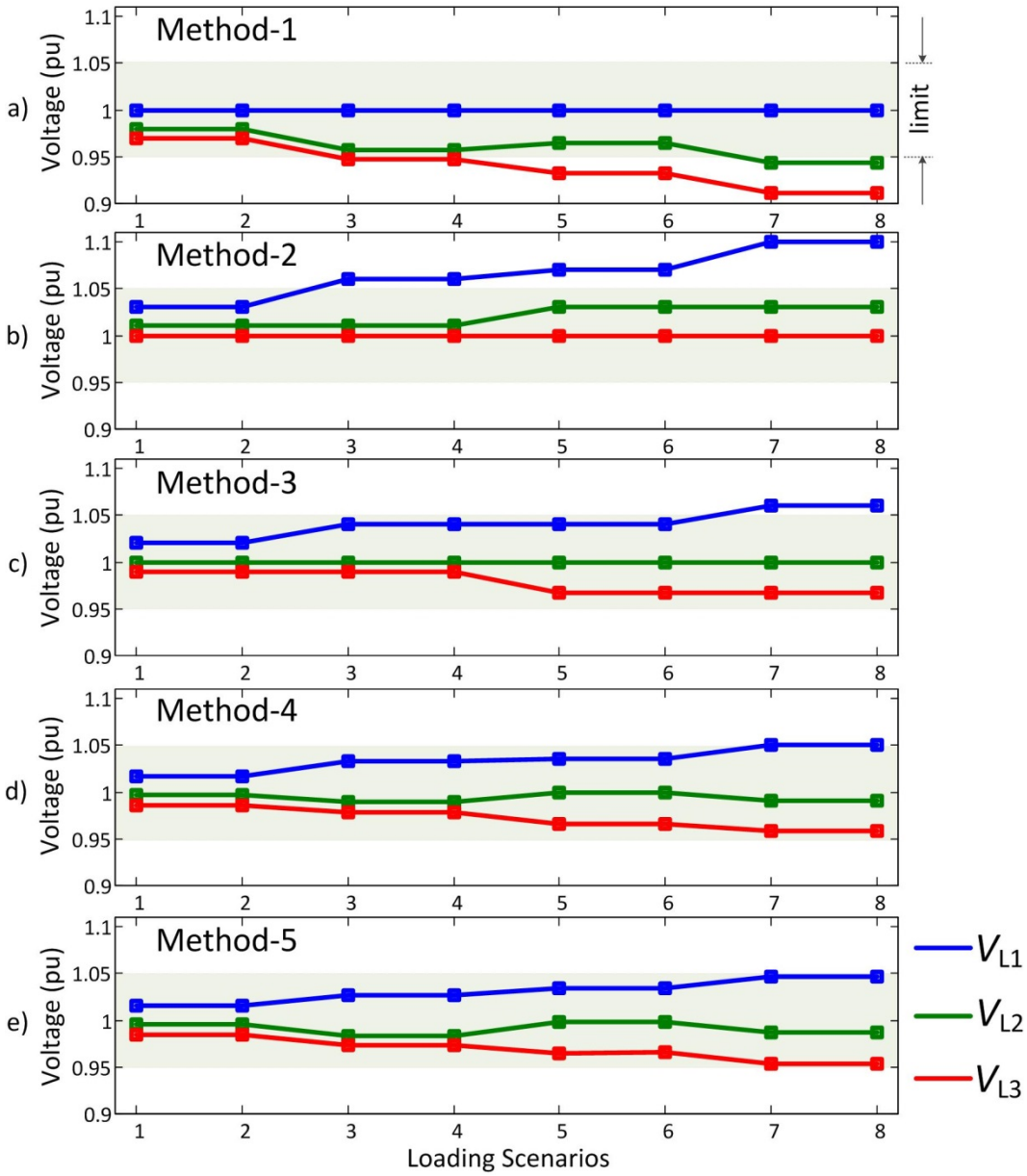

Figure 5.10 Voltage profiles in Configuration-B with various loading scenarios.

Table 5.5 Loading scenarios and load voltage profiles through application of different methods.

Loading Scenarios				V_L (pu)	Method-				
	L1	L2	L3		1	2	3	4	5
1	L	L	L	Maximum	1	1.1	1.06	1.0511	1.046
2	L	L	H	Minimum	0.911	1	0.967	0.9580	0.953
3	L	H	L	Out-of-limits	-0.039	0.05	0.01	0.0011	–
4	L	H	H						
5	H	L	L						
6	H	L	H						
7	H	H	L						
8	H	H	H						

From Figure 5.10 and Table 5.5, it can be seen that voltage deviation among loads is inevitable and therefore should be considered in voltage regulation during MG operation. As shown in Table 5.5 assuming the upper and lower limits equal ±5%, the smallest output of limit load voltage is provided by proposed Method-5, while the largest output of limit load voltage is provided by proposed Method-2. Only using proposed Method-5 can all voltage loads be retained within the acceptable limit without any out-of-limit voltages. In addition, the number of required feedbacks in proposed Method-5 is only 2, while proposed Method-4 requires 3 feedbacks (one from each load); Method-4 is more costly. Method-4 is the average load voltages method, which is widely used in many literatures.

5.2.3. Voltage Regulation in Configuration-C

Consider the network of Figure 5.3 with two branches and three loads in each branch. The network is analysed under eight different loading scenarios as presented in Table 5.5, while the technical parameters are given in Table 5.6.

The voltage regulation methods applied in this configuration are proposed Method-6 and Method-7. The performances of these methods are analysed by measuring load voltages during various loading scenarios. as presented in Table 5.7, the maximum and minimum voltage profiles across all loads are measured to

determine out-of-limits.

Table 5.6 Technical parameters of the network of Configuration-C.

MG line impedance	
(Branch-A)	$R_{C1} = 0.5\ \Omega$, $L_{C1,2,3} = 10$ mH, $R_{C2} = 0.3\ \Omega$, $R_{C3} = 0.4\ \Omega$
(Branch-B)	$R_{C1} = 0.4\ \Omega$, $L_{C1,2,3} = 10$ mH, $R_{C2} = 0.3\ \Omega$, $R_{C3} = 0.2\ \Omega$
MG load	
(Branch-A)	$R_{L1} = 30\ \Omega$, $R_{L2} = 35\ \Omega$,$R_{L3} = 40\ \Omega$, $L_{L1,2,3} = 10$ mH, $C_{L1,2,3} = 1$ mF
(Branch-B)	$R_{L1} = 30\ \Omega$, $R_{L2} = 40\ \Omega$,$R_{L3} = 35\ \Omega$, $L_{L1,2,3} = 10$ mH, $C_{L1,2,3} = 1$ mF
dc/dc converter	$L_i = 4$ mH, $C_i = 1.5$ mF, $R_i = 0.1\ \Omega$

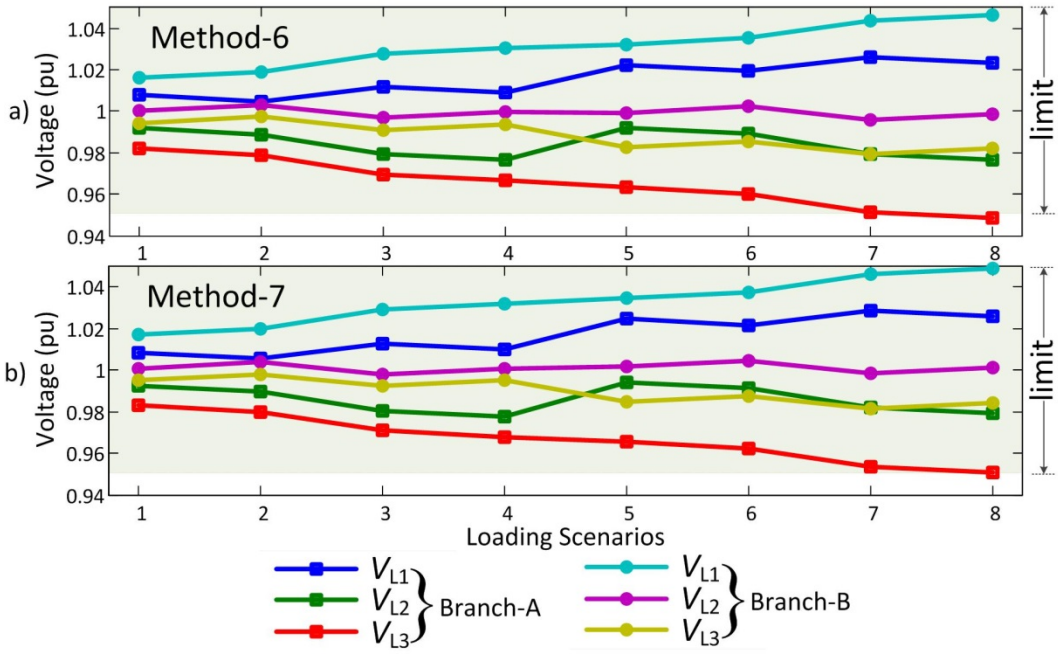

Figure 5.11 Voltage profiles in Configuration-C with various loading scenarios.

Table 5.7 Loading scenarios and load voltage profiles through application of different methods (pu).

Method-6						
	Branch-A			Branch-B		
	V_{L1}	V_{L2}	V_{L3}	V_{L1}	V_{L2}	V_{L3}
Maximum	1.026181	1	1	1.046422	1.002978	1
Minimum	1.004641	0.97642	0.948399	1.016008	0.995977	0.979191
Out of limits	–	–	-0.0016	–	–	–
Average	0.988244			1.006318		
Method-7						
	Branch-A			Branch-B		
	V_{L1}	V_{L2}	V_{L3}	V_{L1}	V_{L2}	V_{L3}
Maximum	1.028945	0.994404	0.982973	1.049139	1.00455	0.996789
Minimum	1.007126	0.979387	0.950861	1.01702	0.99866	0.981828
Out of limits	–	–	–	–	–	–
Average	0.990052			1.00816		

Figure 5.11 and Table 5.7 show that both proposed Method-6 and Method-7 are successful in keeping the voltage of all loads in all branches within the acceptable limits. However, when the load demand is at its peak (i.e. in the eighth loading scenario), V_{L3} in Branch-A is at the lower limit when using proposed Method-6. For a MG with this configuration, proposed Method-7 is more suitable. The average load voltage in each branch is also different, and Branch-B has a higher average load voltage than in Branch-A.

5.2.4. Voltage Regulation and Power Sharing in Configuration-D

Consider the network of Figure 5.4, which comprises of two DGs supplying a load through two unequal line impedances. For a single load in this configuration, proposed Method-8 is applied with the technical parameters presented in Table 5.8.

Table 5.8 Technical parameters of the network of Configuration-D with a single load.

MG line impedance	$R_{C1} = 0.4\ \Omega$, $L_{C1,2} = 10$ mH, $R_{C2} = 0.6\ \Omega$
MG load	$R_{L1} = 30\ \Omega$, $L_{L1} = 10$ mH, $C_{L1} = 1$ mF
dc/dc converter	$L_{i1,2} = 4$ mH, $C_{i1,2} = 1.5$ mF, $R_{i1} = 0.1\ \Omega$, $R_{i2} = 0.3\ \Omega$
DGs ratio	$R_{DG1} = 0.4$, $R_{DG2} = 0.6$

The MG is assumed to be initially in the steady-state condition, and the load demand is assumed to increase three times its initial value at t = 2s. Figure 5.12 shows that the DGs generate unequal voltage magnitudes and currents, according to their designated ratios. The currents generated by DG_1 and DG_2 increase by 0.125 pu (40%) and 0.188 pu (60%), respectively, when compared with the total current load (0.314 pu). It can be concluded that proposed Method-8 can force the DGs to generate their output current with respect to the desired ratios, and can also maintain load voltage at the acceptable limit. The results also show that there is no circulating current among the DGs, even though they are not working at the same voltage level.

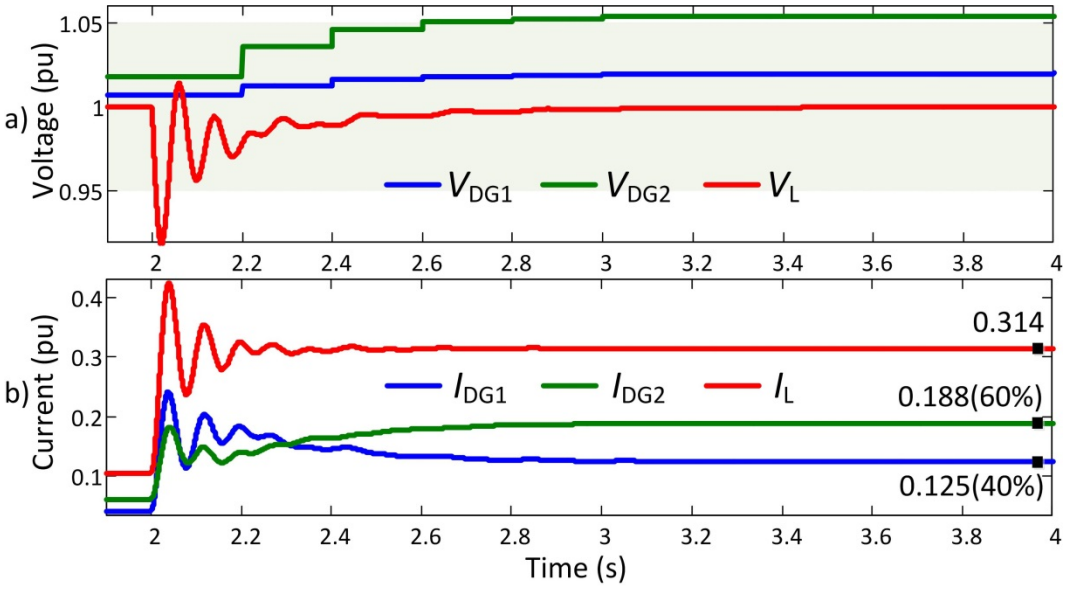

Figure 5.12 Applying Method-8, voltage and current profiles in Configuration-D with a single load and two DGs.

As shown in Figure 5.5, in reality, more than one load can be considered. In this case, proposed Method-9, Method-10, and Method-11 can be used. Consider the network of Figure 5.5 in which two DGs supply three loads through unequal line impedances. The technical parameters are presented in Table 5.9, while the simulation results are presented in Figure 5.13, Figure 5.14, and Figure 5.15. The DGs ratios used in this simulation are $R_{\mathrm{DG1}} = 0.5, R_{\mathrm{DG2}} = 0.3$, and $R_{\mathrm{DG3}} = 0.2$ for DG1, DG2, and DG3, respectively.

Table 5.9 Technical parameters of the network of Configuration-D with multiple loads and DGs.

MG line impedance	$R_{\mathrm{C1}} = 0.4\ \Omega$, , $R_{\mathrm{C2}} = 0.3\ \Omega$, $R_{\mathrm{C3}} = 0.5\ \Omega$, $L_{\mathrm{C1,2,3}} = 10$ mH
MG load	$R_{\mathrm{L1}} = 30\ \Omega$, $R_{\mathrm{L2}} = 25\ \Omega$, $R_{\mathrm{L3}} = 35\ \Omega$, $L_{\mathrm{L1,2,3}} = 10$ mH, $C_{\mathrm{L1.2.3}} = 1$ mF
dc/dc converter	$L_{\mathrm{i1,2}} = 4$ mH, $C_{\mathrm{i1,2}} = 1.5$ mF, $R_{\mathrm{i1}} = 0.1\ \Omega$, $R_{\mathrm{i2}} = 0.3\ \Omega$
DGs ratio	$R_{\mathrm{DG1}} = R_{\mathrm{DG2}} = 0.5$

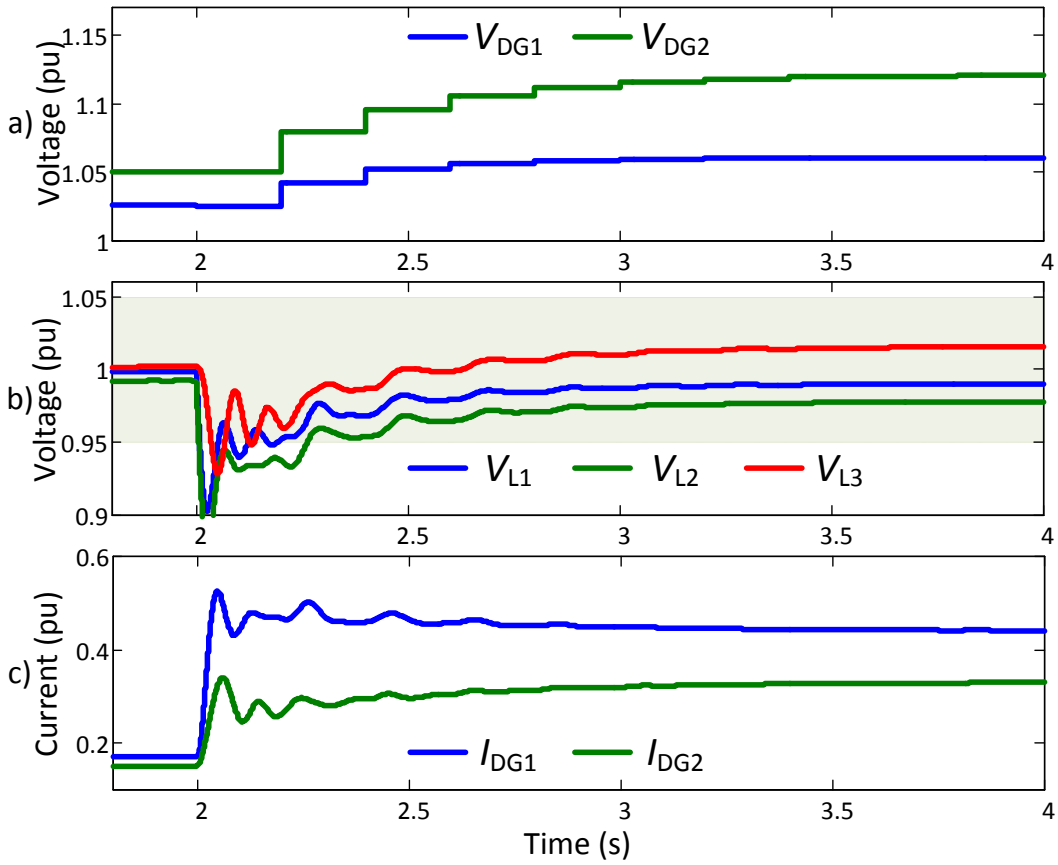

Figure 5.13 Applying Method-9, voltage and current profiles in Configuration-D with three loads and three DGs.

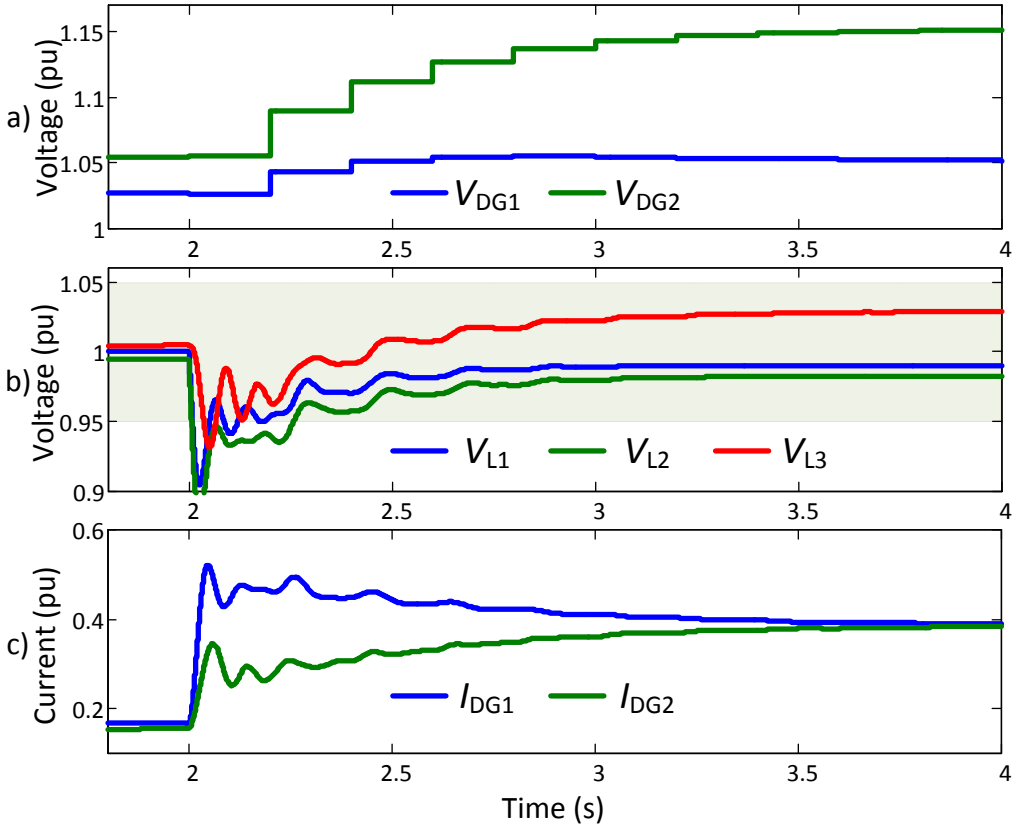

Figure 5.14 Applying Method-10, voltage and current profiles in Configuration-D with three loads and three DGs.

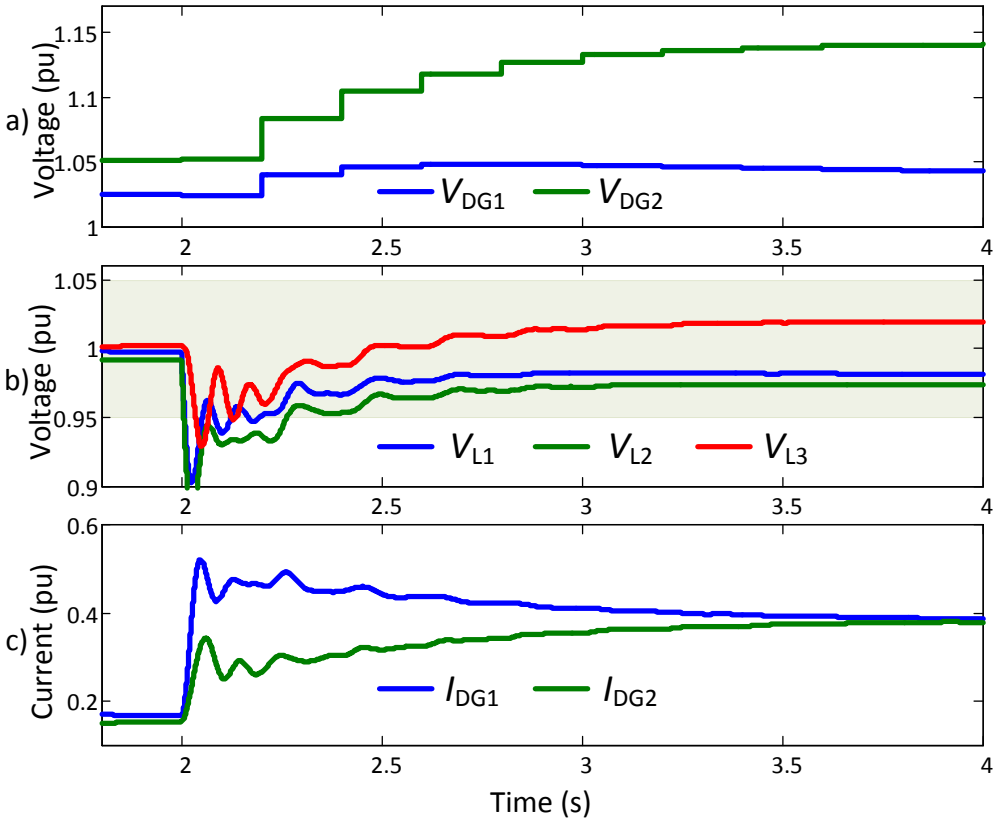

Figure 5.15 Applying Method-11, voltage and current profiles in Configuration-D with three loads and three DGs.

In this simulation, to evaluate and compare the performance of the methods mentioned above, the load demands of L2 and L3 are increased to three times their initial value at t = 2s. Figure 5.13, Figure 5.14, and Figure 5.15 show that all methods are capable of maintaining load voltage within acceptable limits during load demand fluctuations. However, proposed Method-9 cannot achieve precise proportional current sharing because each DG receives voltage feedback only from the closest load. To compensate for the higher load demand, in proposed Method-9, Method-10, and Method-11, the voltage at the output of DG2 is higher than in DG1. However, Method-10 creates the highest DG2 output voltage.

By increasing the number of loads in the DC MG, the response of the system is slower. In Figure 5.12, there is a single load within the MG, while in

Figure 5.13, there are three loads. As seen from these figures, the MG voltage profile — with a lesser number of loads — stabilises faster than the one with more loads.

5.2.5. Voltage Regulation and Power Sharing in Configuration-E

Consider the MG of Figure 5.6 with Configuration-E, in which two parallel-connected DGs supply one load. The technical parameters of this configuration are presented in Table 5.10. To obtain the specific characteristics of this configuration, the voltage regulation between Configuration-E and -D is compared using the same network and equal line impedances.

Table 5.10 Technical parameters of the network of Configuration-E with a single load.

MG line impedance	$R_{\mathrm{C1}} = 0.3\ \Omega$, $L_{\mathrm{C1,2}} = 10$ mH, $R_{\mathrm{C2}} = 0.3\ \Omega$
MG load	$R_{\mathrm{L1}} = 15\ \Omega$, $L_{\mathrm{L1}} = 10$ mH, $C_{\mathrm{L1}} = 1$ mF
dc/dc converter	$L_{\mathrm{i1,2}} = 4$ mH, $C_{\mathrm{i1,2}} = 1.5$ mF, $R_{\mathrm{i1}} = 0.1\ \Omega$, $R_{\mathrm{i2}} = 0.1\ \Omega$
DGs ratio	$R_{\mathrm{DG1}} = R_{\mathrm{DG2}} = 0.5$

Figure 5.16 shows that in both Configuration-D and -E, the proposed voltage regulation method is capable of maintaining the load voltage within the acceptable limits. However, it also reveals that compared to Configuration-E, Configuration-D is more suitable for the application of power/current sharing in the DC MG. In the same DC MG network with an equal total current load (as shown in Figure 5.16(d)), the voltages and currents generated by the DGs in Configuration-D are more proportional to their ratios than in Configuration-E (as shown in Figure 5.16(a) and (c)). In Configuration-E, both the voltage and current in the loads are more influenced by the adjacent DG (in this Case-DG2), and to generate equal/proportional DG power/currents, DG1 is required to produce more voltage magnitude than DG2. However, this required voltage magnitude could exceed the maximum voltage level generated by a dc-dc converter.

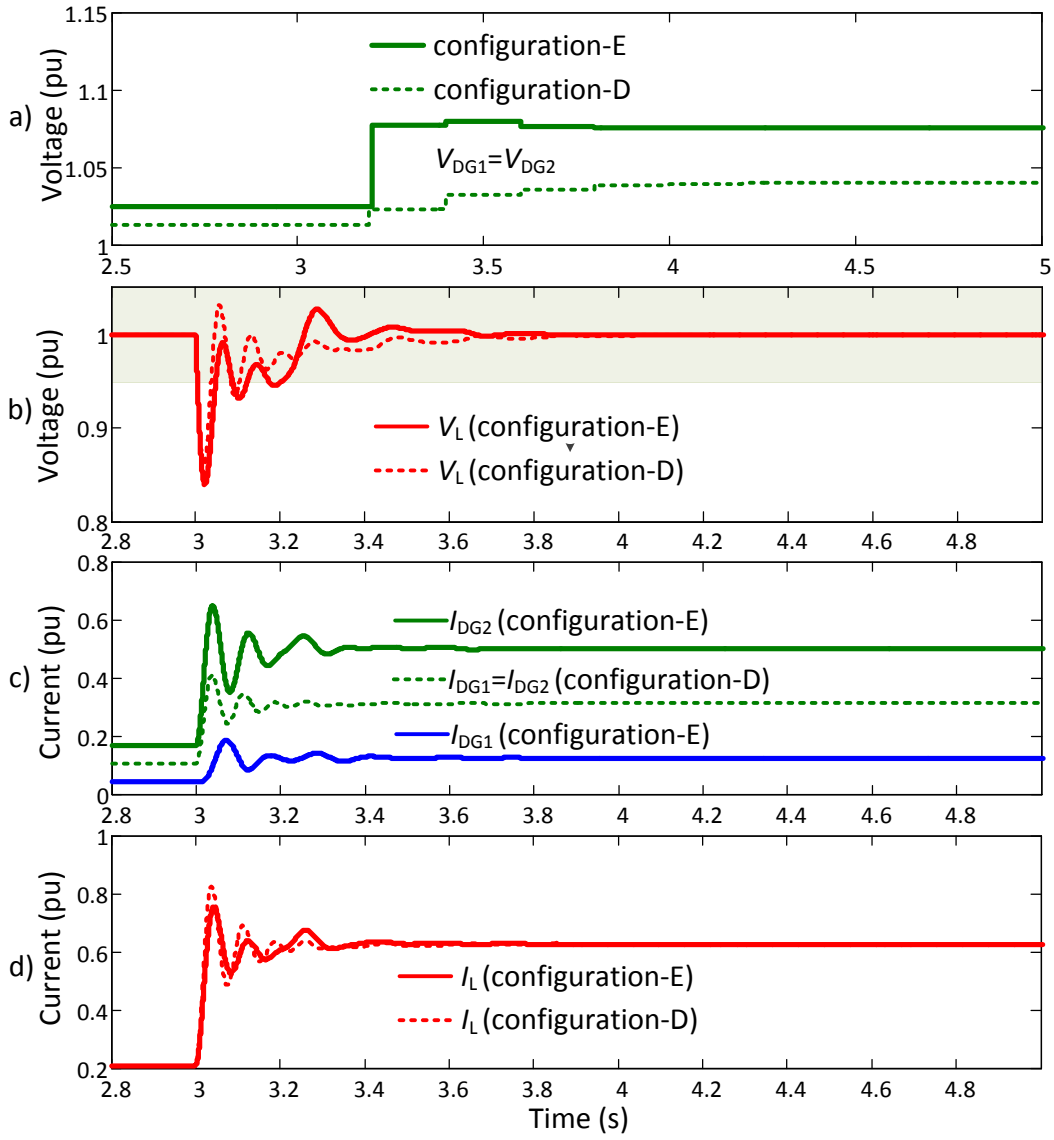

Figure 5.16 Comparison of voltages and currents between Configuration-D and -E in a single load DC MG.

The other possible method for Configuration-E is the use of multiple loads as shown in Figure 5.7. In this configuration, two methods (i.e. Methods-12 and -13) are analysed and compared. The technical parameters of this configuration are presented in Table 5.11.

Table 5.11 Technical parameters of the network of Configuration-E with multiple loads and DGs.

MG line impedance	$R_{\mathrm{C1}} = 0.4\ \Omega$, $L_{\mathrm{C1,2}} = 10$ mH, $R_{\mathrm{C2}} = 0.6\ \Omega$, $R_{\mathrm{C1-L}} = 0.3\ \Omega$, $R_{\mathrm{C1-L}} = 0.6\ \Omega$
MG load	$R_{\mathrm{L1}} = 10\ \Omega$, $L_{\mathrm{L1,2}} = 10$ mH, $C_{\mathrm{L1,2}} = 1$ mF, $R_{\mathrm{L2}} = 15\ \Omega$,
dc/dc converter	$L_{\mathrm{i1,2}} = 4$ mH, $C_{\mathrm{i1,2}} = 1.5$ mF, $R_{\mathrm{i1}} = 0.15\ \Omega$, $R_{\mathrm{i2}} = 0.1\ \Omega$
DGs ratio	$R_{\mathrm{DG1}} = R_{\mathrm{DG2}} = 0.5$

Figure 5.17 and Figure 5.18 show that both methods can mitigate load voltages after increasing load demands. As seen in Figure 5.17(b) and Figure 5.18(b), load voltages can be maintained within acceptable limits during various loading conditions. However, as shown in Figure 5.18(c), only Method-13 can achieve proportional currents between DGs for power/current sharing purposes. In Method-12, the current sharing between DGs cannot be achieved (see Figure 5.17(c)), and more oscillation is created in the DG voltage and current output (see Figure 5.17(a)).

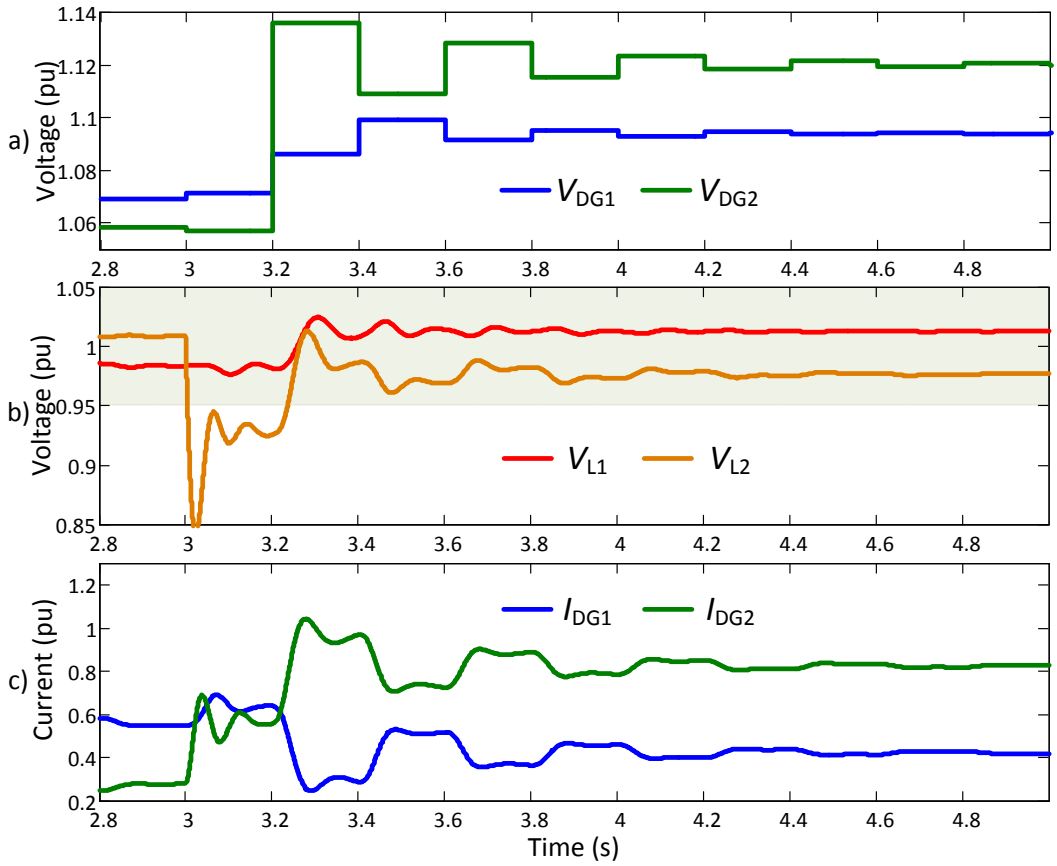

Figure 5.17 Applying Method-12, voltage and current profiles in Configuration-E with multiple loads side and two DGs.

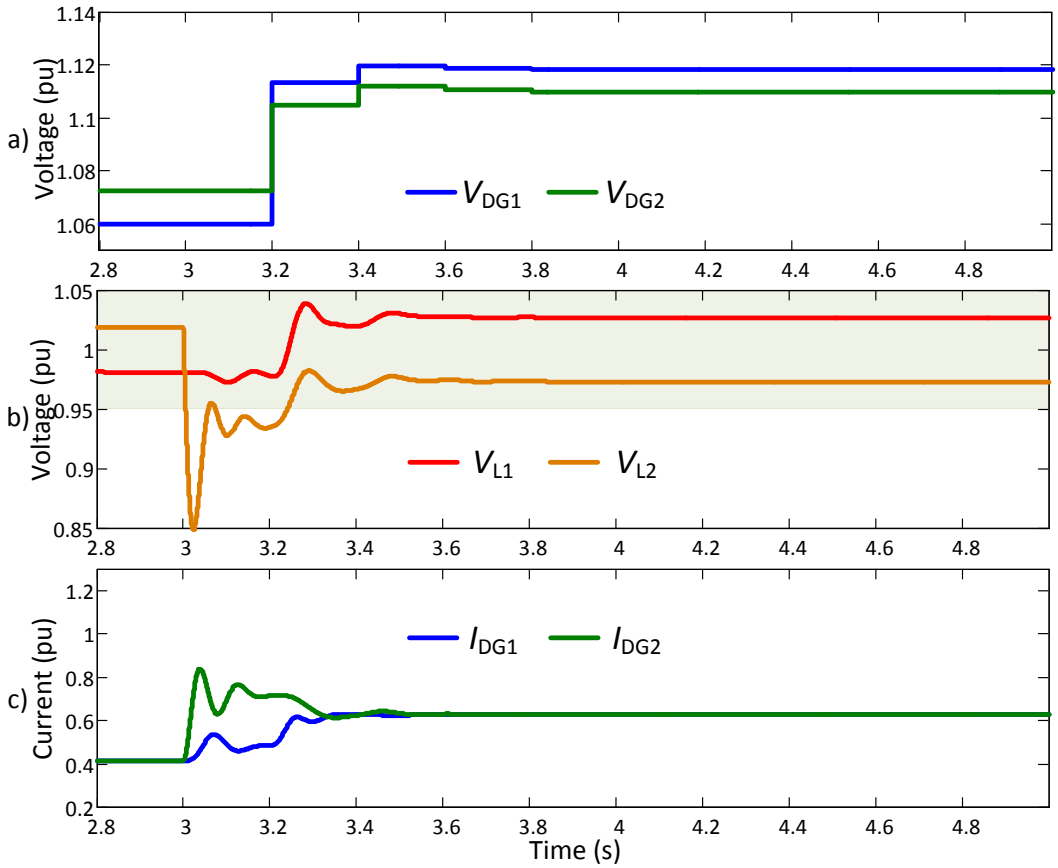

Figure 5.18 Applying Method-13, voltage and current profiles in Configuration-E with multiple loads side and two DGs.

5.2.6. Combination of Several Configurations

Consider the MG of Figure 5.8 with a combination of several configurations and in which three connected DGs supply four loads. The technical parameters of this configuration are presented in Table 5.12. The simulation is conducted with the same DG ratio and equal line impedances.

Table 5.12 Technical parameters of the network of combined configurations with multiple loads and DGs.

MG line impedance	$R_{C1-6} = 0.3\ \Omega$, $L_{C1-6} = 10$ mH
MG load	$R_{L1-6} = 30\ \Omega$, $L_{L1-6} = 10$ mH, $C_{L1-6} = 1$ mF
dc/dc converter	$L_{i1-4} = 4$ mH, $C_{i1-4} = 1.5$ mF, $R_{i1-4} = 0.1\ \Omega$
DGs ratio	$R_{DG1} = \frac{1}{3}$, $R_{DG2} = \frac{1}{3}$, $R_{DG3} = \frac{1}{3}$

In this simulation, to evaluate the performance of the proposed voltage regulation methods as illustrated in (5.9), the load demands of L2 and L4 are increased to three times their initial value at t = 3s and t = 5s, respectively. Figure 5.19 and Figure 5.20 show that the methods used in (5.9) and (5.10) are capable of maintaining the load voltage within the acceptable limits during load demand fluctuations. Fig. 19 and Fig. 20 reveal that the biggest fluctuations in the DC MG loads are occurs in the L2 at t = 3s and L4 at t = 5s when the load demands are increased.

In (5.9), during load demand fluctuations, the voltages are of lower deviation between DGs than in (5.10). However, the method used in (5.9) cannot achieve precise proportional power/current sharing because each DG receives different voltage feedback only from the closest load. The method used in (5.10) generates a higher voltage deviation among DGs compared to the method used in (5.9); this is to compensate for the line impedances in the MG network. The simulation results presented in Figure 5.19 and Figure 5.20 indicate that the different methods (Method-1 to Method-13) can be implemented in the DC MG in many different configurations.

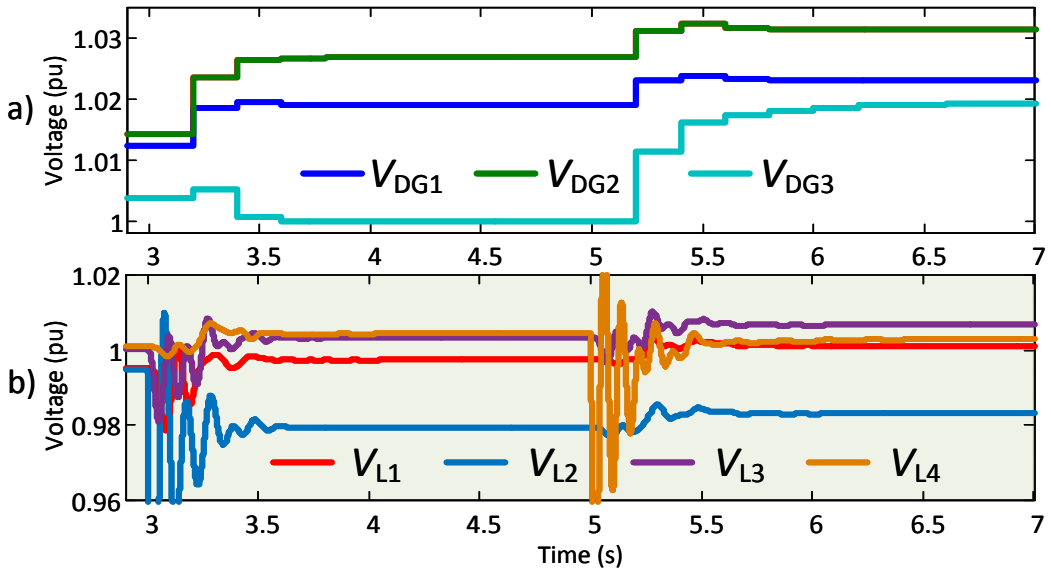

Figure 5.19 Applying (5.9), voltage profiles in a combination of configurations with multiple loads and three DGs.

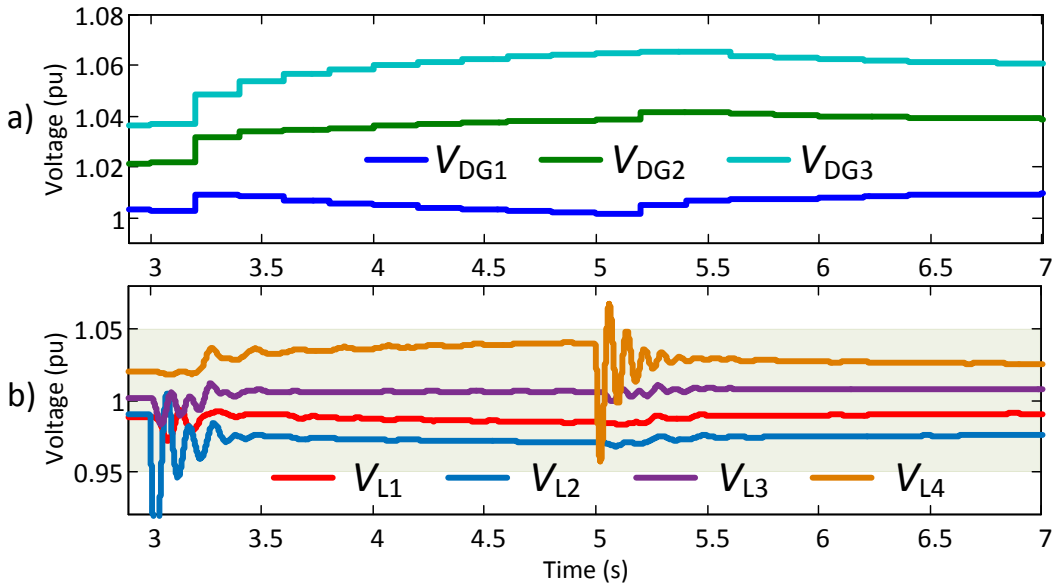

Figure 5.20 Applying (5.10), voltage profiles in combination configurations with multiple loads and three DGs.

5.2.7. Comparison of Discussed Configurations

Table 5.13 presents the comparison of the different DC MG configurations and methods discussed above with respect to number of loads (*L*), number of DGs (*N*), number of parallel loads (*J*), number of branched loads (*M*), number of required feedbacks (*FB*), possibility of voltage regulation (VR), and power/current sharing (PS). This table concludes that all discussed methods can achieve and maintain the voltage at the load point within an acceptable limit; However, while several methods can achieve power/current sharing precisely, others are either imprecise or cannot be implemented. The total number of required feedbacks in the methods that can achieve precise power/current sharing is smaller than that of other methods.

Table 5.13 Comparison of different configurations and methods in DC MGs.

Configuration	Method	L	N	J	M	FB	Possibilities	
							VR	PS
A	1	1	1	1	–	1	✓	NA
B	1	1	1	≥ 1	–	1	✓	NA
	2	≥ 2	1	≥ 2	–	1	✓	NA
	3	≥ 2	1	≥ 3	–	1	✓	NA
	4	≥ 2	1	≥ 3	–	J	✓	NA
	5	≥ 2	1	≥ 3	–	2	✓	NA
C	2-3	≥ 2	1	≥ 1	≥ 2	M	✓	NA
	4	≥ 2	1	≥ 3	≥ 2	$J \times M$	✓	NA
	5	≥ 2	1	≥ 3	≥ 2	$2 \times M$	✓	NA
	7	≥ 2	1	≥ 1	≥ 2	$2 \times M$	✓	NA
D	8	1	≥ 2	1	–	1	✓	✓
	9	≥ 2	≥ 2	≥ 1	–	1	✓	∗
	10	≥ 2	≥ 2	≥ 1	–	N	✓	✓
	11	≥ 2	≥ 2	≥ 1	–	2	✓	✓
E	8	1	≥ 2	≥ 1	≥ 1	$\geq 2 \times M$	✓	∗
	12	≥ 2	≥ 2	≥ 1	≥ 1	$\geq 2 \times M$	✓	×
	13	≥ 2	≥ 2	≥ 1	≥ 1	$\geq 2 \times M$	✓	✓

NA = not applicable, × = cannot be conducted, ∗ : imprecise, ✓ : precise.

5.3. Summary

This chapter presents various circuit configurations for DC MGs and the possibilities for both voltage regulation and power sharing. The specific characteristics of each configuration are discussed, analysed and simulated. The simulation results indicate that the proposed voltage regulation and power sharing methods can achieve the desired voltage and generated DG current precisely and within predefined acceptable limits. The required feedback signals in loads can be varied according to the proposed methods. While all configurations can employ the proposed voltage regulation technique, several configurations cannot

implement the power/current sharing technique due to its natural characteristics. This specific configuration characteristic cannot be applied a simultaneous voltage regulation and power sharing whatever the applied methods due to its natural characteristic according to Kirchhoff's law.

Chapter 6: Centralised and Distributed Data Communication in Microgrids

In this Chapter, two proposed algorithms/methods are proposed and discussed. The new algorithm for establishing the shortest communication infrastructure is presented in the first sub-chapter, and the centralised and distributed MG data communication scheme is discussed in the second sub-chapter.

6.1. New Algorithm for Establishing the Shortest Distance Communication Infrastructure in Microgrids

The communication infrastructure for connecting MG communication devices can be deployed using the following methods:

- In the path of an electric distribution network, as shown in Figure 6.1(a). This method is simple to install, maintain and repair; however, the distance of the communication infrastructure can be long. This method is more suitable for wired communication infrastructure or for established electrical facilities.
- Square area, as shown in Figure 6.1(b). In this method, all of the areas where the MG operates are covered by wireless (repeater) signals. This design is suitable for wind or photovoltaic farms, or for use in a crowded area where large sensors, meters or actuators can be monitored and controlled.
- Point-to-point connection, as shown in Figure 6.1(c). This method requires a mathematical calculation to define the shortest distance between any two points. This method is appropriate for any new installation of communication infrastructure, or for where there are longer distances between DGs, ESSs, and loads.

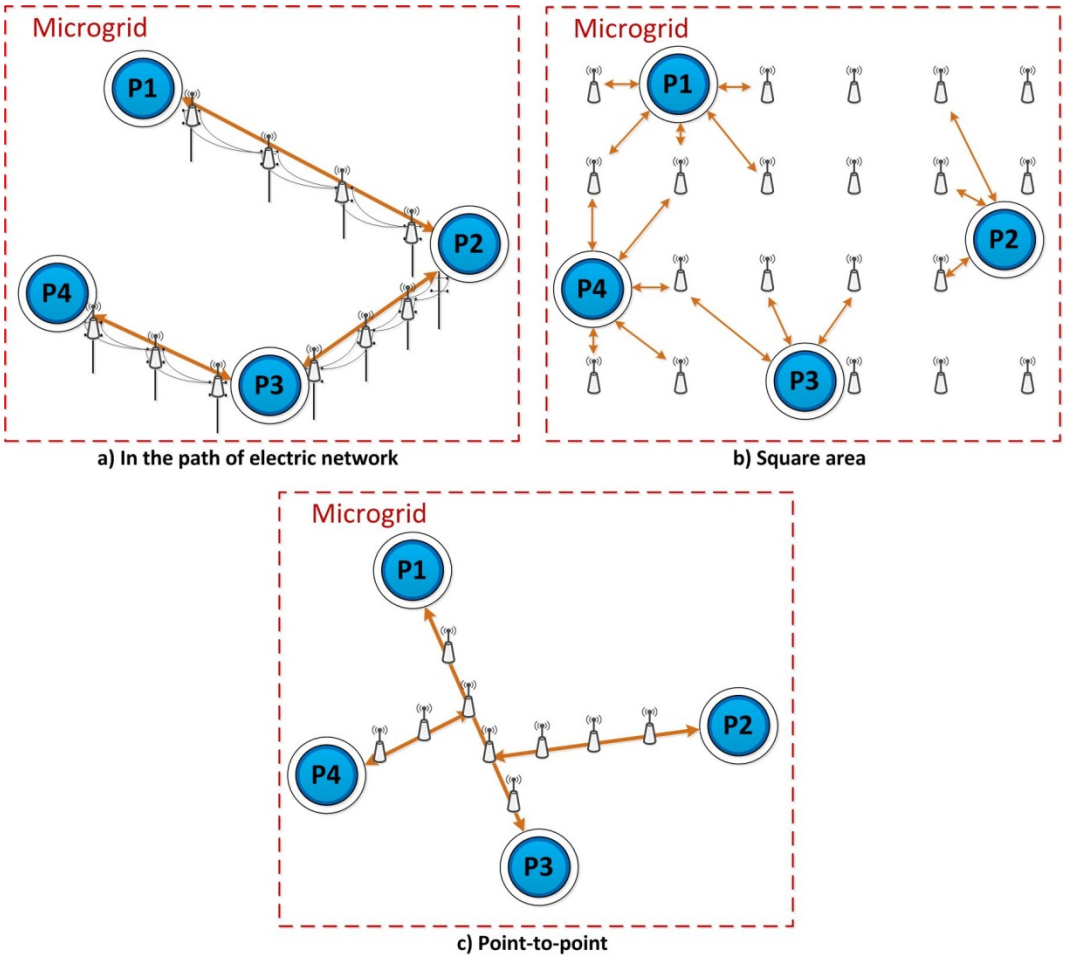

Figure 6.1 Three possible layouts of MG communication infrastructure. P1, P2, P3, and P4 represent the MG points of DGs, ESSs, or loads, connected via communication devices.

As discussed in Sections 2.4 and 2.5, the MG communication infrastructure affects the communication delay, the type of communication technology used, and also which data communication scheme is applied. The options presented in Figure 6.1(a) and Figure 6.1(b) can be directly implemented without any further mathematical algorithm. However, for the point-to-point option, as illustrated in Figure 6.1(c), a further mathematical algorithm is required. When connecting all points, the shorter the overall distance, the less the installation cost. The shortest distance algorithm for communication infrastructure is therefore discussed and developed in this section. The point-to-point method can be developed using different approaches as follows:

6.1.1. Direct Connection Approach

The Direct Connection approach directly connects the DGs, ESSs, or loads points to the MG central controller, as shown in Figure 6.2. This method may lead to the longest communication infrastructure in the MG. If the location of the MG central controller location is not initially assigned, the algorithm can define it so that it is the shortest possible distance from all DGs. All required data to be processed in the MG — such as voltage magnitude, current, active/reactive power, frequency, etc. — are transmitted from DGs, ESSs, or loads points to the MG central controller; or from Point P_k to P_m via the MG central controller. Using this communication infrastructure approach, MG data communication and exchange is conducted via the MG central controller connection; therefore, communication bandwidth and robustness are essential. The advantages of this approach include easy implementation, flexibility for plug-and-play, and a smaller communication delay. Wired/wireless Ethernet/IoT, GSM/cellular, Wi-Max, and also radio frequency-based communication technology can be implemented in this approach.

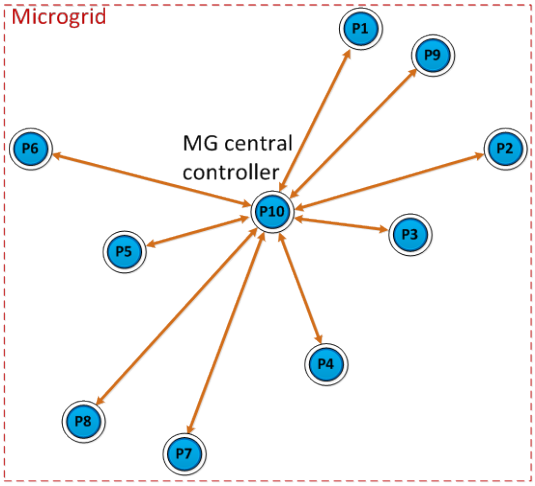

Figure 6.2 Direct Connection approach for MG communication infrastructure.

6.1.2. Joined Path Approach

The main idea of the Joined Path approach is based on the Direct Connection approach yet eliminates some of the paths. If a DG controller is connected to the MG controller through the other DG communication infrastructure, it is possible to form one common path (shared communication infrastructure), as illustrated in Figure 6.3. The joined communication

infrastructure increases the communication delay for transmitting data from the points to the MG central controller; however, the joined paths have a shorter total distance and will therefore decrease the installation costs. Also important to note is that the junction point requires an additional communication device to act as transmitter and receiver between the points of two or more communication devices. This approach is suitable for wired communication, ZigBee, Bluetooth, and radio frequency-based communication technology.

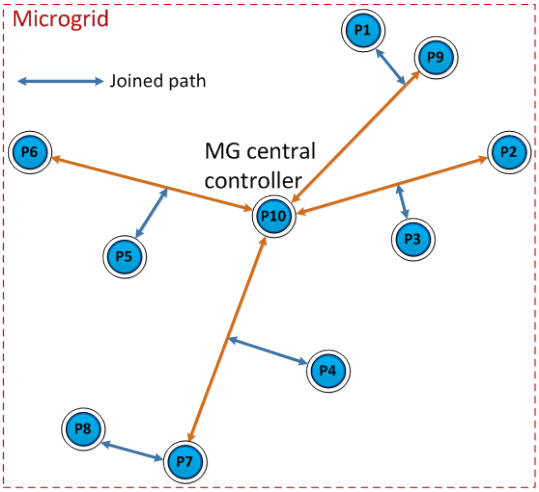

Figure 6.3 Joined Path approach for MG communication infrastructure.

To define the joined path in this approach, the proposed step-by-step algorithms are:

- The location of the points, which represent the location of the DGs, ESSs, and loads, are based on the Cartesian coordinates as (x, y).
- The original distance from each point to the MG central controller as:

$$\Delta D_k = \sqrt{\sum \Delta(y_k, y_C)^2, \Delta(x_k, x_C)^2}, \forall k \epsilon \{P_1, \cdots, P_{CD}\} \quad (6.1)$$

where $_{CD}$ and $_{C}$ are the total number of points to be connected in the communication devices, and the location of the MG central controller respectively.

- The joined path can be established by joining adjacent communication paths. The adjacent paths can be defined by an absolute angle deviation ($\Delta\theta$) in which ($\Delta\theta$ <45^0):

$$\Delta\theta_{k-l} = \left|\Delta\frac{(y_k, y_C)}{(x_k, x_C)}, \Delta\frac{(y_l, y_C)}{(x_l, x_C)}\right|, \forall k\epsilon\{P_1, \cdots, P_{CD-1}\}, \forall l\epsilon\{P_2, \cdots, P_{CD}\} \quad (6.2)$$

- The shortest original distance point to the MG central controller is joined to one of the longest original distance points in the adjacent communication path. The shortest distance from P_l to the junction point in the path of P_k is found by employing (6.1). The joined path distance ($\Delta D_l{}'$) must be shorter than the original distance (ΔD_l). The parameters used in this approach are illustrated in Figure 6.4.

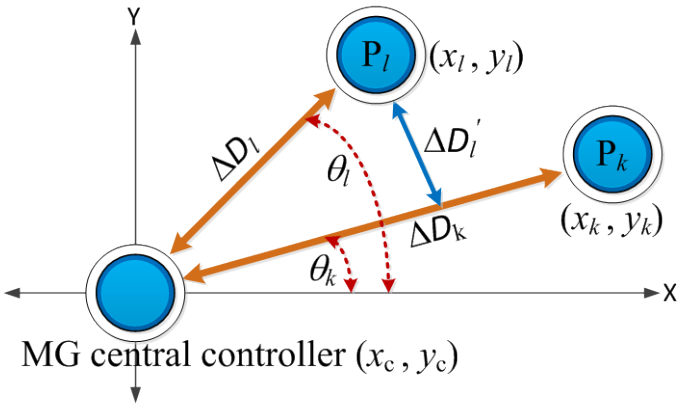

Figure 6.4 Parameters in the Joined Path approach.

6.1.3. Longest Joined Path Approach

The Longest Joined Path approach modifies and develops the Joined Path approach by increasing the absolute angle deviation ($\Delta\theta$) so that more communication paths can be joined to the common communication path. As discussed in the Joined Path approach, the common communication path is the longest original distance from the point to the MG central controller. The joined paths can be amalgamated into the common path when the joined path distance ($\Delta D_k{}'$) is shorter than the original distance to the MG central controller (ΔD_k). Equations (6.1) and (6.2) are used in this approach to determine the common communication path and also the joined paths. This approach is illustrated in Figure 6.5.

In the Longest Joined Path approach, the communication delay for transmitting data from the points to the MG central controller is higher than in the

Joined Path approach. This is due to the increased number of connected points in the communication devices. The total distance, on the other hand, decreases and thereby leads to a reduction in communication infrastructure installation costs. This approach is suitable for wired communication, ZigBee, Bluetooth, and radio frequency-based communication technology.

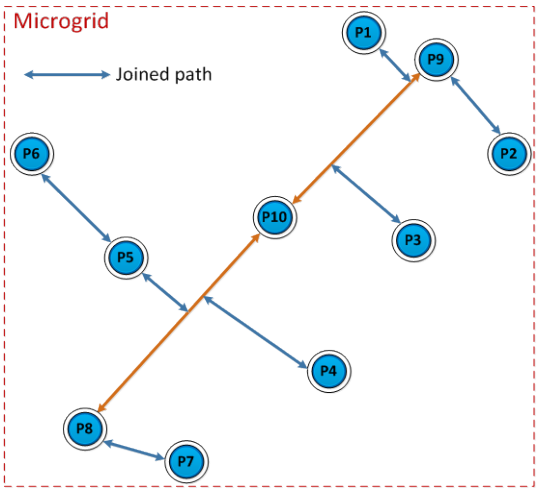

Figure 6.5 The Longest Joined Path approach for MG communication infrastructure.

6.1.4. Shortest Distance Matrix Approach

The communication infrastructure in the Shortest Distance Matrix approach is determined by the shortest distance between two adjacent points in the communication devices. The remaining points are then connected to the other shortest distance points so that all points are connected in the MG network. This approach requires a more complex mathematical algorithm than the previously discussed approaches. However, this approach is the least expensive in terms of communication installation costs, because it can produce the shortest total distance. Due to the complex mathematical algorithm, this approach is not suitable for frequently plug-and-play units of MG DGs, ESSs or loads, but it is suitable for wired communication, ZigBee, Bluetooth, and radio frequency-based communication technology.

Using this approach, it is not necessary to calculate the distance between the points to the MG central controller. Instead, the distance point-to-point is calculated in the form of a matrix and using Equation (6.1). As shown in Figure

6.6, this approach may create isolated communication networks when two adjacent points are very close to each other, but to prevent this, the 2nd, then 3rd, etc. shortest distance is also chosen. For example, Figure 6.6 shows that the shortest distance to P1 is from P9 (and vice versa), and the shortest distance to P3 is from P10 (and vice versa). As shown in Figure 6.6(a), when using only the shortest distance, this approach creates two isolated communication networks. However, when the 2nd shortest distance is also applied, as shown in Figure 6.6(b), all MG points are connected in a single communication network as requested.

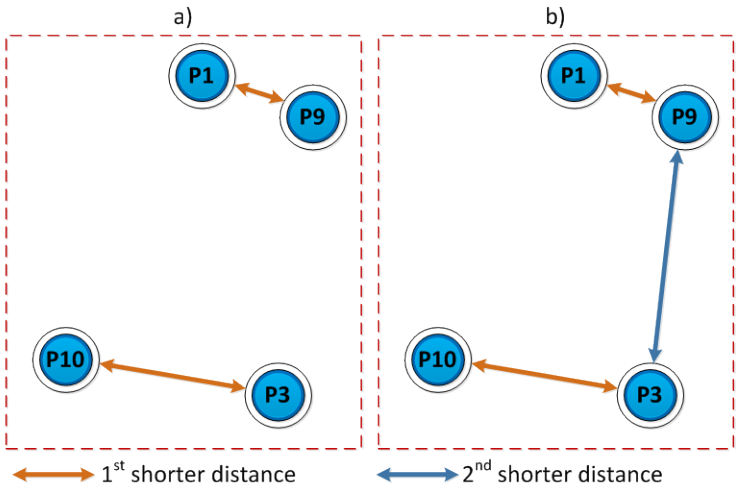

Figure 6.6 The possibility of creating an isolated communication network when using the only shortest distance.

The algorithm of the matrix's shortest approach is presented in the flow chart of Figure 6.7.

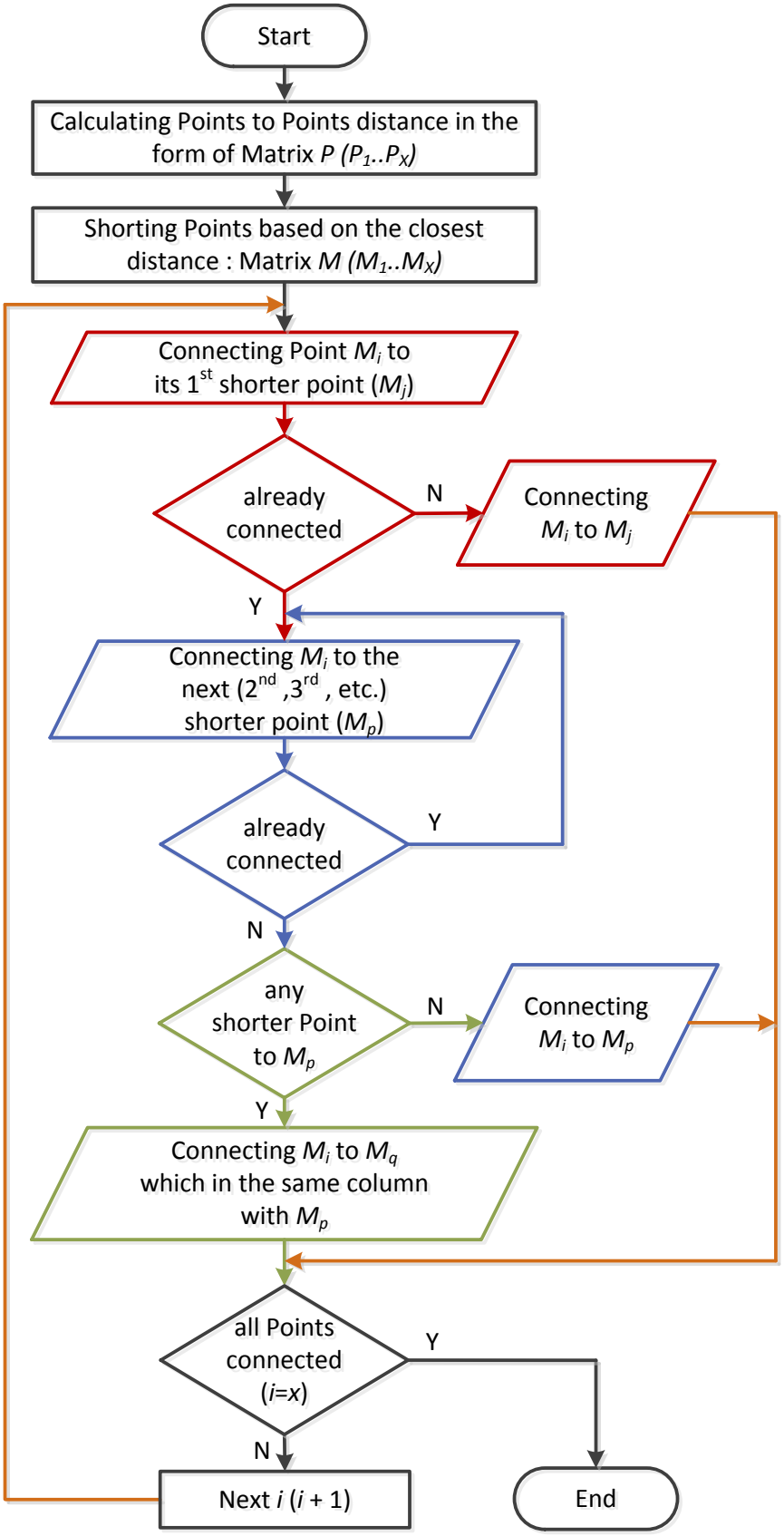

Figure 6.7 Flowchart of the proposed Shortest Distance Matrix approach.

Let us consider a MG with x = 10 points in its communication devices, which each represent the locations of the DGs, ESSs and loads. As shown in Figure 6.2,Figure 6.3, and Figure 6.5, the coordinates of P1 to P10 are (6400, 19400), (8000, 17800), (6800, 16000), (5600, 14300), (3000, 16000), (2000, 18000), (3500, 13000), (2400, 13600), (7000, 19000) and (5100, 16200), respectively. The following matrix P represents the distance point-to-point by implementing (6.1):

$$P = \begin{array}{c} \begin{array}{cccccccccc} P_1 & P_2 & P_3 & P_4 & P_5 & P_6 & P_7 & P_8 & P_9 & P_{10} \end{array} \\ \begin{bmatrix} 0 & 226 & 342 & 516 & 481 & 462 & 703 & 705 & 72 & 345 \\ 226 & 0 & 216 & 424 & 531 & 600 & 658 & 700 & 156 & 331 \\ 342 & 216 & 0 & 208 & 380 & 520 & 446 & 501 & 301 & 171 \\ 516 & 424 & 208 & 0 & 311 & 516 & 247 & 328 & 490 & 196 \\ 481 & 531 & 380 & 311 & 0 & 224 & 304 & 247 & 500 & 211 \\ 462 & 600 & 520 & 516 & 224 & 0 & 522 & 442 & 510 & 358 \\ 703 & 658 & 446 & 247 & 304 & 522 & 0 & 125 & 695 & 358 \\ 705 & 700 & 501 & 328 & 247 & 442 & 125 & 0 & 709 & 375 \\ 72 & 156 & 301 & 490 & 500 & 510 & 695 & 709 & 0 & 338 \\ 345 & 331 & 171 & 196 & 211 & 358 & 358 & 375 & 338 & 0 \end{bmatrix} \begin{array}{c} P_1 \\ P_2 \\ P_3 \\ P_4 \\ P_5 \\ P_6 \\ P_7 \\ P_8 \\ P_9 \\ P_{10} \end{array} \end{array}$$

1st shorter distance 2nd shorter 3rd shorter

To prevent the creation of an isolated communication network, the variables must be renamed. Firstly, P1 is renamed M1, and then because the 1st shortest distance to P1 is from P9, P9 is renamed M2. The 1st shortest distance to P9 is from P1; however because P1 is already used as M1, the 2nd shortest distance to P9 is selected instead. The 2nd shortest distance to P9 is from P2, and P2 is renamed as M3. This sorting and renaming continues, as proposed in the flow-chart of Figure 6.7, until all points are selected.

Once all variables have been renamed, the approach then starts by determining the shortest distance point from M1, which is M2. The shortest distance point from M2 is M1; however, because M1 has previously been connected, the 2nd shortest distance from M2 is chosen instead. The 2nd shortest distance from M2 is M3, and this is shown by the arrows over the M matrix. The approach process continues until all points are connected. It is to be noted that if there is a closer point in the same row of the M matrix, then this should be

connected instead of the second shortest point. The completed M matrix and the arrow for determining the Shortest Distance Matrix approach are given below.

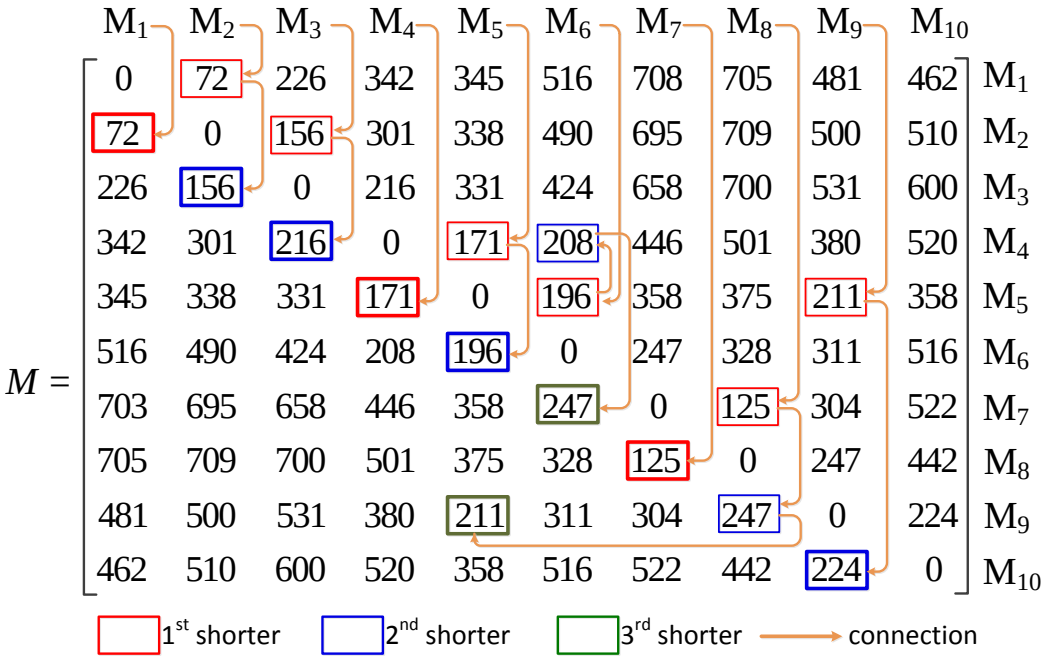

6.1.5. Simulation Results and Numerical Analysis

The above-discussed approaches are modelled and numerically simulated in MATLAB for the MGs illustrated in Figure 6.2,Figure 6.3, and Figure 6.5. The MG central controller varies in location, and in this simulation, the locations are defined as (5100, 16200), (3500, 14500), (4000, 18000), (7000, 15000), (6000, 18000), and (8000, 12000). Figure 6.8, Figure 6.9, Figure 6.10, and Figure 6.11 present the communication infrastructure results after implementing the proposed approaches.

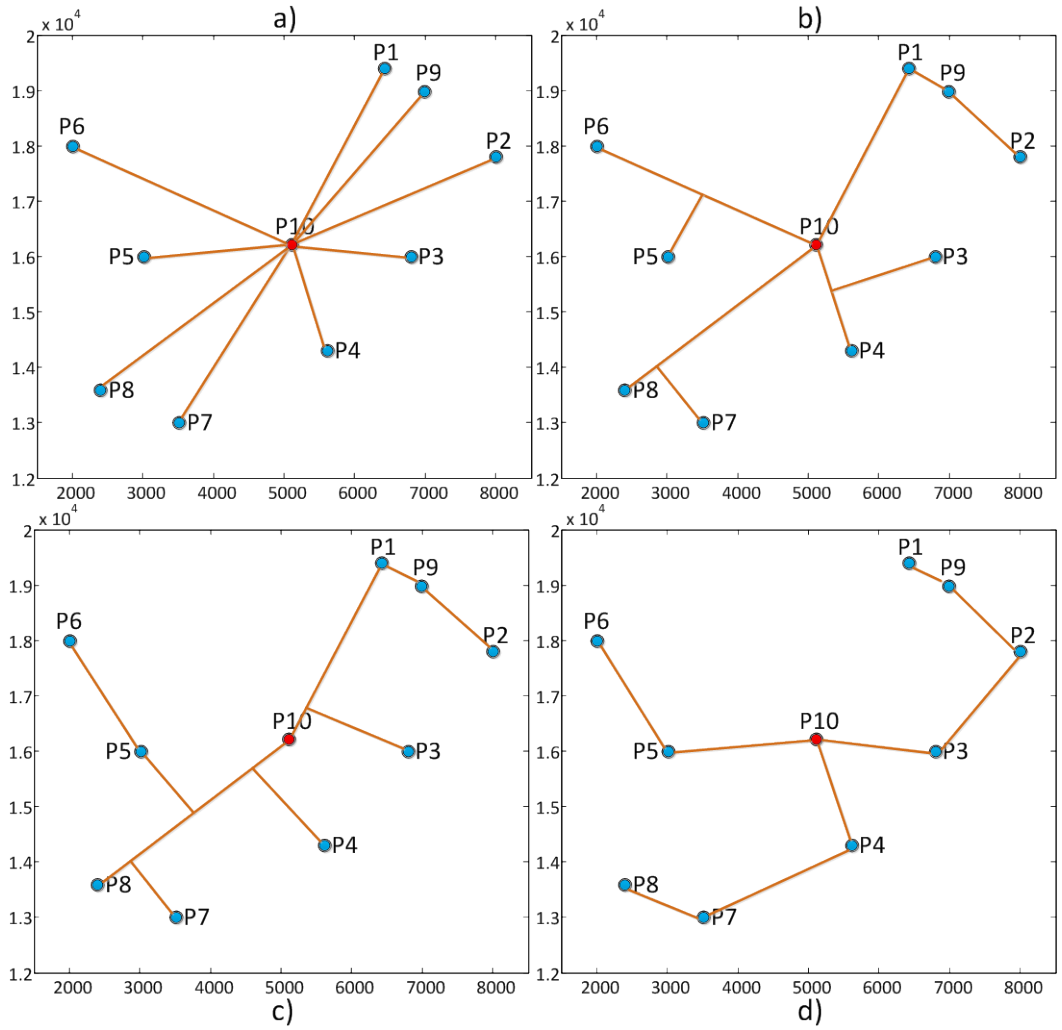

Figure 6.8 Communication infrastructure simulation results when MG central controller is located at (5100, 16200), using proposed approaches: a) Direct Join, b) Joined Path, c) Longest Joined Path, and d) Shortest Distance Matrix.

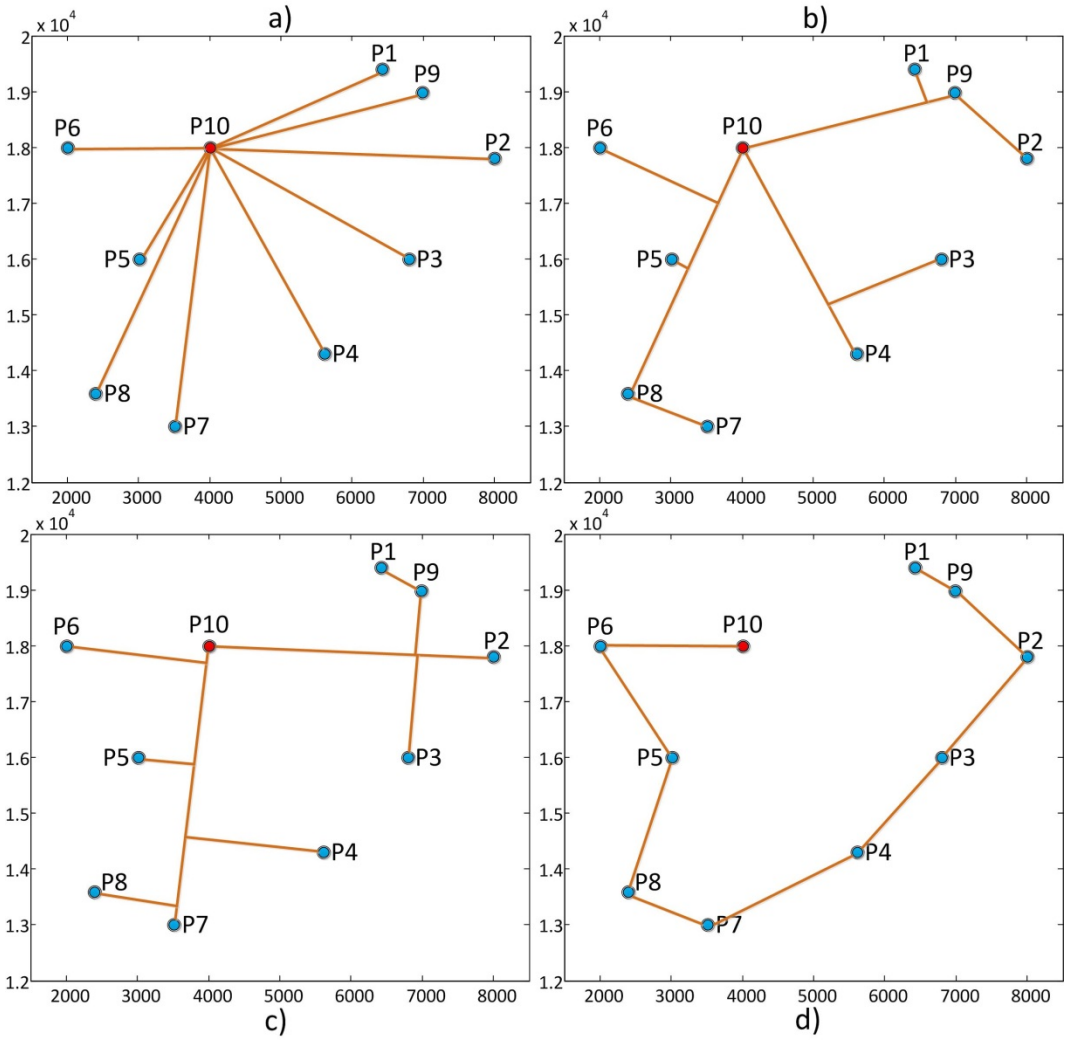

Figure 6.9 Communication infrastructure simulation results when MG central controller is located at (4000, 18000), using proposed approaches: a) Direct Connection, b) Joined Path, c) Longest Joined Path, and d) Shortest Distance Matrix.

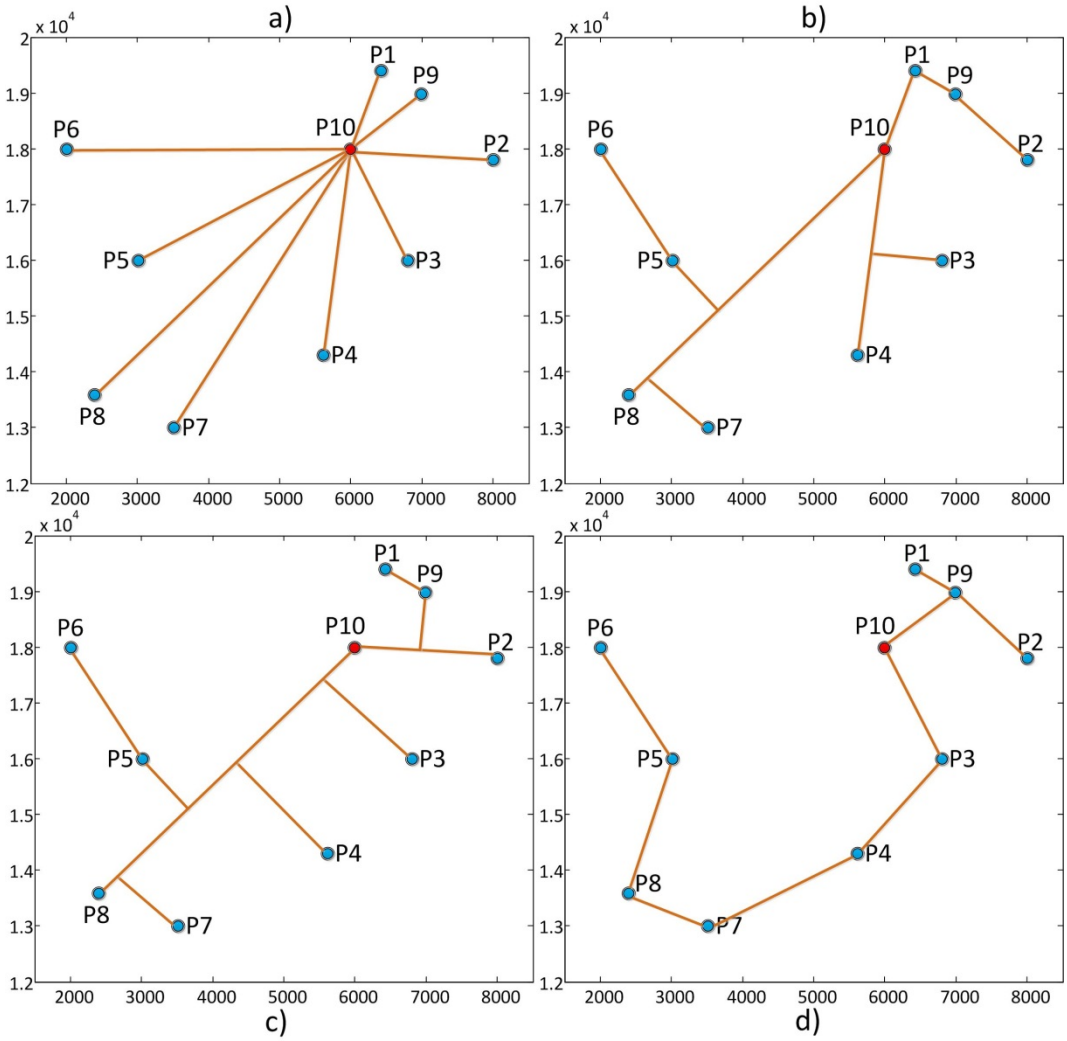

Figure 6.10 Communication infrastructure simulation results when MG central controller is located at (6000, 18000), using proposed approaches: a) Direct Connection, b) Joined Path, c) Longest Joined Path, and d) Shortest Distance Matrix.

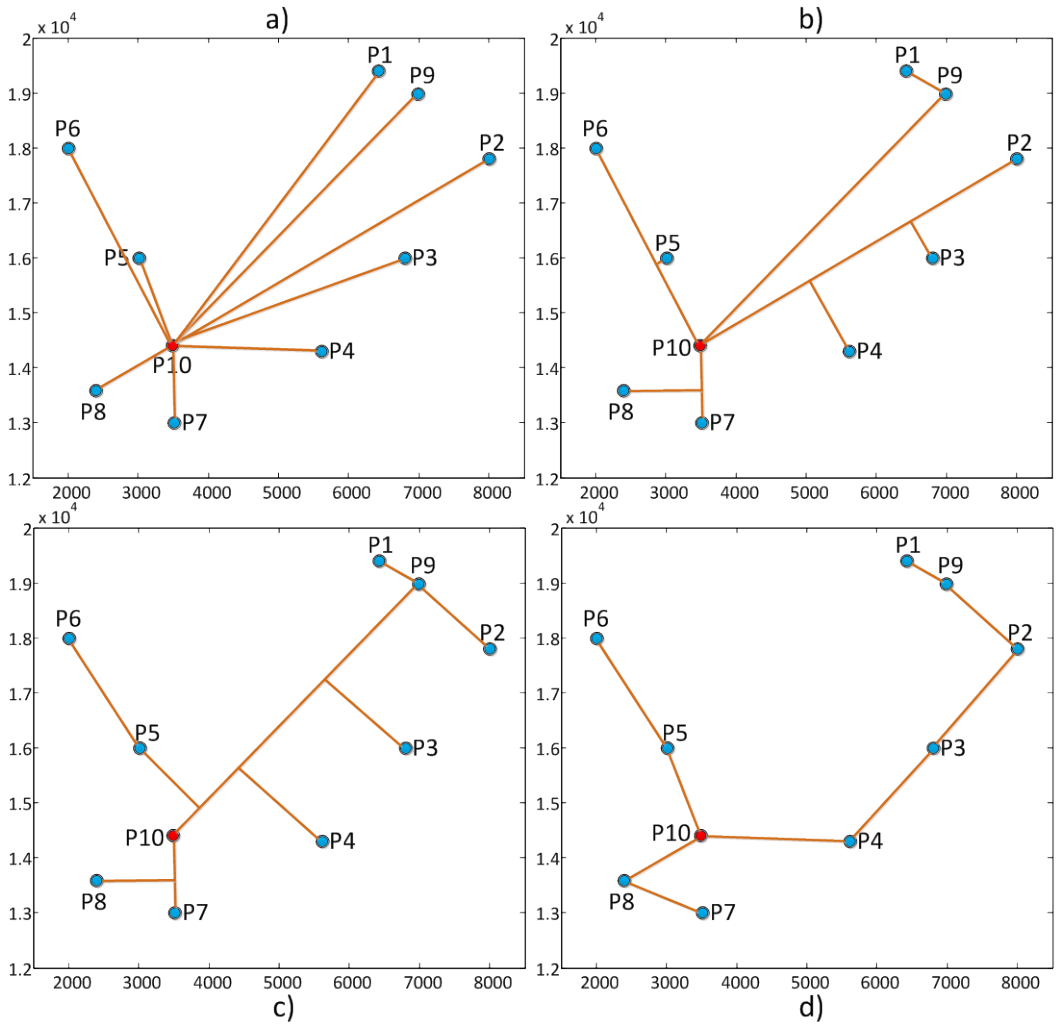

Figure 6.11 Communication infrastructure simulation results when MG central controller is located at (3500, 14500), using proposed approaches: a) Direct Connection, b) Joined Path, c) Longest Joined Path, and d) Shortest Distance Matrix.

Using the proposed Direct Connection approach in Figure 6.8(a), the total distance of communication infrastructure is 26,846.51 metres. However, when applying the proposed Shortest Distance Matrix approach, as shown in Figure 6.8(d), the total distance of communication infrastructure is reduced to 16,191.29 metres. In the proposed Direct Connection approach, all communication infrastructures from P1 to P10 are defined as dedicated. However, in the proposed Joined Path, Longest Joined Path, and Shortest Distance Matrix approaches, the communication infrastructures are shared. This shared communication infrastructure — used for data exchange between the DG, ESS, and load points of the communication devices — increases both data latency and communication delay in the MG [123].

The value of data latency can be approximated using the time occupation ratio (TODR), which is the ratio of the period each DG controller takes to transmit data to the MG central controller. A higher TODR correlates to a lower probability of data latency in the network. The TODR depends on the number of communication devices that share the same communication infrastructure. The TODR is calculated and presented in (3.1), and is not re-discussed in this section.

According to (3.1), the total distance of the communication infrastructure directly affects the installation costs, while the probability of data latency and communication delay can be compared between the proposed Direct Connection, Joined Path, Longest Joined Path, and Shortest Distance Matrix approaches, then numerically analysed and predicted. Table 6.1 shows a comparison of the total distance of the required communication infrastructure, using the four different approaches, and also presents the TODR with varied locations of the MG central controller (discussed above).

Table 6.1 Simulation summary of four different approaches for defining the Shortest Distance Communication Infrastructure in MGs.

MG Central Controller (x, y)	Direct connection		Joined Path			Longest Joined Path			Shortest Matrix		
	Total Distance (m)	TODR (%)	Total Distance (m)		TODR (%)	Total Distance (m)		TODR (%)	Total Distance (m)		TODR (%)
(5100, 16200)	26,846.51	900	19,036	–29.1%	400	17,580.34	–34.5%	200	16,191.29	–39.7%	300
(3500 , 14500)	31,019.76	900	20,685	–33.3%	400	17,562.18	–43.4%	300	15,128.33	–51.2%	301
(4000 , 18000)	31,360.71	900	19,172	–38.9%	300	18,657.86	–40.5%	200	16,960.1	–45.9%	100.971
(7000 , 15000)	32,792.5	900	21,906	–33.2%	400	17,275.88	–47.3%	101.2	15,464.29	–52.8%	177
(6000 , 18000)	29,636.62	900	18,645	–37.1%	300	17,952.49	–39.4%	150	16,365.05	–44.8%	202
(8000 , 12000)	53,264.61	900	24,988	–53.1%	97	21,273.7	–60.1%	102	18,284.26	–65.7%	152
Average		900		–37.4%	316		–44.2%	175.5		–50.0%	205.5

Table 6.1 shows that the shortest distance is achieved using the proposed Shortest Distance Matrix approach, which when compared to the Direct Connection approach, can reduce the total distance of the required communication infrastructure by up to 50%. The proposed Joined Path and Longest Joined Path approaches, when compared to the Direct Connection approach, reduce the total distance of the required communication infrastructure by up to 37.4% and 44.2%, respectively; however, the possibility of data latency and communication delay, which are represented by TODR, is increased. The average TODR — using the proposed Joined Path, Longest Joined Path, and Shortest Distance Matrix approaches — is 316%, 175.5%, and 205.5%, respectively, instead of the maximum TODR of 900%. The decrease in TODRs correspond to the possible increase of the communication delays. When implementing the Joined Path, Longest Joined Path, and Shortest Distance Matrix approaches, communication delays increase by 2.84, 5.13, and 4.37 times more than the proposed Direct Connection approach, respectively.

The impact of these communication delays on the operation of the MG are discussed and evaluated in the next section.

6.2. Proposed Centralised and Distributed Data Communication Scheme for Microgrids

As discussed in Sections 2.4 and 6.1, the data communication infrastructure and technology determines the type of the data communication scheme that can be applied and implemented on the MG. In this thesis and in many other published papers, data communication can be classified as a centralised data communication scheme, which is when the required data is transmitted from DGs, ESSs, or loads to the MG central controller [40], [41]. The MG central controller calculates and processes the received data, according to the implemented technique, before re-transmitting to the DGs, ESSs, and loads. In a distributed data communication scheme, all the required data is transmitted and exchanged between the DGs and ESSs without any coordination from the MG central controller [16], [17], [40].

According to (4.1), the load currents are supplied by the generated currents of all MG DGs. In a steady-state condition, the DGs generate the proportional current output according to their current ratio. However, voltage and current outputs generated proportionally require continuous data updating and proper synchronisation among DGs. Un-synchronised/randomly updating voltage and current outputs lead to an over/un-proportionally supplied current on the load side. Therefore, to achieve a proportional/designated voltage and current on the load side, periodic synchronisation among DGs for updating outputs is essential and performed via the proposed centralised and distributed data communication schemes as illustrated in Figure 6.12.

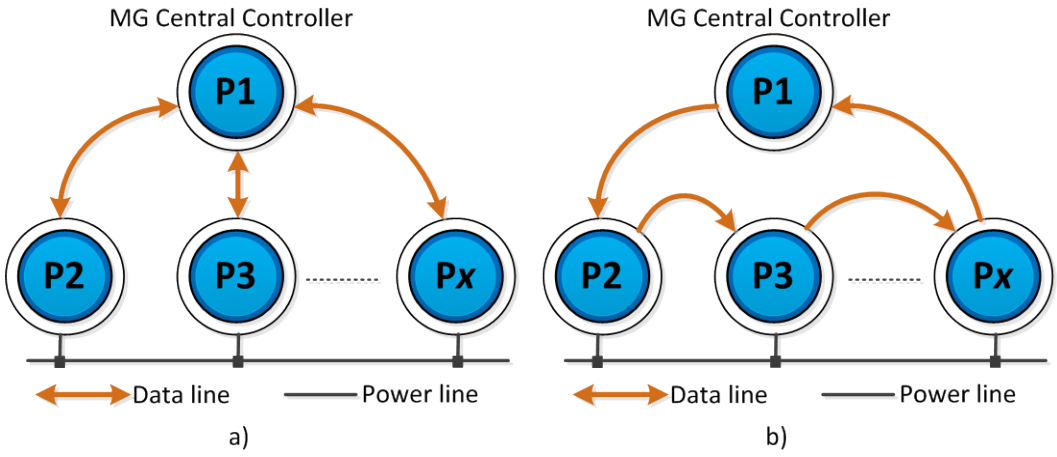

Figure 6.12 The proposed MG data communication scheme with: a) centralised data, b) distributed data.

Table 4.2 summarises the required data to be exchanged and transmitted, using the proposed voltage and power/current load sharing method that is presented in Equations (4.5) to (4.11). In the proposed centralised data communication scheme, I_{DG} and V_{DG} are transmitted from the DGs to the MG central controller to determine R_{DG} and $I_{\mathrm{T}}/P_{\mathrm{T}}$. The data $I_{\mathrm{T}}/P_{\mathrm{T}}$ is then calculated by the MG central controller and transmitted back to the DGs for re-calculating and updating of R^{*}_{DG}. To determine N, the data s_{DG} is transmitted to the MG central controller by the DGs. On the other hand, in the proposed distributed data communication scheme, all the above required data are transmitted to the next closest DG. The updated DG outputs are performed only when the above data is received in full from the previous closest DG. The proposed data flow in a

distributed scheme is designed to prevent data collision; it also shortens queues in the communication line.

In summary, in the proposed centralised data communication scheme, DG outputs are updated simultaneously, while in the proposed distributed data communication scheme, the DG outputs are updated sequentially. The data flow transmissions and flowcharts of the proposed centralised and distributed MG data communication schemes are illustrated in Figure 6.13 and Figure 6.14, respectively.

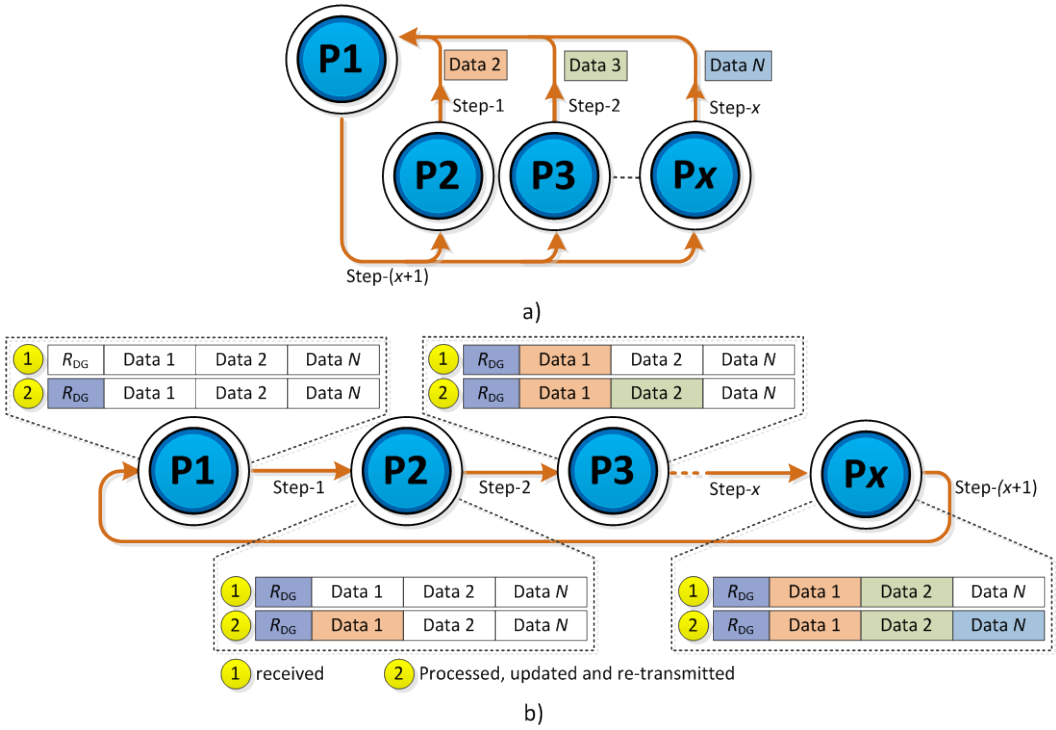

Figure 6.13 Data transmission flow of the proposed MG data communication scheme with: a) centralised scheme, b) distributed scheme.

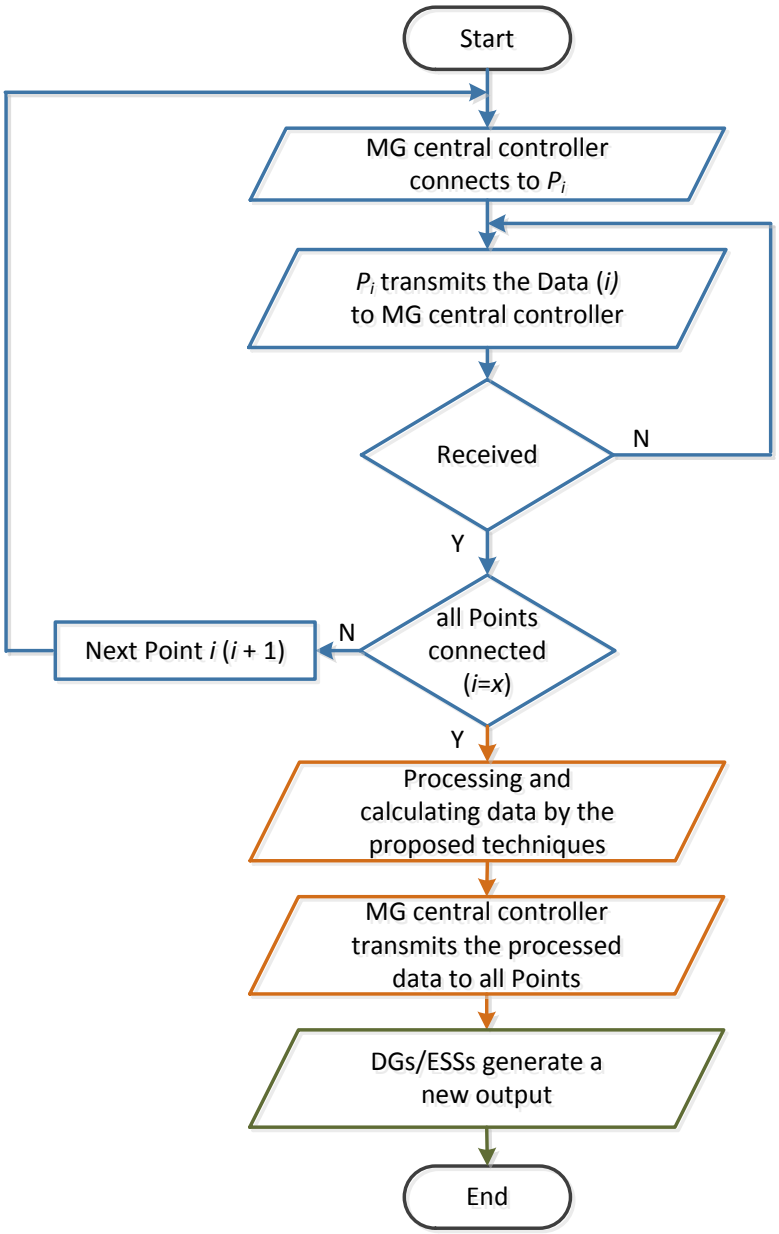
Start
MG central controller connects to P_i
P_i transmits the Data (i) to MG central controller
Received
N
Y
all Points connected (i=x)
N
Next Point i (i + 1)
Y
Processing and calculating data by the proposed techniques
MG central controller transmits the processed data to all Points
DGs/ESSs generate a new output
End

a)

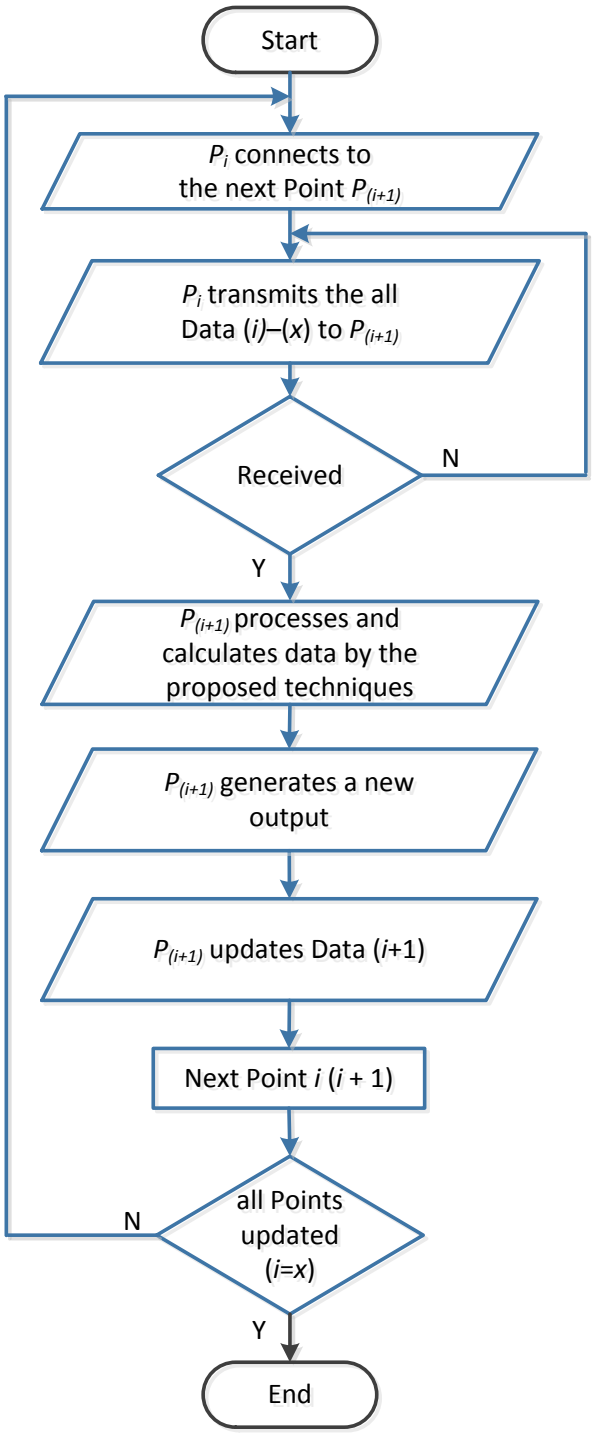

b)

Figure 6.14 One-cycle processing flowchart of the proposed MG data communication scheme with: a) centralised scheme, b) distributed scheme.

In the proposed technique, all received data are saved in the DG controllers and in the MG central controller, and then used in the calculations until a new value is received. Upon failure in the communication system, the proposed control

technique continues to function using the stored data. To prevent and eliminate communication failure problems, each communication technology has a protocol, such as the re-transmittal of the confirmation code to the transmitter [122]. Therefore, in this thesis, we assume that all transmitted data are received in a good and acceptable condition by the receiver.

6.2.1 Communication Delays

As discussed in Chapter 4, the proposed voltage regulation and power sharing method requires a specific time delay of T_{P}. Communication delay is unavoidable and must be considered in MG operation. There are several MG processes that contribute to the total delay in the MG operation; these include:

- Data latency affected by communication infrastructure (T_{IF}) is the probability of communication delay in different communication infrastructures. As discussed in Chapter 3 and [52], this delay can be approximated and predicted by the value of the TODR. According to Table 6.1, the average TODR of the proposed Joined Path, Longest Joined Path and Shortest Distance Matrix approaches are 2.84, 5.13, and 4.37 times lower than the proposed Direct Connection approach. This delay also incorporates the delay effects of several factors including: communication topology; protocol; frequency; security and modulation; landscape; data queue; packet loss and collision; signal strength; number of hops and routes; and clusters [53], [58], [79], [130], [131].
- Propagation delay (T_{PG}) is the required period for an electromagnetic signal to reach its destination point. However, because the speed of an electromagnetic signal in the air is equal to the speed of light, we can neglect the propagation delay.
- The data packet period (T_{DF}) is the required period for transmitting a single packet data. This delay is dependent on what communication bandwidth and technology is employed. The calculation of T_{DF} is presented in Chapter 3 and based on ZigBee communication technology. It is important to note that there is always the possibility of unsuccessful data transfer, and maximum number of data re-transmissions is up to 3x [122].

- DC-DC converter processing delay (T_{DC}) is the required period for a DC-DC converter to generate a steady-state designated output (voltage or current). This delay depends on many parameters, including the type of the converter, capacity, etc., and falls approximately between 1-20ms [31], [126], [127]. A value of $T_{\mathrm{DC}} = 10\mathrm{ms}$ is assumed in this thesis.
- Controller delay (T_{CL}), is the required period for the controller to process all inputs according to the proposed/implemented techniques. This delay includes the period for fetching data from sensors or actuators. A Digital controller (usually a micro-controller-based technology) and the employed clock can be up to 100 MHz. $T_{\mathrm{CL}} = 1\mathrm{ms}$ is assumed here.

According to the proposed data transmission flow in Figure 6.13 and the proposed one-cycle processing flowchart in Figure 6.14, total delay in the proposed centralised and distributed data communication schemes can be calculated and predicted.

The total time delay in the proposed centralised data communication scheme (T_{Cen}) is formulated as:

$$T_{\mathrm{Cen}} = \sum T_{\mathrm{DF}k} \times T_{\mathrm{IF}}, \forall k \epsilon \{1 \cdots (x-1)\}, T_{\mathrm{DC}j}, T_{\mathrm{CL}j}, \forall j \epsilon \{1 \cdots N)\} \tag{6.3}$$

It is to be noted that: the T_{DF} for the MG central controller requires connection to all points; the T_{DF} for the DGs/ESSs transmit data to the MG central controller (i.e. $V_{\mathrm{DG}}, I_{\mathrm{DG}}, s_{\mathrm{DG}}$), the T_{DF} for the loads transmits data to the MG central controller (i.e. V_{L}); and the T_{DF} for the MG central controller transmits the updated data to all DGs/ESSs (i.e. N, P_{T} or I_{T}, R^{*}_{DG}).

On the other hand, the total time delay required in the proposed distributed data communication scheme (T_{Den}) is formulated as:

$$T_{\mathrm{Den}} = \sum T_{\mathrm{DF}k} \times T_{\mathrm{IF}}, \forall k \epsilon \{1 \cdots x\}, T_{\mathrm{CL}j}, T_{\mathrm{DC}j}, \forall j \epsilon \{1 \cdots N\} \tag{6.4}$$

where T_{DF} is the required period for transmitting all data as presented in Table 4.2.

6.2.2 Dynamic Performance Evaluation

The dynamic performance of the proposed techniques with a DC MG spreading location, as discussed in Figure 6.8, is examined and modelled in MATLAB/Simulink. The DC MG network consists of four DGs and six load points. The power line connection and the simplified circuit diagram are illustrated in Figure 6.15. The technical parameters of the DC MG under consideration are summarised in Table 6.2.

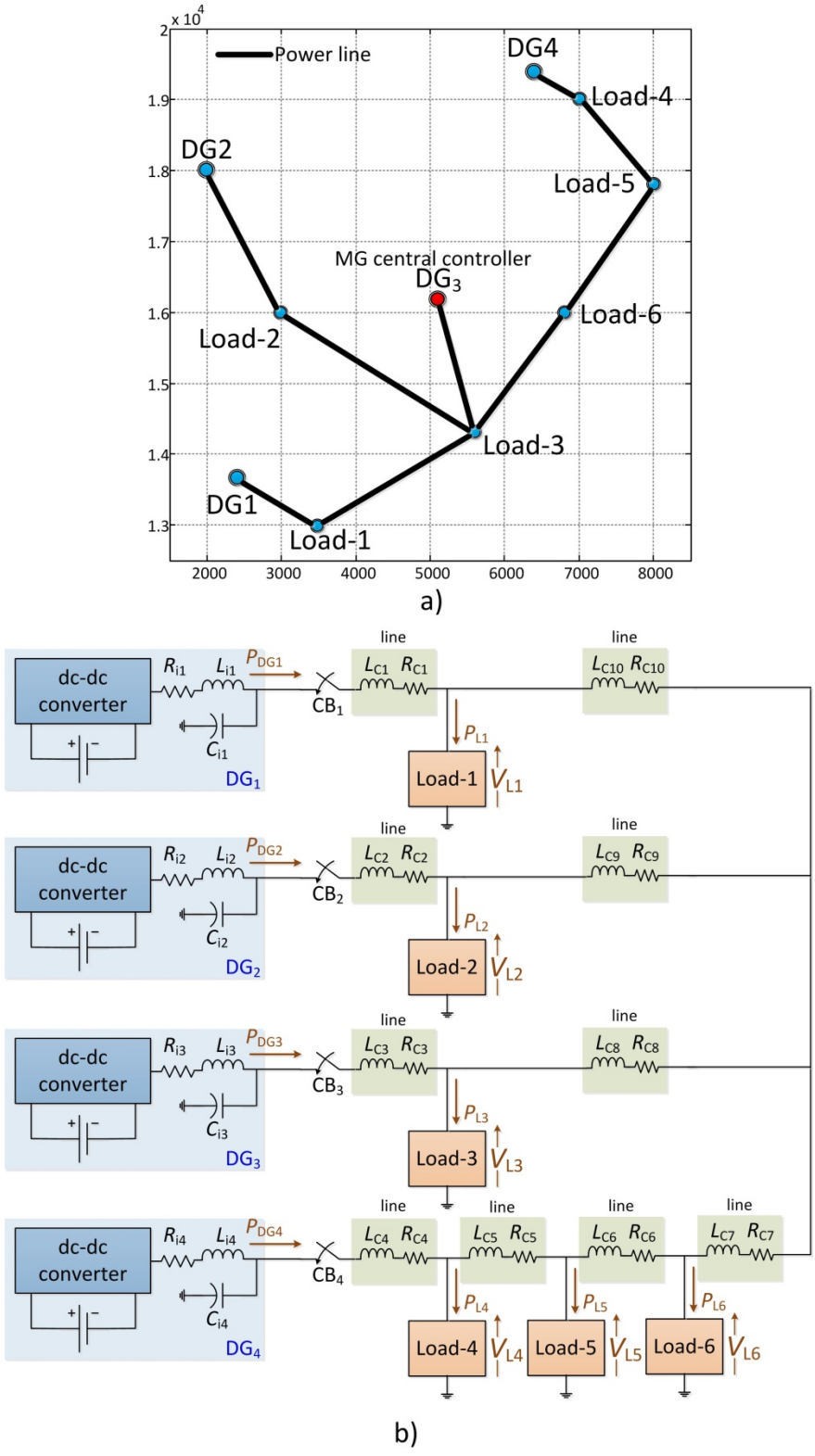

Figure 6.15 a) The power line connections and their spreading location, and b) the simplified circuit of the DC MG for both the centralised and distributed data communication simulations.

Table 6.2 Considered technical parameters for data communication scheme simulation.

Base	220 V, 70 A, 34 kW
Lines	$R_{\mathrm{C1..10}} = 0.1\ \Omega$, $R_{\mathrm{C2}} = 0.2\ \Omega$, $L_{\mathrm{C1..10}} = 10$ mH
Loads	capacity ≈ 5kW, $R_{\mathrm{L1..6}} = 10\ \Omega$, $L_{\mathrm{L1..6}} = 10$ mH, $C_{\mathrm{L1..6}} = 1$ mF
DG_1	Capacity ≈ 6kW, Vmax = 250V, $L_{\mathrm{i}} = 4$ mH, $C_{\mathrm{i}} = 1.5$ mF, $R_{\mathrm{i}} = 0.1\ \Omega$
DG_2	Capacity ≈ 11kW, Vmax = 270V, $L_{\mathrm{i}} = 4$ mH, $C_{\mathrm{i}} = 1.5$ mF, $R_{\mathrm{i}} = 0.1\ \Omega$
DG_3	Capacity ≈ 11kW, Vmax = 270V, $L_{\mathrm{i}} = 4$ mH, $C_{\mathrm{i}} = 1.5$ mF, $R_{\mathrm{i}} = 0.1\ \Omega$
DG_4	Capacity ≈ 6kW, Vmax = 250V, $L_{\mathrm{i}} = 4$ mH, $C_{\mathrm{i}} = 1.5$ mF, $R_{\mathrm{i}} = 0.1\ \Omega$

The DC MG is initially assumed to be in a steady-state condition, and the voltages at the load points are within an acceptable limit. The employed voltage and power/current load sharing techniques are the proposed techniques discussed in Chapter 4, and as proposed in Method-11 of Chapter 5. The voltage load feedback $\left(V_{\mathrm{L}}^{\mathrm{fb}}\right)$ is defined as avg$(V_{\mathrm{L}i}^{\max}, V_{\mathrm{L}i}^{\min}, \forall i \epsilon \{1 \cdots 6\})$

According to the proposed data flows in Figure 6.13, the proposed sequential charts in Figure 6.14, Equations (6.3) and (6.4), and the required transmittal period using ZigBee-based technology in Table 4.2, the T_{P} for the proposed centralised and distributed data communication schemes for a DC MG comprising of four DGs and six loads points is summarised in Table 6.3. When a higher bandwidth communication technology is employed, the period of T_{P} is smaller than the values presented in Table 6.3. For instance, the bandwidth of the Ethernet-based communication technology is up to 100 Mbps or up to 40 x faster than the ZigBee-based communication technology; thereby, in this case, the $\sum T_{\mathrm{DF}}, T_{\mathrm{IF}}$ is smaller than the values in Table 6.3. However, to examine the performance of the proposed methods in this thesis, the maximum delay is used instead of the minimum delay.

Table 6.3. The required periods for centralised and distributed data communication scheme in different communication infrastructures.

Centralised Data Communication Scheme				
Communication Infrastructure Approaches	$\sum T_{\mathrm{DF},} T_{\mathrm{IF},}(\mu s)$	$\sum T_{\mathrm{DC}}(\mathrm{ms})$	$\sum T_{\mathrm{CL}}(\mathrm{ms})$	$\sum T_{\mathrm{P}}(\mathrm{ms})$
Direct Connection	10612	10	1	21.612
Joined Path	30138	10	1	41.138
Longest Joined	54439	10	1	65.439
Shortest Distance	46374	10	1	57.374
Distributed Data Communication Scheme				
Direct Connection	128800	40	4	172.800
Joined Path	365792	40	4	409.792
Longest Joined	660744	40	4	704.744
Shortest Distance	562856	40	4	606.856

Table 6.3 shows that in the proposed centralised data communication scheme, the periods of T_{P} are implemented for just one-cycle to update the DG outputs. When the analysis is conducted on the proposed distributed data communication scheme, the periods of T_{P} are implemented for the total number of DGs and load cycles. When updating each DG individually, the required periods differ between DGs, as illustrated in Figure 6.13(b) and Figure 6.14(b).

In this simulation, the DG power ratios are proportionally defined based on their capacity, i.e. $R_{\mathrm{DG1}} = R_{\mathrm{DG4}} = \frac{6}{34}$, and $R_{\mathrm{DG2}} = R_{\mathrm{DG3}} = \frac{11}{34}$; hence while the loads are at peak demand, it is required the power to flow from DG_1, DG_2 and DG_3 to DG_4. The maximum load demand is simulated at $t = 3$ s. Using the proposed Shortest Distance Matrix approach communication infrastructure, the impacts of the proposed centralised and distributed data communication schemes on the voltage regulation and power sharing of the DC MG in Figure 6.15 is shown in Figure 6.16 and Figure 6.17.

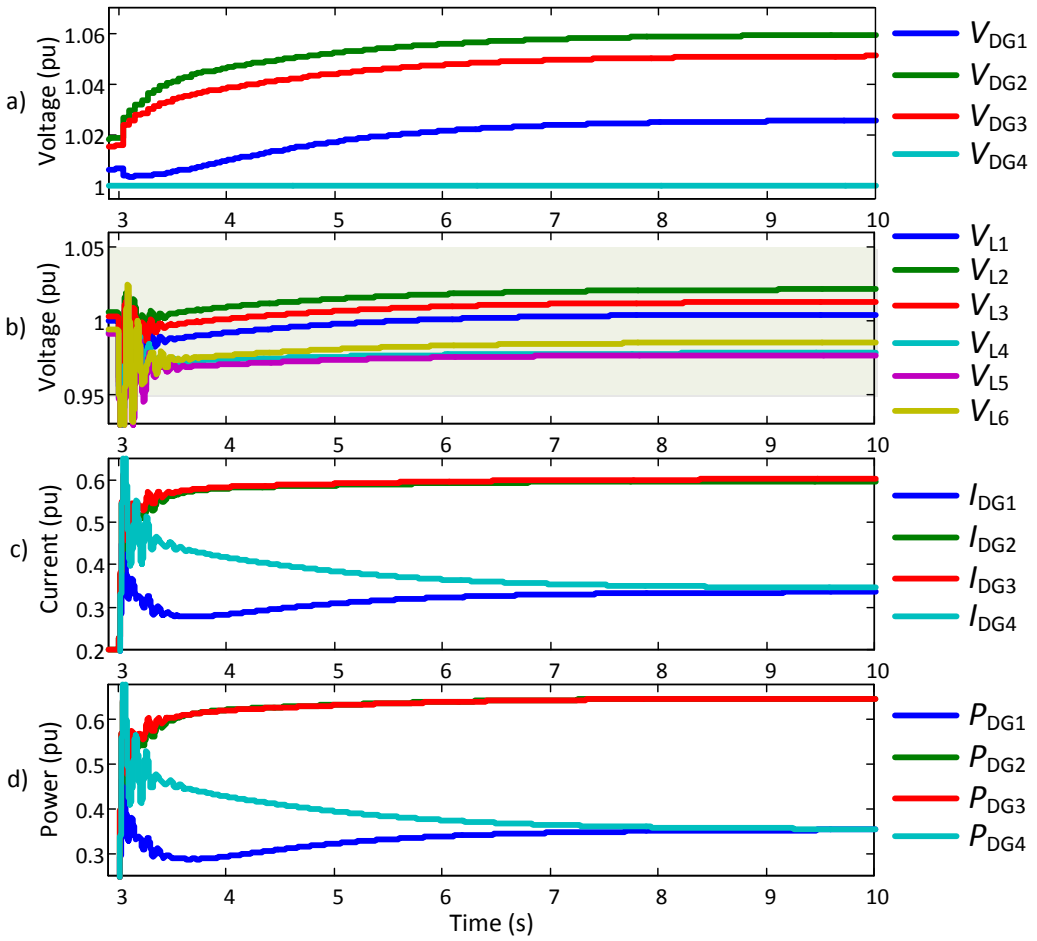

Figure 6.16 Voltage, current, and power profiles of the DC MG in the proposed centralised data communication simulation.

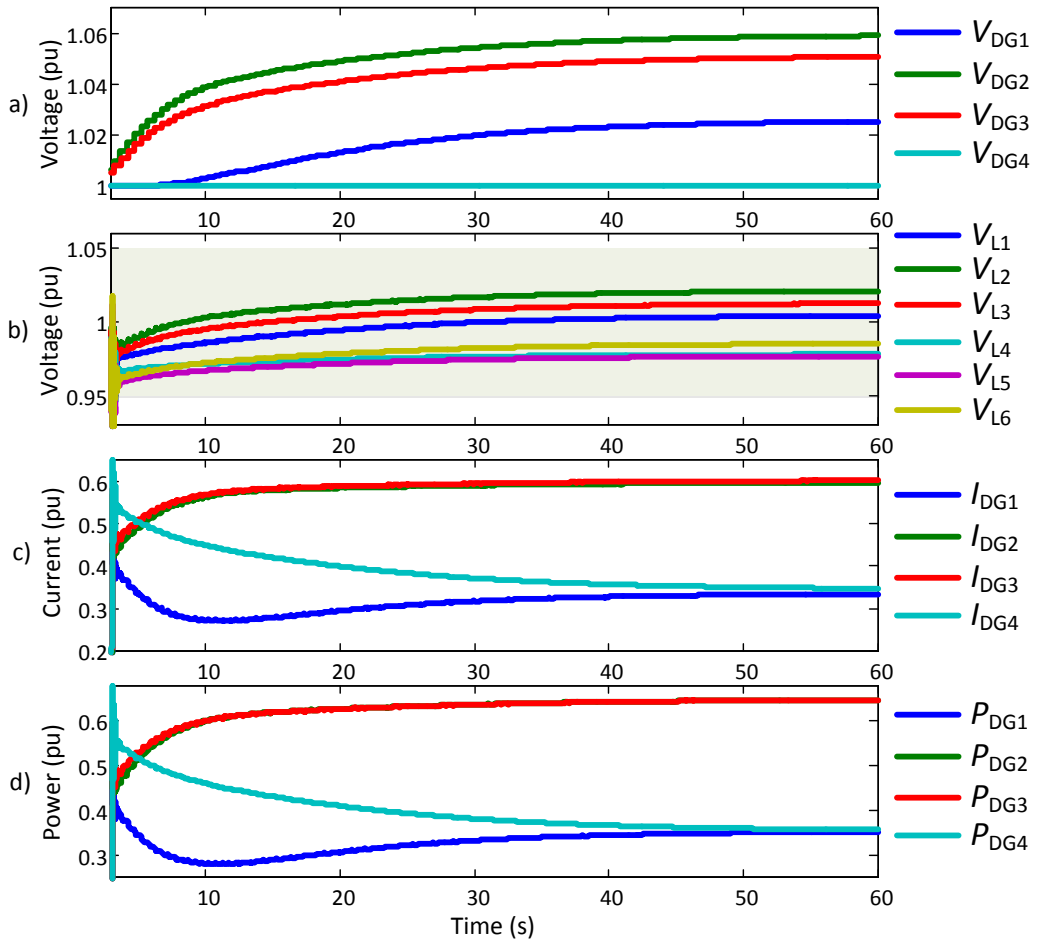

Figure 6.17 Voltage, current, and power profiles of the DC MG in the proposed distributed data communication simulation.

The simulation results reveal that the proposed centralised and distributed data communication schemes can maintain all voltage loads within the acceptable limit during fluctuation of load demands as shown in Figure 6.16(b) and Figure 6.17(b). The results also indicate that the DGs can generate power at precisely the designated rate as depicted in Figure 6.16(d) and Figure 6.17(d). DG_1, DG_2 and DG_3 generate higher voltage outputs than DG_4; this is to provide the required power for Load-4 and Load-5, which are closer to DG_4, as shown in Figure 6.16(a) and Figure 6.17(a). Power sharing in the DC MG can be achieved faster using the proposed centralised data communication scheme than the distributed scheme. In the proposed centralised data communication scheme, proportional and precisely generated DG power is achieved at $t =< 10$ s, while in the proposed distributed scheme, designated power is achieved around $t = 60$ s, as depicted in Figure 6.16(d) and Figure 6.17(d).

Circulating currents do not occur during the simulation, even though there are dissimilarities between the DG output voltages and the DG generated power, as illustrated in Figure 6.16(c) and Figure 6.17(c).

The one-cycle processing for voltage regulation and power/current load sharing in the DC MG is clearly illustrated and explained for both the proposed centralised and distributed data communication schemes in Figure 6.18(a) and (b), respectively. According to the proposed flowchart in Figure 6.14(a) and (b) and as shown in Figure 6.18(a), all DGs in the proposed centralised data communication scheme update their output upon receiving the required data from the MG central controller . In the proposed distributed scheme, as shown in Figure 6.18(b), the DGs update their outputs only after receiving the required data from another DG

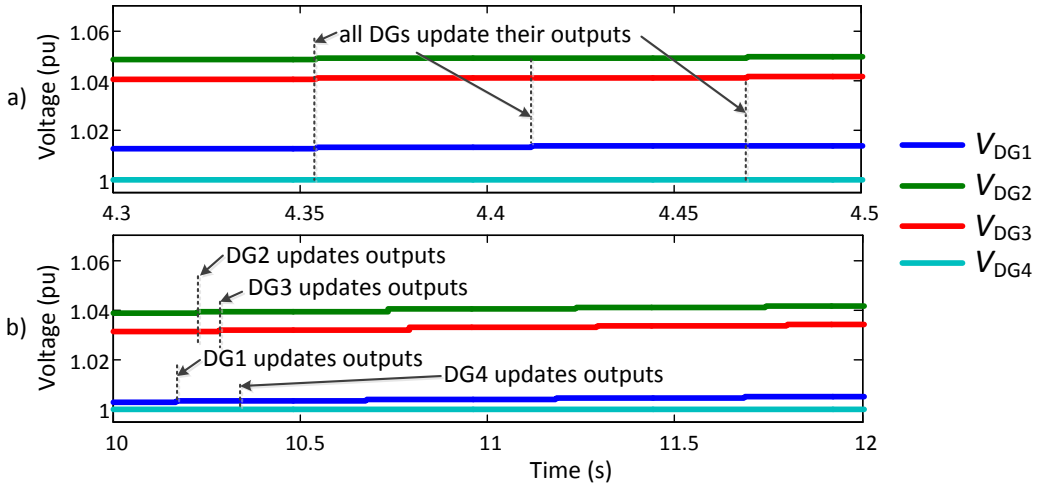

Figure 6.18 The DG one-cycle processing for updating outputs using: a) centralised, and b) distributed data communication scheme.

6.3. Summary

Data communication among DGs, ESSs, loads and other units in MG is required and essential for MG operational. However, establishing data communication infrastructure in the MG leads to a significant installation cost. Therefore, defining shorter distances for data communication in the MG is an important economic issue to be considered. Four different approaches for communication infrastructure in MG are presented, discussed, and simulated in this chapter. Using numerical analyses in Matlab/Simulink, it can be shown that

the required total distance of communication infrastructure in MG is reduced by implementing the proposed approaches. However, the probability of data latency of the MG communication network might be increased.

The impacts of the proposed communication infrastructure approaches in the dc MG operation are examined by implementing the proposed centralized and decentralized data communication schemes. In the proposed centralized scheme, the synchronization among DGs for updating outputs is conducted by MG central controller by transmitting the required data to all DGs at the time. While in the proposed decentralized scheme, updating DG outputs are performed after receiving the required data from another DG. The simulation results indicate that the proposed centralized and decentralized data communication schemes can maintain all loads voltages within acceptable limit during fluctuations of load demands. Meantime the designated and proportional generated power by DGs can be achieved precisely.

As demonstrated through simulation studies, the dynamic operation of an MG with the proposed technique and such a large communication delay can be realized successfully. The communication delay becomes smaller when using higher bandwidth communication technologies such as Wi-Fi. Thereby, any other communication technology listed in Table 2.1 with a smaller delay can be employed without any negative impacts on the performance of the proposed technique.

Chapter 7: Conclusion and Future Works

In this chapter, the conclusion and future works are drawn and discussed. The conclusion is presented in the first sub-chapter, and the future work is discussed in the second sub-chapter.

7.1. Conclusion

A ZigBee-based wireless data communication system is presented in this thesis for future MGs. The proposed communication system is responsible for transmitting several electrical parameters from the local controller of each DG to the MG central controller and vice versa. The standard ZigBee data frame is used to transmit the data, and a new coding is presented for the data payload section of this frame. The new coding represents each of the above-mentioned data, their values, dimensions, and origin (i.e. from a sensor, meter, etc.) in binary or text format. As proposed in this thesis, the data payload section can either be composed of a fixed number of bits or variable number of bits.

The data transmission delay is affected by the selection of the binary/text format, the fixed/variable number of bits for the data payload, and also the carrier frequency. Through several numerical analyses, a comparison of the expected data transmission delay is provided, as well as the maximum number of symbols that can be used to transmit data in those MGs with several DGs. These analyses are carried out for the above-mentioned data sets, and then the relevant transmission delays are calculated in each format/coding configuration. From these analyses, it can be seen that to cover a vast area, ZigBees with a carrier frequency of 868 MHz or 915 MHz are required; however, these results also show an increase in data transmission delay. A 2.45 GHz ZigBee can be used over shorter distances, and produces a much smaller data transmission delay.

The PSCAD/EMTDC-based simulations show that the droop control system needs to be located within the local controller of each DG; otherwise, there is a greater possibility of system instability due to communication delays, even for the ZigBees with the fastest processing time. The communication delay — caused by transferring the droop control set-points from the MG central controller and MG

main CB status, to the local controller of each DG — does not affect the dynamic performance of the MG system, even for the ZigBee with the slowest processing time.

This thesis also proposes a new technique which simultaneously facilitates voltage regulation at the load points of a DC MG and proper power/current sharing amongst the existing active DGs. The results indicate that the proposed technique can retain MG voltage within acceptable limits while adjusting the output currents/powers of the DGs to realize the desired ratio; this is irrespective of load demand variations and the unequal and unknown impedances of the MG lines. The thesis verifies the successful dynamic operation of the system, considering the maximum processing delay time imposed by the communication system. The studies also illustrate the successful dynamic operation of the MG, using the proposed technique, under different loading conditions and various load types; upon failure of the data communication system; and with DGs with plug and play characteristics. The proposed technique is practical, easy to implement, and adaptable to any DC MG configuration, regardless of the number and locations of the DGs and their loads.

This thesis presents and discusses the various circuit configurations for DC MGs, made up of single/multi-source and single/multi-loads in a serial/parallel circuit, and their potential use for voltage regulation and power/current sharing. The specific characteristics of each configuration are discussed, analysed and simulated. The simulation results indicate that the proposed voltage regulation and power sharing methods can precisely achieve the desired DG voltage and generated current, and within predefined acceptable limits. The required feedback signal of the loads can be varied according to the proposed method. While all configurations can employ the proposed voltage regulation technique, several configurations cannot implement the power/current sharing technique due to its natural characteristics.

Data communication among DGs, ESSs, loads, and other units in the MG is required and essential for MG operation. However, establishing data communication infrastructure in the MG leads to significant installation costs. Therefore, for economic reasons, it is important to consider and define shorter distances for MG data communication. Four different approaches to MG

communication infrastructure are presented, discussed, and simulated in this thesis. Using numerical analyses in Matlab/Simulink, it is shown that the required total distance of communication infrastructure in an MG is reduced by implementing the proposed approach; however, the probability of data latency in the MG communication network might be increased. The impact of the proposed communication infrastructure approach on DC MG operation is examined by implementing the proposed centralised and distributed data communication schemes. In the proposed centralised scheme, DG synchronization for output updates is conducted by the MG central controller and the required data is transmitted to all DGs at the same time. In the proposed distributed scheme, the updating of DG outputs is performed only after the required data is received from the previous DG. The simulation results indicate that both the proposed centralised and distributed data communication schemes can maintain all voltages loads within acceptable limits during fluctuation of load demands. The designated and proportional DC generated power can also be achieved precisely.

7.2. Future Works

Suggested future works for the proposed system presented, discussed and simulated in this thesis are:

- Through numerical analysis, the required voltage load feedbacks for the DG controllers can be approximated and predicted to reduce communication installation costs and improve the robustness of the data communication system. Hence, the required data communication should only be employed for transmitting and exchanging data between the DGs and the MG central controller.
- Experimental results can be collated and compared using by a small-scale DC MG system. This study requires several fields of study, and an expensive installation start-up such as a DC MG network with various loads, DGs controller, a DC-DC converter, and communication system.

References

[1] Z. Liu, C. Su, H. Hoidalen, and Z. Chen, "A Multi-Agent System Based Protection and Control Scheme for Distribution System with Distributed Generation Integration," *IEEE Trans. Power Deliv.*, vol. 32, no. 1, pp. 536–545, 2017.

[2] K. Das, A. Nitsas, M. Altin, A. D. Hansen, and P. E. Sørensen, "Improved Load-Shedding Scheme Considering Distributed Generation," *IEEE Trans. Power Deliv.*, vol. 32, no. 1, pp. 515–524, 2017.

[3] R. H. Lasseter and P. Paigi, "Microgrid: a conceptual solution," in *IEEE 35th Annual Power Electronics Specialists Conference (IEEE Cat. No.04CH37551)*, 2004, pp. 4285–4290.

[4] I. Serban and C. Marinescu, "Control Strategy of Three-Phase Battery Energy Storage Systems for Frequency Support in Microgrids and with Uninterrupted Supply of Local Loads," *IEEE Trans. Power Electron. Electron.*, vol. 29, no. 9, pp. 5010–5020, 2014.

[5] Y. Gu, X. Xiang, W. Li, and X. He, "Mode-Adaptive Decentralized Control for Renewable DC Microgrid With Enhanced Reliability and Flexibility," *IEEE Trans. Power Electron.*, vol. 29, no. 9, pp. 5072–5080, 2014.

[6] E. Planas, J. Andreu, J. I. Gárate, I. Martínez De Alegría, and E. Ibarra, "AC and DC technology in microgrids: A review," *Renew. Sustain. Energy Rev.*, vol. 43, pp. 726–749, 2015.

[7] J. Zhao and F. Dörfler, "Distributed control and optimization in DC microgrids," *Automatica*, vol. 61, pp. 18–26, 2015.

[8] M. M. Salem, N. I. Elkalashy, Y. Atia, and T. A. Kawady, "Modified Inverter Control of Distributed Generation for Enhanced Relaying Coordination in Distribution Networks," *IEEE Trans. Power Deliv.*, vol. 8977, no. c, pp. 1–1, 2016.

[9] Y.-S. Kim, E.-S. Kim, and S.-I. Moon, "Distributed Generation Control Method for Active Power Sharing and Self-Frequency Recovery in an Islanded Microgrid," *IEEE Trans. Power Syst.*, vol. 32, no. 1, pp. 544–551, 2017.

[10] J. J. Jamian, H. A. Illias, K. Gia Ing, and H. Mokhlis, "Optimum distribution network operation considering distributed generation mode of operations and safety margin," *IET Renew. Power Gener.*, vol. 10, no. 8, pp. 1049–1058, 2016.

[11] M. M. A. Mahfouz and M. A. H. El-Sayed, "Smart grid fault detection and classification with multi-distributed generation based on current signals approach," *IET Gener. Transm. Distrib.*, vol. 10, no. 16, pp. 4040–4047, 2016.

[12] J. Lin, W. Yu, N. Zhang, X. Yang, H. Zhang, and W. Zhao, "A Survey on Internet of Things : Architecture , Enabling Technologies , Security and Privacy , and Applications," *IEEE Internet Things J.*, vol. 4662, no. c, pp. 1–17, 2017.

[13] S. A. Saleh, E. Ozkop, and A. S. Aljankawey, "The Development of a Coordinated Anti-Islanding Protection for Collector Systems with Multiple Distributed Generation Units," *IEEE Trans. Ind. Appl.*, vol. 52, no. 6, pp. 4656–4667, 2016.

[14] A. Sendin, “Communication Technologies , Networks , and Strategies for Practical Smart Grid Deployments : From Substations to Meters,” in *Communication and Networking in Smart Grids*, 1st Editio., Y. Xiao, Ed. New York: CRC Press, 2012, pp. 241–275.
[15] B. L. R. Stojkoska and K. V Trivodaliev, “A review of Internet of Things for smart home : Challenges and solutions,” *J. Clean. Prod.*, vol. 140, pp. 1454–1464, 2017.
[16] S. Moayedi and A. Davoudi, “Distributed Tertiary Control of DC Microgrid Clusters,” *IEEE Trans. Power Electron.*, vol. 31, no. 2, pp. 1717–1733, 2016.
[17] V. Nasirian, S. Moayedi, A. Davoudi, and F. Lewis, “Distributed Cooperative Control of DC Microgrids,” *IEEE Trans. Power Electron.*, vol. 30, no. 4, pp. 2288–2303, 2014.
[18] P. García, P. Arboleya, B. Mohamed, A. C. Vega, and M. C. Vega, “Implementation of a hybrid distributed / centralized real-time monitoring system for a DC / AC microgrid with energy storage capabilities,” *IEEE Trans. Ind. Informatics*, vol. 3203, no. 1551, pp. 1–10, 2016.
[19] N. C. F. Tse, J. Y. C. Chan, W. Lau, J. T. Y. Poon, and L. L. Lai, “Real-Time Power-Quality Monitoring With Hybrid Sinusoidal and Lifting Wavelet Compression Algorithm,” *IEEE Trans. Power Deliv.*, vol. 27, no. 4, pp. 1718–1726, 2012.
[20] M. S. Manikandan, S. R. Samantaray, and I. Kamwa, “Simultaneous denoising and compression of power system disturbances using sparse representation on overcomplete hybrid dictionaries,” *IET Gener. Transm. Distrib.*, vol. 9, no. 11, pp. 1077–1088, 2015.
[21] Y. Huang, A. Pang, and P. Hsiu, “Distributed Throughput Optimization for ZigBee Cluster-Tree Networks,” *IEEE Trans. Parallel Distrib. Syst.*, vol. 23, no. 3, pp. 513–520, Mar. 2012.
[22] H. Y. Tung, K. F. Tsang, K. T. Chui, H. C. Tung, H. R. Chi, G. P. Hancke, and K. F. Man, “The Generic Design of a High-Traffic Advanced Metering Infrastructure Using ZigBee,” *IEEE Trans. Ind. Informatics*, vol. 10, no. 1, pp. 836–844, 2014.
[23] C. Tseng, “Coordinator Traffic Diffusion for Data-Intensive Zigbee Transmission in Real-time Electrocardiography Monitoring.,” *IEEE Trans. Biomed. Eng.*, vol. 60, no. 12, pp. 3340–3346, Jun. 2013.
[24] I. Hwang, D. Lee, and J. Baek, “Home network configuring scheme for all electric appliances using ZigBee-based integrated remote controller,” *IEEE Trans. Consum. Electron.*, vol. 55, no. 3, pp. 1300–1307, Aug. 2009.
[25] J. M. Guerrero, J. C. Vasquez, J. Matas, L. G. de Vicuna, and M. Castilla, “Hierarchical Control of Droop-Controlled AC and DC Microgrids : A General Approach Toward Standardization,” *IEEE Trans. Ind. Electron.*, vol. 58, no. 1, pp. 158–172, 2011.
[26] F. Nejabatkhah and Y. W. Li, “Overview of Power Management Strategies of Hybrid AC/DC Microgrid,” *IEEE Trans. Power Electron.*, vol. 30, no. 12, pp. 7072–7089, 2015.
[27] J. J. Justo, F. Mwasilu, J. Lee, and J. W. Jung, “AC-microgrids versus DC-microgrids with distributed energy resources: A review,” *Renew. Sustain. Energy Rev.*, vol. 24, pp. 387–405, 2013.
[28] V. Nayanar, N. Kumaresan, and N. G. Ammasai Gounden, “Wind-driven SEIG supplying DC microgrid through a single-stage power converter,”

Eng. Sci. Technol. an Int. J., vol. 19, no. 3, pp. 1600–1607, 2016.

[29] M. S. Rahman, M. J. Hossain, and J. Lu, "Coordinated control of three-phase AC and DC type EV–ESSs for efficient hybrid microgrid operations," *Energy Convers. Manag.*, vol. 122, pp. 488–503, 2016.

[30] A. Khorsandi, M. Ashourloo, and H. Mokhtari, "A Decentralized Control Method for a Low-Voltage DC Microgrid," *IEEE Trans. ENERGY Convers.*, vol. 29, no. 4, pp. 793–801, 2014.

[31] B. C. Bao, X. Zhang, J. P. Xu, and J. P. Wang, "Critical ESR of output capacitor for stability of fixed off-time controlled buck converter," *IET Trans. Electron. Lett.*, vol. 49, no. 4, pp. 4–5, 2013.

[32] M. A. Setiawan, F. Shahnia, R. P. S. Chandrasena, and A. Ghosh, "Data Communication Network and its Delay Effect on the Dynamic Operation of Distributed Generation Units in a Microgrid," in *IEEE PES Asia-Pacific Power and Energy Engineering Conference (APPEEC)*, 2014, pp. 1–6.

[33] N. Yang, B. Nahid-Mobarakeh, F. Gao, D. Paire, A. Miraoui, and W. Liu, "Modeling and stability analysis of multi-time scale DC microgrid," *Electr. Power Syst. Res.*, vol. 140, pp. 906–916, 2016.

[34] H. Lotfi, A. Khodaei, and A. Indices, "AC Versus DC Microgrid Planning," *IEEE Trans. Smart Grid*, vol. 8, no. 1, pp. 296–304, 2017.

[35] P. A. Madduri, J. Poon, J. Rosa, M. Podolsky, E. A. Brewer, and S. R. Sanders, "Scalable DC Microgrids for Rural Electrification in Emerging Regions," *IEEE J. Emerg. Sel. Top. Power Electron.*, vol. 4, no. 4, pp. 1195–1205, 2016.

[36] M. Farhadi and O. Mohammed, "Adaptive Energy Management in Redundant Hybrid DC Microgrid for Pulse Load Mitigation," *IEEE Trans. Smart Grid*, vol. 6, no. 1, pp. 54–62, 2015.

[37] K. A. Alobeidli, M. H. Syed, M. S. El Moursi, and H. H. Zeineldin, "Novel Coordinated Voltage Control for Hybrid Micro-Grid With Islanding Capability," *IEEE Trans. Smart Grid*, vol. 6, no. 3, pp. 1116–1127, 2015.

[38] J. Xiao and P. Wang, "Hierarchical Control of Hybrid Energy Storage System in DC Microgrids," *IEEE Trans. Ind. Electron.*, vol. 62, no. 8, pp. 4915–4924, 2015.

[39] N. R. Tummuru, M. K. Mishra, and S. Srinivas, "Dynamic Energy Management of Renewable Grid Integrated Hybrid Energy Storage System," *IEEE Trans. Ind. Electron.*, vol. 62, no. 12, pp. 7728–7737, 2015.

[40] X. Lu, J. M. Guerrero, K. Sun, and J. C. Vasquez, "An Improved Droop Control Method For DC Microgrids Based On Low Bandwidth Communication With DC Bus Voltage Restoration And Enhanced Current Sharing Accuracy," *IEEE Trans. Power Electron.*, vol. 29, no. 4, pp. 1800–1812, 2014.

[41] S. Anand, B. G. Fernandes, and J. M. Guerrero, "Distributed Control to Ensure Proportional Load Sharing and Improve Voltage Regulation in Low-Voltage DC Microgrids," *IEEE Trans. Power Electron.*, vol. 28, no. 4, pp. 1900–1913, 2013.

[42] C. N. Papadimitriou, E. I. Zountouridou, and N. D. Hatziargyriou, "Review of hierarchical control in DC microgrids," *Electr. Power Syst. Res.*, vol. 122, pp. 159–167, 2015.

[43] N. Yang, D. Paire, F. Gao, A. Miraoui, and W. Liu, "Compensation of droop control using common load condition in DC microgrids to improve voltage regulation and load sharing," *Int. J. Electr. Power Energy Syst.*,

vol. 64, pp. 752–760, 2015.
[44] R. Asad and A. Kazemi, “A novel distributed optimal power sharing method for radial dc microgrids with different distributed energy sources,” *Energy*, vol. 72, pp. 291–299, 2014.
[45] M. Sechilariu, B. C. Wang, and F. Locment, “Supervision control for optimal energy cost management in DC microgrid: Design and simulation,” *Int. J. Electr. Power Energy Syst.*, vol. 58, pp. 140–149, 2014.
[46] S. Augustine, M. K. Mishra, and N. Lakshminarasamma, “Adaptive Droop Control Strategy for Load Sharing and Circulating Current Minimization in Low-Voltage Standalone DC Microgrid,” *IEEE Trans. Sustain. ENERGY*, vol. 6, no. 1, pp. 132–141, 2015.
[47] A. Khorsandi, M. Ashourloo, H. Mokhtari, and R. Iravani, “Automatic droop control for a low voltage DC microgrid,” *IET Gener. Transm. Distrib.*, vol. 10, no. 1, pp. 41–47, 2016.
[48] S. Augustine, N. Lakshminarasamma, and M. K. Mishra, “Control of photovoltaic-based low-voltage dc microgrid system for power sharing with modified droop algorithm,” *IET Power Electron.*, vol. 9, no. 6, pp. 1132–1143, 2016.
[49] A. P. N. Tahim, D. J. Pagano, E. Lenz, and V. Stramosk, “Modeling and Stability Analysis of Islanded DC Microgrids Under Droop Control,” *IEEE Trans. Power Electron.*, vol. 30, no. 8, pp. 4597–4607, 2015.
[50] Z. Akhtar and M. A. Saqib, “Microgrids formed by renewable energy integration into power grids pose electrical protection challenges,” *Renew. Energy*, vol. 99, pp. 148–157, 2016.
[51] V. C. Güngör, D. Sahin, T. Kocak, S. Ergüt, C. Buccella, C. Cecati, and G. P. Hancke, “Smart Grid Technologies : Communication Technologies and Standards,” *IEEE Trans. Ind. Informatics*, vol. 7, no. 4, pp. 529–539, 2011.
[52] M. A. Setiawan, F. Shahnia, S. Rajakaruna, and A. Ghosh, “ZigBee-Based Communication System for Data Transfer Within Future Microgrids,” *IEEE Trans. Smart Grid*, vol. 6, no. 5, pp. 2343–2355, 2015.
[53] B. Wang, M. Sechilariu, and F. Locment, “Intelligent DC Microgrid With Smart Grid Communications : Control Strategy Consideration and Design,” *IEEE Trans. Smart Grid*, vol. 3, no. 4, pp. 2148–2156, 2012.
[54] A. Usman and S. H. Shami, “Evolution of Communication Technologies for Smart Grid applications,” *Renew. Sustain. Energy Rev.*, vol. 19, pp. 191–199, Mar. 2013.
[55] F. Gómez-cuba, R. Asorey-cacheda, and F. J. González-castaño, “Smart Grid Last-Mile Communications Model and Its Application to the Study of Leased Broadband,” *IEEE Trans. Smart Grid*, vol. 4, no. 1, pp. 5–12, 2013.
[56] Q. Shafiee, T. Dragicevic, J. C. Vasquez, and J. M. Guerrero, “Hierarchical control for multiple DC-microgrids clusters,” *IEEE Trans. Energy Convers.*, vol. 29, no. 4, pp. 922–933, 2014.
[57] T. Dragi, J. C. Vasquez, and D. Skrlec, “Supervisory Control of an Adaptive-Droop Regulated DC Microgrid With Battery Management Capability,” *IEEE Trans. Power Electron.*, vol. 29, no. 2, pp. 695–706, 2014.
[58] H. Li, J. Bin Song, and Q. Zeng, “Adaptive Modulation in Networked Control Systems with Application in Smart Grids,” *IEEE Commun. Lett. S*, vol. 17, no. 7, pp. 1305–1308, 2013.
[59] X. Lu, K. Sun, J. M. Guerrero, J. C. Vasquez, L. Huang, and J. Wang,

"Stability Enhancement Based on Virtual Impedance for DC Microgrids With Constant Power Loads," *IEEE Trans. Smart Grid*, vol. 6, no. 6, pp. 2770–2783, 2015.

[60] T. Dragicevic, X. Lu, J. C. Vasquez, and J. M. Guerrero, "DC Microgrids - Part I: A Review of Control Strategies and Stabilization Techniques," *IEEE Trans. Power Electron.*, vol. 31, no. 7, pp. 4876–4891, 2016.

[61] N. Langhammer and R. Kays, "Performance Evaluation of Wireless Home Automation Networks in Indoor Scenarios," *IEEE Trans. Smart Grid*, vol. 3, no. 4, pp. 2252–2261, Dec. 2012.

[62] C. Zhang, W. Ma, and C. Sun, "A switchable high-speed fiber-optic ring net topology and its method of high-performance synchronization for large-capacity power electronics system," *Int. J. Electr. Power Energy Syst.*, vol. 57, pp. 335–349, May 2014.

[63] S. Yoon, S. Jang, Y. Kim, and S. Bahk, "Opportunistic Routing for Smart Grid With Power Line Communication Access Networks," *IEEE Trans. Smart Grid*, vol. 5, no. 1, pp. 303–311, 2014.

[64] N. Radhika and V. Vanitha, "Smart Grid Test Bed Based on Gsm," *Procedia Eng.*, vol. 30, no. 2011, pp. 258–265, Jan. 2012.

[65] Y. Zhang, L. Wang, W. Sun, R. C. Green II, and M. Alam, "Distributed Intrusion Detection System in a Multi-Layer Network Architecture of Smart Grids," *IEEE Trans. Smart Grid*, vol. 2, no. 4, pp. 796–808, Dec. 2011.

[66] T. Liu, Y. Liu, Y. Mao, Y. Sun, X. Guan, W. Gong, and S. Xiao, "A Dynamic Secret-Based Encryption Scheme for Smart Grid Wireless Communication," *IEEE Trans. Smart Grid*, vol. 5, no. 3, pp. 1175–1182, May 2014.

[67] N. C. Batista, R. Melício, J. C. O. Matias, and J. P. S. Catalão, "Photovoltaic and wind energy systems monitoring and building/home energy management using ZigBee devices within a smart grid," *Energy*, vol. 49, no. 1, pp. 306–315, 2013.

[68] S. Ahmad, "Smart metering and home automation solutions for the next decade," in *2011 International Conference on Emerging Trends in Networks and Computer Communications (ETNCC)*, 2011, pp. 200–204.

[69] C. Deng, X. Xiao, Z. Fu, G. Liu, H. Yang, and J. Liu, "Terrestrial-Satellite Hybrid Backbone Communication Network for Smart Power Grid," *Energy Procedia*, vol. 12, pp. 27–36, Jan. 2011.

[70] T. N. Le, W.-L. Chin, and H.-H. Chen, "Standardization and Security for Smart Grid Communications Based on Cognitive Radio Technologies -- A Comprehensive Survey," *IEEE Commun. Surv. Tutorials*, vol. 19, no. 1, pp. 423–445, 2017.

[71] F. M. Sallabi, a. M. Gaouda, a. H. El-Hag, and M. M. a. Salama, "Evaluation of ZigBee Wireless Sensor Networks Under High Power Disturbances," *IEEE Trans. Power Deliv.*, vol. 29, no. 1, pp. 13–20, Feb. 2014.

[72] P. Valdastri, a. Menciassi, and P. Dario, "Transmission Power Requirements for Novel ZigBee Implants in the Gastrointestinal Tract," *IEEE Trans. Biomed. Eng.*, vol. 55, no. 6, pp. 1705–1710, Jun. 2008.

[73] Y. Zhang and Q. Li, "Exploiting ZigBee in Reducing WiFi Power Consumption for Mobile Devices," *IEEE Trans. Mob. Comput.*, vol. 13, no. 12, pp. 2806–2819, 2014.

[74] P. Yi, S. Member, A. Iwayemi, C. Zhou, and S. Member, “Developing ZigBee Deployment Guideline Under WiFi Interference for Smart Grid Applications,” *IEEE Trans. Smart Grid*, vol. 2, no. 1, pp. 110–120, 2011.
[75] Digi International Inc., *XBee ® /XBee-PRO ® RF Modules*. Minnetonka, MN: Digi International Inc., 2009.
[76] Y.-K. Chen, Y.-C. Wu, C.-C. Song, and Y.-S. Chen, “Design and Implementation of Energy Management System With Fuzzy Control for DC Microgrid Systems,” *IEEE Trans. Power Electron.*, vol. 28, no. 4, pp. 1563–1570, Apr. 2013.
[77] J. Huang, H. Wang, Y. Qian, and C. Wang, “Priority-Based Traffic Scheduling and Utility Optimization for Cognitive Radio Communication Infrastructure-Based Smart Grid,” *IEEE Trans. Smart Grid*, vol. 4, no. 1, pp. 78–86, Mar. 2013.
[78] E. A. A. Coelho, D. Wu, J. M. Guerrero, J. C. Vasquez, T. Dragičević, Č. Stefanović, and P. Popovski, “Small-Signal Analysis of the Microgrid Secondary Control Considering a Communication Time Delay,” *IEEE Trans. Ind. Electron.*, vol. 63, no. 10, pp. 6257–6269, 2016.
[79] X. Lu, K. Sun, J. M. Guerrero, J. C. Vasquez, and L. Huang, “State-of-Charge Balance Using Adaptive Droop Control for Distributed Energy Storage Systems in DC Microgrid Applications,” *IEEE Trans. Ind. Electron.*, vol. 61, no. 6, pp. 2804–2815, 2014.
[80] M. A. Abusara, S. M. Sharkh, and J. M. Guerrero, “Improved droop control strategy for grid-connected inverters,” *Sustain. Energy, Grids Networks*, vol. 1, pp. 10–19, 2015.
[81] Y. Gu, W. Li, and X. He, “Frequency-Coordinating Virtual Impedance for Autonomous Power Management of DC Microgrid,” *IEEE Trans. Power Electron.*, vol. 30, no. 4, pp. 2328–2337, 2015.
[82] N. L. Diaz, T. Dragiˇ, and J. M. Guerrero, “Intelligent Distributed Generation and Storage Units for DC Microgrids — A New Concept on Cooperative Control Without Communications Beyond Droop Control,” *IEEE Trans. Smart Grid*, vol. 5, no. 5, pp. 2476–2485, 2014.
[83] S. Sanchez and M. Molinas, “Large Signal Stability Analysis at the Common Coupling Point of a DC Microgrid : A Grid Impedance Estimation Approach Based on a Recursive Method,” *IEEE Trans. ENERGY Convers.*, vol. 30, no. 1, pp. 122–131, 2015.
[84] P. Zhang, H. Zhao, H. Cai, J. Shi, and X. He, “Power decoupling strategy based on ‘virtual negative resistor’for inverters in low-voltage microgrids,” *Iet Power Electron.*, vol. 9, no. 5, pp. 1037–1044, 2016.
[85] Y. Guan, J. M. Guerrero, X. Zhao, J. C. Vasquez, and X. Guo, “A New Way of Controlling Parallel-Connected Inverters by Using Synchronous-Reference-Frame Virtual Impedance Loop - Part I: Control Principle,” *IEEE Trans. Power Electron.*, vol. 31, no. 6, pp. 4576–4593, 2016.
[86] H. Kakigano, Y. Miura, and T. Ise, “Distribution voltage control for DC microgrids using fuzzy control and gain-scheduling technique,” *IEEE Trans. Power Electron.*, vol. 28, no. 5, pp. 2246–2258, 2013.
[87] A. Tah and D. Das, “An Enhanced Droop Control Method for Accurate Load Sharing and Voltage Improvement of Isolated and Interconnected DC Microgrids,” *IEEE Trans. Sustain. Energy*, vol. 7, no. 3, pp. 1194–1204, 2016.
[88] X. Zhou, F. Tang, P. C. Loh, X. Jin, and W. Cao, “Four-Leg Converters

with Improved Common Current Sharing and Selective Voltage-Quality Enhancement for Islanded Microgrids," *IEEE Trans. Power Deliv.*, vol. 31, no. 2, pp. 522–531, 2016.

[89] P. H. Huang, P. C. Liu, W. Xiao, and M. S. El Moursi, "A Novel Droop-Based Average Voltage Sharing Control Strategy for DC Microgrids," *IEEE Trans. Smart Grid*, vol. 6, no. 3, pp. 1096–1106, 2015.

[90] J. Chi, P. Wang, J. Xiao, Y. Tang, and F. H. Choo, "Implementation of Hierarchical Control in DC microgrids," *IEEE Trans. Ind. Electron.*, vol. 61, no. 8, pp. 4032–4042, 2014.

[91] L. Meng, Q. Shafiee, G. F. Trecate, H. Karimi, D. Fulwani, X. Lu, and J. M. Guerrero, "Review on Control of DC Microgrids and Multiple Microgrid Clusters," *IEEE J. Emerg. Sel. Top. Power Electron.*, vol. 5, no. 3, pp. 928–948, 2017.

[92] M. Farhadi and O. a. Mohammed, "Real-time operation and harmonic analysis of isolated and non-isolated hybrid DC microgrid," *IEEE Trans. Ind. Appl.*, vol. 50, no. 4, pp. 2900–2909, 2014.

[93] Z. Wang, W. Wu, and B. Zhang, "A Distributed Control Method With Minimum Generation Cost for DC Microgrids," *IEEE Trans. Energy Convers.*, vol. 31, no. 4, pp. 1462–1470, 2016.

[94] A. A. Mohamed, A. T. Elsayed, T. A. Youssef, and O. A. Mohammed, "Hierarchical control for DC microgrid clusters with high penetration of distributed energy resources," *Electr. Power Syst. Res.*, vol. 148, pp. 210–219, 2017.

[95] Y. Zhang and Y. Li, "Energy Management Strategy for Supercapacitor Virtual Impedance," *IEEE Trans. Power Electron.*, vol. 32, no. 4, pp. 2704–2716, 2017.

[96] W. W. Weaver, R. D. Robinett, G. G. Parker, and D. G. Wilson, "Energy storage requirements of dc microgrids with high penetration renewables under droop control," *Int. J. Electr. Power Energy Syst.*, vol. 68, pp. 203–209, 2015.

[97] Z. Zhang, Y. Cai, Y. Zhang, D. Gu, and Y. Liu, "A Distributed Architecture Based on Microbank Modules With Self-Reconfiguration Control to Improve the Energy Efficiency in the," *IEEE Trans. POWER Electron.*, vol. 31, no. 1, pp. 304–317, 2016.

[98] S. Lu, L. Wang, T. Lo, and A. V Prokhorov, "Integration of Wind Power and Wave Power Generation Systems Using a DC Microgrid," *IEEE Trans. Ind. Appl.*, vol. 51, no. 4, pp. 2753–2761, 2015.

[99] N. Liu, Q. Chen, X. Lu, J. Liu, and J. Zhang, "A Charging Strategy for PV-Based Battery Switch Stations Considering Service Availability and Self-Consumption of PV Energy," *IEEE Trans. Ind. Electron.*, vol. 62, no. 8, pp. 4878–4889, 2015.

[100] M. Mahdi and J. Soltani, "A robust control strategy for a grid-connected multi-bus microgrid under unbalanced load conditions," *Int. J. Electr. Power Energy Syst.*, vol. 71, pp. 68–76, 2015.

[101] E. Unamuno and J. A. Barrena, "Hybrid ac/dc microgrids - Part I: Review and classification of topologies," *Renew. Sustain. Energy Rev.*, vol. 52, pp. 1251–1259, 2015.

[102] J. Singh, P. Veeraraghavan, and S. Singh, "QoS multicast routing using Explore Best Path," *Comput. Commun.*, vol. 29, no. 15, pp. 2881–2894, Sep. 2006.

[103] C. W. Duin, “Two fast algorithms for all-pairs shortest paths,” *Comput. Oper. Res.*, vol. 34, no. 9, pp. 2824–2839, Sep. 2007.
[104] R. Ahmed, M. F. Bari, S. R. Chowdhury, M. G. Rabbani, R. Boutaba, and B. Mathieu, “Route: Routing on Names,” *IEEE/ACM Trans. Netw.*, vol. 24, no. 5, pp. 3073–3083, 2016.
[105] C. Wu, C. Deng, L. Liu, J. Han, J. Chen, S. Yin, and S. Wei, “A Multi-Objective Model Oriented Mapping Approach for NoC-based Computing Systems,” *IEEE Trans. Parallel Distrib. Syst.*, vol. 28, no. 3, pp. 662–676, 2017.
[106] X. Fang, D. Yang, P. Gundecha, and G. Xue, “MAP : Multi-Constrained Anypath Routing in Wireless Mesh Networks,” *IEEE Trans. Mob. Comput.*, vol. 12, no. 10, pp. 1893–1906, 2013.
[107] K. Chen and H. Shen, “SMART: Utilizing Distributed Social Map for Lightweight Routing in Delay-tolerant Networks,” *IEEE/ACM Trans. Netw.*, vol. 22, no. 5, pp. 1545–1558, 2014.
[108] C. Pschierer, B. Gilbert, C. DeBisschop, and S. Van Der Stricht, “Aerodrome mapping databases supporting taxi routing functions,” *IEEE Aerosp. Electron. Syst. Mag.*, vol. 28, no. 10, pp. 4–13, 2013.
[109] T. Wang, D. Zhang, X. Zhou, X. Qi, H. Ni, and H. Wang, “Mining Personal Frequent Routes via Road Corner Detection,” *IEEE Trans. Syst. MAN, Cybern. Syst.*, vol. 46, no. 4, pp. 445–458, 2016.
[110] F. Rupi, S. Bernardi, and J. Schweizer, “Map-matching algorithm applied to bicycle global positioning system traces in Bologna,” *IET Intell. Transp. Syst.*, vol. 10, no. 4, pp. 244–250, 2016.
[111] B. Ma, Y. Feng, X. Jia, G. Wang, J. Zhang, R. Li, and F. Shi, “Vehicle routing in urban areas based on the Oil Consumption Weight -Dijkstra algorithm,” *IET Intell. Transp. Syst.*, vol. 10, no. 7, pp. 495–502, 2016.
[112] E. Unamuno and J. A. Barrena, “Hybrid ac/dc microgrids - Part II: Review and classification of control strategies,” *Renew. Sustain. Energy Rev.*, vol. 52, pp. 1123–1134, 2015.
[113] F. Shahnia, R. P. S. Chandrasena, S. Rajakaruna, and A. Ghosh, “Primary control level of parallel distributed energy resources converters in system of multiple interconnected autonomous microgrids within self-healing networks,” *IET Gener. Transm. Distrib.*, vol. 8, no. 2, pp. 203–222, Feb. 2014.
[114] T. a. Papadopoulos, A. I. Chrysochos, and G. K. Papagiannis, “Narrowband power line communication: Medium voltage cable modeling and laboratory experimental results,” *Electr. Power Syst. Res.*, vol. 102, pp. 50–60, Sep. 2013.
[115] A. Cataliotti, G. Cipriani, V. Cosentino, D. D. Cara, V. Di Dio, S. Guaiana, N. Panzavecchia, and G. Tinè, “A prototypal architecture of a IEEE 21451 network for smart grid applications based on power line communications,” *IEEE Sens. J.*, vol. 15, no. 5, pp. 2460–2467, 2015.
[116] E. Padilla, “Towards Smart Integration of Distributed Energy Resources Using Distributed Network Protocol Over Ethernet,” *Smart Grid, IEEE …*, vol. 5, no. 4, pp. 1686–1695, 2014.
[117] J. J. Nielsen, N. K. Pratas, and P. Popovski, “What can wireless cellular technologies do about the upcoming smart metering traffic?,” *IEEE Commun. Mag.*, vol. 53, no. 9, pp. 41–47, 2015.
[118] A. Cama, F. G. Montoya, J. Gómez, J. L. De La Cruz, and F. Manzano-

Agugliaro, “Integration of communication technologies in sensor networks to monitor the Amazon environment,” *J. Clean. Prod.*, vol. 59, pp. 32–42, Nov. 2013.

[119] N.-K. C. Nair and L. Zhang, “SmartGrid: Future networks for New Zealand power systems incorporating distributed generation,” *Energy Policy*, vol. 37, no. 9, pp. 3418–3427, Sep. 2009.

[120] H. R. Baghaee, M. Mirsalim, and G. B. Gharehpetian, “Power Calculation using RBF Neural Networks to Improve Power Sharing of Hierarchical Control Scheme in Multi - DER Microgrids,” *IEEE J. Emerg. Sel. Top. Power Electron.*, vol. 4, no. 4, pp. 1217–1225, 2016.

[121] L. Che, M. Shahidehpour, A. Alabdulwahab, and Y. Al-Turki, “Hierarchical coordination of a community microgrid with AC and DC microgrids,” *IEEE Trans. Smart Grid*, vol. 6, no. 6, pp. 3042–3051, 2015.

[122] IEEE Computer Society, *IEEE Standards 802.15.4*, 1st Editio., no. October. New York: The Institute of Electrical and Electronics Engineers, Inc., 2003.

[123] W. Stallings, *Data and Computer Communication : Eight edition*, Eight. New Jersey: Pearson Prentice Hall, 2007.

[124] R. P. S. Chandrasena, F. Shahnia, A. Ghosh, and S. Rajakaruna, “Secondary Control in Microgrids for Dynamic Power Sharing and Voltage / Frequency Adjustment,” in *Australasian Universities Power Engineering Conference (AUPEC)*, 2014, vol. 1, no. October, pp. 1–8.

[125] Y. H. Liao, H. C. Chen, H. C. Cheng, Y. L. Ke, and Y. T. Li, “A novel control strategy of circulating currents in paralleled single-phase boost converters with different power sharing for microgrid applications,” *IEEE Trans. Ind. Appl.*, vol. 50, no. 2, pp. 1304–1312, 2014.

[126] J. Wang, B. Bao, J. Xu, G. Zhou, and W. Hu, “Dynamical Effects of Equivalent Series Resistance of Output Capacitor in Constant On-Time Controlled Buck Converter,” *IEEE Trans. Ind. Electron.*, vol. 60, no. 5, pp. 1759–1768, 2013.

[127] X. Zhang, J. Xu, B. Bao, and G. Zhou, “Asynchronous-Switching Map-Based Stability Effects of Circuit Parameters in Fixed Off-Time,” *IEEE Trans. Power Electron.*, vol. 31, no. 9, pp. 6686–6697, 2016.

[128] Y. Xia, Y. Peng, H. Hu, Y. Wang, and W. Wei, “Advanced unified decentralised control method with voltage restoration for DC microgrids,” *IET Renew. Power Gener.*, vol. 10, no. 6, pp. 861–871, 2016.

[129] T. Morstyn, B. Hredzak, G. D. Demetriades, and V. G. Agelidis, “Unified Distributed control for DC microgrids operating modes,” *IEEE Trans. Power Syst.*, vol. 31, no. 1, pp. 802–812, 2016.

[130] H. Liang, A. K. Tamang, W. Zhuang, and X. S. Shen, “Stochastic Information Management in Smart Grid,” *IEEE Commun. Surv. Tutorials*, vol. 16, no. 3, pp. 1746–1770, 2014.

[131] Z. Shi, R. Sun, R. Lu, L. Chen, J. Chen, and X. Sherman Shen, “Diverse Grouping-Based Aggregation Protocol with Error Detection for Smart Grid Communications,” *IEEE Trans. Smart Grid*, vol. 6, no. 6, pp. 2856–2868, 2015.

[132] R. Majumder, “Aggregation of microgrids with DC system,” *Electr. Power Syst. Res.*, vol. 108, pp. 134–143, 2014.

Every reasonable effort has been made to acknowledge the owners of copyright material. I would be pleased to hear from any copyright owner who has been omitted or incorrectly acknowledged.